CRANFIELD UNIVERSITY

ATMA PRAKASH

PREDICTION OF NO_X EMISSIONS FOR AN RQL COMBUSTOR USING A STIRRED REACTOR MODELLING APPROACH

SCHOOL OF AEROSPACE TRANSPORT AND MANUFACTURING

PHD THESIS

Academic Year: 2015

Supervisor: DR VISHAL SETHI
DR DEVAIAH K NALIANDA

SEPTEMBER 2015

CRANFIELD UNIVERSITY

SCHOOL OF AEROSPACE TRANSPORT AND MANUFACTURING

PHD THESIS

Academic Year 2015

ATMA PRAKASH

PREDICTION OF NO_X EMISSIONS FOR AN RQL COMBUSTOR USING A STIRRED REACTOR MODELLING APPROACH

Supervisor: DR VISHAL SETHI
DR DEVAIAH K NALIANDA

SEPTEMBER 2015

This thesis is submitted in fulfilment of the requirements for the degree of Doctor of Philosophy

EXECUTIVE SUMMARY

In an effort to reduce NO_X emissions both in the landing and take-off (LTO) cycle as well as in cruise, significant research has been conducted on novel aero-engine low emissions combustor design concepts. Preliminary combustor design and emissions prediction software tools are becoming increasingly important during the conceptual design phase of aero-engine combustors. They allow a large number of designs to be explored, in a relatively short amount of time, thereby identifying the most promising designs to consider for further development.

There are three methods for NO_X emission prediction; correlations, stirred reactor models and CFD models. Correlation methods are derived from experimental results and are therefore only applicable for combustors for which data is available. The stirred reactor modelling approach provides a reasonably good compromise with respect to computational time and robustness relative to correlation and CFD based methods. The stirred reactor method assumes finite rate chemistry inside the combustor using simplified chemical kinetic models. The basic concept of the reactor-based method is to split the combustor into a number of reactors (perfectly or partially stirred) to compute the overall emissions.

The primary objective of this doctoral research was to assess the suitability and limitations of the stirred reactor modelling approach to predict NO_X emissions of a Rich-Burn Quick-Quench and Lean-Burn (RQL) combustor concept. The geometry of the RQL combustor and the model constraints were assumed from a NASA test rig experiment. The stirred reactor emission prediction model developed was verified using this test data. The results suggest that, based on the modelling assumptions made, the stirred reactor modelling approach is able to capture the trends of emissions (with changing boundary conditions) even though there are discrepancies in the absolute values. This suggests that the stirred reactor model is a useful tool during the preliminary design phase to quantify the impact of changes in boundary conditions/design parameters on changes in NO_X emissions.

An additional assessment was performed to assess the sizing requirements for the RQL combustor design to meet the certification criteria for altitude relight at 10,000m. The results highlight and assess the combustor design requirements for a successful relight at 10,000m. The minimum reference area required and a reference diameter for a “pessimistic” θ parameter curve and an “optimistic” θ parameter curve is analysed respectively.

To the author’s best knowledge the application of a stirred reactor modelling approach to compute NO_X emissions of an RQL combustor has not been done before and is therefore the contribution to knowledge of this research.

Keywords:

NOX, CO, Combustor, Emission Prediction, Novel Combustor, RQL, Stirred Reactor & Shale gas

ACKNOWLEDGEMENTS

First and foremost, I would like to express my deepest gratitude to my parents as this PhD would not have happened without their love and support throughout my life. Therefore, I would like to dedicate my PhD thesis to my parents, brother and my loving wife Vandana who has been a great motivator for me.

I would like to express my sincere gratitude to my supervisors, Dr Vishal Sethi and Dr Devaiah K Nalianda. Dr Sethi has not only guided me as my supervisor, he has been my mentor, and my adviser who has supported me professionally and gave me friendly suggestions when needed. I will always be indebted to his dedicated guidance and support throughout the entire research project and beyond. Also, I would like to extend my gratitude to Dr Nalianda for his educational and informative informal talks which has rejuvenated me every time I met him.

I am grateful to Professor P. Pilidis for giving me the opportunity to pursue the doctoral study at Cranfield University with scholarship. I really enjoyed the lectures by Professor P. Pilidis, Professor R. Singh, and late Dr K. W. Ramsden. Their lectures have helped me build a strong foundation in the area of gas turbine technology. I would also like to thank Nicola and Gill who were always there to help.

I would like to thank all my friends whom I met at Cranfield University. I will always cherish those beautiful moments which I shared with them in the last four years at Cranfield.

I would like to thank the team of Cranfield Speakers Toastmaster club to help me in learning the art of public speaking. Especially, I would like to mention the contribution of Jim, Becky, John Schell, Paul, Andy and Daniel for helping me prepare and evaluate my speeches.

I would like to express my gratitude to the CSA, especially to Sue, Glenda, Martin, and Stewart for being there during the organisation of the cultural festivals for societies. The doctoral study at Cranfield University has been a great journey for me and I will cherish those memories for the rest of my life.

TABLE OF CONTENTS

LIST OF FIGURES

LIST OF TABLES

LIST OF ABBREVIATIONS

ACARE	Advisory Council for Aeronautical Research in Europe
BPR	Bypass Ratio
BFF	Boeing Fuel Flow
CAEP	Committee on Aviation Environmental Protection
CFC	Chloral Fluoro Carbon
CFD	Computational Fluid Dynamics
CH_4	Methane
CO	Carbon Monoxide
CO_2	Carbon Dioxide
CU	Cranfield University
CUTF	Cranfield University Turbofan
DAC	Dual Annular Combustor
DLN	Dry Low NO_X
DZ	Dilution Zone
$EINO_X$	Emission Index for NO_X
FAR	Fuel to air ratio
FBN	Fuel Bound NO_X
FF	Flame Front
GE	General Electric
H_2O	Water
HO_2	Peroxy radicals
ICAO	International Civil Aviation Organization
IZ	Intermediate zone
LAQ	Local Air Quality
LDI	Lean direct injection
LHV	Lower Heating Value

LPP	Lean Pre-mixed Pre vaporised
LTO	Landing and take-off cycle
NASA	National Aeronautics and Space Administration
NO_X	Oxides of Nitrogen
N_2O	Nitrous oxide
NO_2	Nitrogen dioxide
NW	Near Wall
O_2	Oxygen
O_3	Ozone
OPR	Overall pressure ratio
P	Pressure
P & W	Pratt and Whitney
PaSR	Partially-stirred reactor
PDF	Gaussian Probability Density Function
PERM	Partially Evaporated & Rapid Mixing Combustor
PR	Pressure Ratio
PSR	Perfectly-Stirred Reactor
PSRS	Series of Perfectly-Stirred Reactors
PZ	Primary Zone
QQ	Quick-Quench
R-CHO	Aldehydes
RQL	Rich-burn Quick-quench Lean-burn combustor
SARPs	Standards and Recommended Practices
SMD	Sauter mean diameter
SO_X	Oxides of Sulphur
TAPS	Twin Annular Premixed Swirl Combustor
TERA	Techno-economic Environmental and Risk Analysis

UHC	Unburned Hydrocarbons
UV	Ultra-Violet

GLOSSARY

A_n	Nozzle area
A_{ref}	Reference Area
C	Empirical Constant = 2.5
d_j	Diameter of the Jet Entry Orifice
D_{ref}	Reference diameter
ρ	Density
ρ_{jets}	Jet flow density
ρ_{main}	Main flow density
δ_{amb}	Free stream and ISA sea level static pressure ratio
$EIHC$	Emission index of Hydro carbon
$EICO$	Emission index of carbon mono-oxide
f	Mixture fraction
f_m	Mixture fraction mean value
F1	Fraction of air entering the flame front rich-burn reactor
F2	Fraction of rich-burn to quick-mix near-wall reactor effluent gases
F3	Fraction of air to near wall quick-mix reactor
F4	Fraction of air to quick-quench core reactor
F_N	Nett Thrust
F_G	Gross Thrust
F_D	Momentum Drag
g	Gram
γ	Specific heat at constant pressure to that at constant volume ratio
H	Humidity Factor
H	Channel Height (Mentioned appropriately)
J	Jet-to-Crossflow Momentum Flux Ratio
kg	Kilogram

$\dot{m}_A$	Combustor airflow rate, kg/s
m_{pz}	Primary zone airflow rate, kg/s
M	Mach number
M_a	Mach number
MR	Jet-to-Crossflow Mass Flow Ratio
n	Number of Circular Jet Orifices to Optimize Mixing
η_c	Combustion efficiency
$\eta_{overall}$	Overall efficiency
$\eta_{propulsive}$	Propulsive efficiency
$\eta_{thermal}$	Thermal efficiency
ω	Specific humidity
P_3	Combustor inlet pressure
P_{amb}	Inlet ambient pressure
p_n	Nozzle Exit Static Pressure
p_0	Air Static Pressure
P_v	Saturation vapour pressure
$\emptyset$	Equivalence ratio
φ	Relative humidity
q	Fuel to air ratio
R	Gas constant
$REIHC$	Reference emission index of Hydro carbon
$REICO$	Reference emission index of carbon mono-oxide
S	Orifice Spacing
S	Mixing or unmixedness parameter
σ	Standard deviation of the mixture fraction
θ	Entry Angle of the Jet to the Crossflow
θ	Theta Parameter (mentioned appropriately)
θ_{amb}	Free stream and ISA Sea level static temperature ratio

t	Residence time
t_e	Fuel evaporation time
T_3	Combustor inlet temperature
T_{amb}	Ambient temperature
T_c	Combustor temperature
T_{eq}	Equivalent Temperature
T_{pz}	Primary zone temperature
T_{st}	Stoichiometric flame temperature
θ	Theta Parameter
V_c	Volume of the combustor
V_e	Volume employed in fuel evaporation in combustor
V_J	Jet Velocity
V_{jets}	Jet flow Velocity
V_{main}	Main flow Velocity
V_0	Inlet air velocity
W	Mass flow rate
W_B	Bypass mass flow rate
W_c	Core mass flow rate
W_f	Fuel flow rate
W_{ff}	Fuel flow factor
Y_{max}	Maximum Radial Penetration of the Jet Centreline

1 INTRODUCTION

1.1 Project Context

The world has witnessed a drastic techno-economic development in the last century due to which transport, trade and logistics have improved the lifestyle of the public. The Aviation industry has transformed the way of travelling across globe. Now it is more economic, comfortable and accessible to travel. Unfortunately, this revolution in aviation has brought various environmental issues; gaseous emissions and noise nuisance. These gaseous emissions disrupt the eco-system normal operating process. In addition to the CO_2 released by in-flight jet engines, aviation industry also contributes to greenhouse gas emissions from ground airport vehicles and transport used by passengers and staffs to access the airport. While the principal greenhouse gas emission from powered aircraft in flight is CO_2, other emissions include nitric oxide, nitrogen dioxide, water vapour and particulates (soot and sulphate particles), sulphur oxides, carbon monoxide, and unburned hydrocarbons (UHC).

These gases have serious implications on the global environment and pose a great risk for human health explained in section 2. The NO_X (NO and NO_2) is a major concern; especially around the airports locality, where it can create ozone gas which is harmful to the wellbeing. Moreover, aviation is the only reason for high altitude cruise NO_X which plays a major role in the ozone layer depletion in the stratosphere [1]. Depletion of ozone layer allows the solar Ultra-Violet (UV) rays to penetrate the Earth leading to skin related diseases.

Contribution of civil aviation to global greenhouse emissions has been estimated at around 2% by the International Civil Aviation Organisation (ICAO). According to the 2010 ICAO Environmental report, air travel is growing at an average rate of 4.8% per year and it is expected to increase further [2]. The Advisory Council for Aeronautical Research in Europe (ACARE) which is a European advisory body in a public-private partnership between the European Commission, aviation industry leaders and academia has established ambitious

goals in flightpath 2050 to reduce CO_2 emissions by 75% per passenger kilometre, NO_X emissions by 90% per passenger kilometre and to reduce perceived noise by 65% by 2050 [3] [4].

The ICAO has been taking continuous efforts to regulate the aircraft emissions by formulating stringent policies on emission reduction. Therefore, aviation industry is looking ways to reduce the emissions not only due to its global climatic impact and health hazard, but to meet stringent emission standards set up by ICAO, CAEP & ACARE.

In case of stationary gas turbines, emission regulations tends to vary from one country to another due to different legislations which is supplemented by local or site-specific regulations and ordinances governing the size and usage of the plant under consideration and the type of fuel used [5]. The NOx emission for stationary gas turbines engines in the USA is regulated by EPA (United States Environmental Protection Agency), more details may be found in [6]. The emissions of UHC, particulate matter, and SOx are negligibly small for the large number of gas turbine engines burning natural gas. Therefore, most of the drive towards more stringent regulations for stationary gas turbines has been directed at NOx. In the United States, the Environmental Protection Agency (EPA) has promulgated emissions standards [7], which depend on the engine's input energy and intended use (utility or industrial). On July 6th 2006, the EPA proposed, the NOx limits for stationary gas turbines as:

- 42 ppmv below 3 MW, 25 ppmv (3–110 MW) and 15 ppmv (above 110 MW) for new electricity-producing turbine-firing natural gas
- The NOx limits for new electricity-producing turbines firing fuels other than natural gas are: 96 ppmv below 3 MW (4000 HP); 74 ppmv (3–110 MW); and 42 ppmv (above 110 MW).

A new amendment rule was proposed by the EPA on 29th August 2012 for stationary gas turbines engine combustion. These amendments were proposed to amend the NOx emissions standard for stationary combustion turbines that burn multiple fuels. The detailed description about the amendments are mentioned by the EPA federal register [8]. One of the programs to move

towards greener energy generation is SunShot energy storage solutions project under the Sustainable and Holistic Integration of Energy Storage and Solar PV (SHINES) program which develops and demonstrates integrated photovoltaic (PV) and energy storage solutions that are scalable, secure, reliable, and cost-effective [9]. This is the first funding program as shown in Figure 1-1 within the Department of Energy focusing exclusively on connecting renewable power to storage.

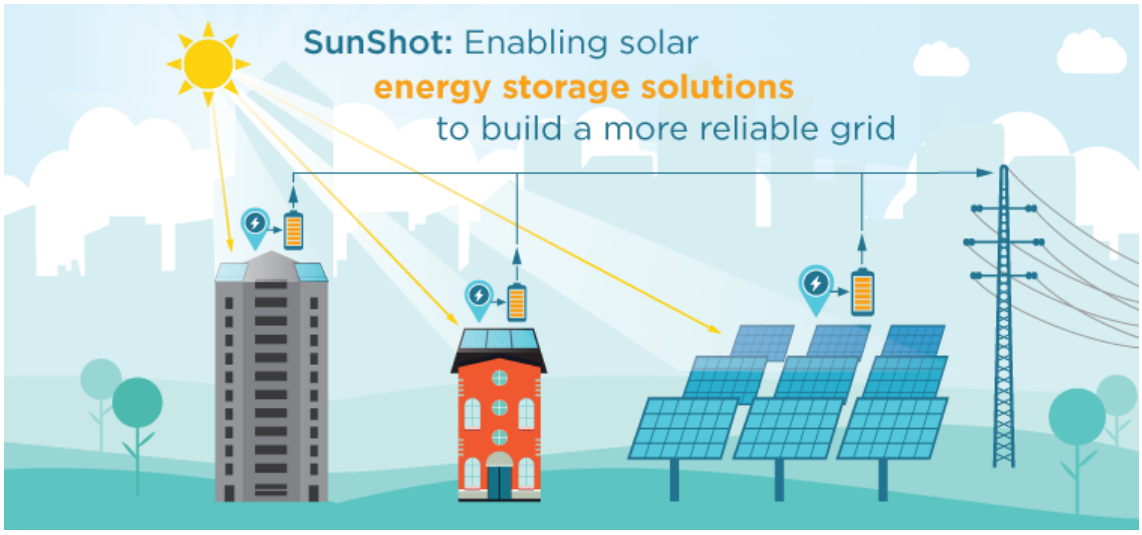

Figure 1-1 SunShot Project [9]

The formation of pollutants during combustion depends on various parameters such as inlet pressure, temperature, combustor geometry, airflow, and fuel distribution inside the combustor [5]. The formation rate of NO_X increases with flame temperature, peaking at air-fuel ratios close to stoichiometric [10].

In particular, requirement for the larger aircraft to carry more passengers with lower fuel cost has led the aviation industries in moving to the higher bypass ratio engine designs. As, the bypass ratio of large turbofans increases, the resulting power requirements of the larger fan mandate increases requiring more energy to be extracted from the low-pressure turbine. This typically leads to higher pressures, combustion temperatures, and therefore higher NO_X production. In fact, the increase in total aviation NO_X emissions has grown rapidly than total fuel consumption over the last few decades because of the

higher pressure ratios (and therefore combustion temperatures) demanded by the more fuel-efficient high-bypass-ratio engines [11].

Therefore, in order to minimize the NO_X emission in the combustor, the time spent in the high flame temperature region must be minimized. Novel combustor design concepts limits the temperature, varies the mass flow distribution in different zones, and resident time in order to reduce the overall NO_X emission below the current ICAO legislation levels. As, novel low emission combustors show a promising way to curb down the aircraft emissions and compliance with the stringent regulations, this research focuses on the novel combustor designs concept and the suitability of a NO_X emission prediction method for an aircraft engine.

This section leads to the following research questions that this study aims at answering:-

- What are novel emission combustor designs which can be adopted for aircraft engines to comply with the ICAO legislation and which is more suitable for this study?
- Which emission prediction method is suitable for modelling the NO_X formation in the novel combustor design and why?
- Are the developed model's NO_X predictions, verified with the public domain test rig data?
- How sensitive is the developed model for the combustor input parameters such as temperature, pressure, fuel/air flow and geometry?
- Is the novel combustor suitable for flying in an altitude re-lighting conditions?
- Can the developed NO_X prediction model be robust for alternative fuels?

1.2 Project Objectives

Based on the research questions, following objectives of the doctoral research are derived and mentioned below:

- Selection of a method to predict NO_X emission for novel aero engine combustors.
- Development of a novel low emission combustor model using the selected prediction method to predict NO_X.
- Verification of the NO_X emission predictions model with the test rig data available in public domain.
- Assessment of the novel combustor design suitability for flying in an altitude re-lighting conditions.
- In order to check the robustness of the model for alternative fuel, addition of four types of liquid natural shale gas fuel in the model.

1.3 Novel Aspects

The novel aspect of this research involves the development of a NO_X emission prediction model using stirred reactor modelling approach for an RQL combustor. The geometry of the RQL combustor and the model constraints were assumed from a NASA test rig experiment and the stirred reactor NO_X emission prediction model developed is verified using this test data. Sensitivity study of the developed model is performed by varying inlet air in various zones to assess the effects on NO_X emissions in the developed RQL model. An additional assessment is performed to assess the sizing requirements for the RQL combustor design to meet the certification criteria for altitude relight at 10,000m.

1.4 Methodology

In order to achieve all the thesis objectives, a research methodology has been followed. First, a literature review is performed on all the NOx emission prediction method available for gas turbine engines. Therefore, empirical, semi-empirical correlation, CFD and stirred reactor method has been researched to find the viable method for this study. Then, the stirred rector model is selected based on the criteria such as computational speed, time taken to execute, flexibility in adapting to different aircraft models present at Cranfield University. In the second step, engine models are selected based on public domain data

availability to calculate the engine performance in the TURBOMATCH in-house Cranfield University engine performance software.

In the third step, output from the engine performance model such as combustor inlet temperature, pressure, fuel flow and mass flow is introduced in the developed RQL model, based on stirred reactor approach to predict NO_X. In the fourth step, the NO_X prediction results from RQL emission prediction model is verified with the NASA RQL test rig experiment [12]. Finally, a detailed case study is performed on sizing and altitude relight capability of RQL combustor using the test rig RQL combustor geometry as a baseline.

The novelty of the methodology lies in the use of the reactor based model instead of a correlation method or CFD method for RQL NO_X emissions prediction. Furthermore, the verification of an RQL model based on the stirred reactor method with the NASA test rig experiment has been performed for the first time in RQL combustion research.

1.5 Thesis Structure

The first part of chapter 2 provides an overview of the mechanism involved in formation of the pollutants and their impact on environment. The second part described the ICAO regulations and NO_X emissions standards for aircraft certifications. The third part covered different methods used in the industry to predict emissions from a jet engine combustor and research conducted on the novel combustor design to reduce emissions. Finally, after identifying the gap in the literature, the last part presented the reasoning for choosing the stirred reactor method in predicting NO_X emissions of a gas turbine RQL combustor.

Chapter 3 describes in detail the development of the emission prediction model “Hephaestus” for RQL combustor using stirred reactor approach. Second part of the chapter explains the developed RQL combustor model’s assumptions and constraints in developing the model. The result output from the model and the verification with a NASA test rig experiment is covered in the 4^{th} chapter. The

later part covered the sensitivity analysis of the RQL model for NO_X prediction by varying the various input parameters of the combustor.

Furthermore, the last part of the chapter four critiqued the NASA RQL combustor suitability for aircraft integration, and the basic criterion for altitude re-light capability of the RQL combustor is analysed. Then required sizing suggestions for a RQL combustor to satisfy the altitude re-light capability is discussed in the last part of the chapter.

The chapter 5 concludes with the discussion and further recommendation of work to be continued after this study.

The list of published papers from outcome of this study is mentioned in the appendix A. The Appendix B shows the input file for the developed RQL model with all the input parameters such as, pressures, temperature, fuel flow, air mass flow rate and the geometry of the combustor.

Additionally, in order to investigate the robustness of the emission prediction model to accommodate alternative fuels, Appendix C describes the modelling of four types of natural shale gas fuels in the emission prediction tool and their NO_X predictions for conventional combustor.

2 LITERATURE REVIEW

The first part of this chapter describes the mechanism of NO_X formation and its effects on environment and human health. The second part of the chapter gives an overview of the ICAO regulations and emissions standards for aircraft certification. The third part of this chapter covers the different methods used in the aviation industry to reduce NO_X emission from a jet engine combustor and research conducted on the various novel low NO_X combustor designs. Finally, at the end of the chapter, problem definition and challenges associated with the chosen novel low NO_X combustor design are provided.

2.1 Introduction

In spite of much advancement in fuel-efficient and less polluting turbofan and turboprop engines, the rapid growth of air travel in recent years has contributed to an increase in total emissions. According to the ICAO, the contribution of civil aircraft to global greenhouse emissions has been estimated at around 2%. The Committee on Aviation Environmental Protection (CAEP), which assists ICAO in the formulation of new policies on aircraft noise and emissions, has presented a number of policies in the last decade in order to curb down the aviation emissions. Due to these emission regulations, the aviation industry is looking into the ways to cut down its global emission imprints.

The next section gives an insight into the various aviation pollutants form during combustion and its environmental & human health impacts.

2.2 Emissions from the Aircraft

2.2.1 Introduction

Main greenhouse gases which result in significant increase in global warming are carbon dioxide (CO_2), methane (CH_4), nitrous oxide (N_2O), chloro-fluoro-carbons (CFCs) and also troposphere ozone (O_3). Apart from producing CO_2 as the principal greenhouse gas pollutant from an aircraft, it emits; nitric oxide & nitrogen dioxide together known as Oxides of Nitrogen (NO_X), water vapour

(H_2O) , particulates (soot and sulphate particles), sulphur oxides, carbon monoxide (CO), and unburned hydrocarbons (UHC).

Carbon dioxide and water vapour are not considered as the pollutants because they are usual by products of complete combustion of a hydrocarbon fuel. However, both contribute to global warming and only way to reduce their production is by burning less fuel. Thus, improvement in engine thermal efficiency not only reduces operating costs but carbon dioxide and water vapour pollutants as well. Section 2.3 explains how engine efficiency impacts on aircraft emission.

Pollutant formation during combustion reaction is dependent on different parameters such as flame temperature, residence time, atomisation of the fuel, fuel-air homogeneity and combustor design. Figure 2-1 shows the principal pollutants formed during aircraft combustion.

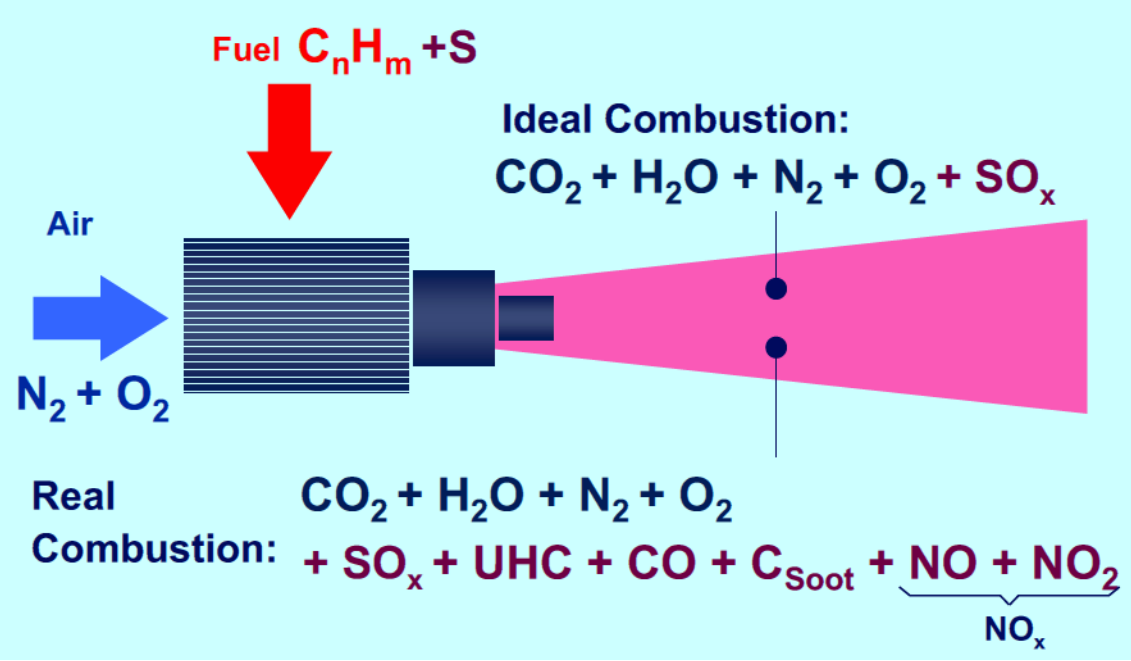

Figure 2-1: Emissions from the Aircrafts [13]

The pollutants emitted from an aircraft are mentioned below:

- Carbon dioxide (CO_2)
- Water vapour (H_2O)
- Carbon Monoxide (CO)
- Unburned hydrocarbon (UHC)
- Oxides of sulphur (SO_X)
- Smoke
- Oxides of Nitrogen (NO_X)

These pollutants are the gaseous emissions from the aircraft which have direct or in-direct impact on human health and environment. Figure 2-2 shows the gas turbine engine emissions characteristics for different engine power settings.

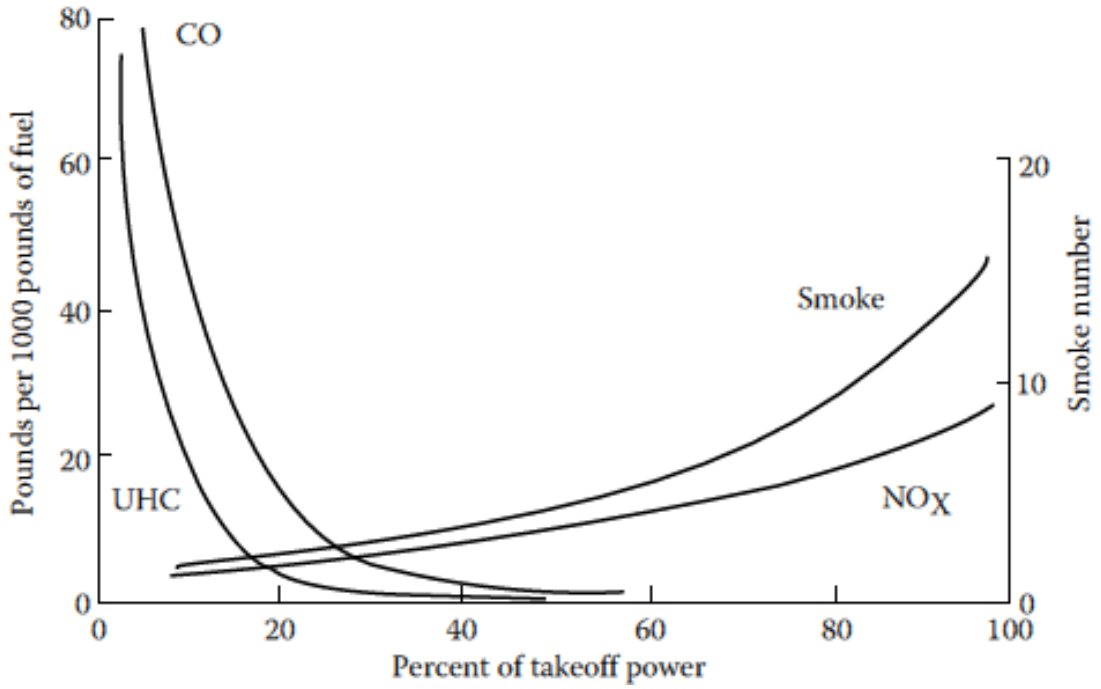

Figure 2-2: Emission characteristics of gas turbine engines [5]

2.2.2 Carbon Dioxide CO_2

The increase in burning of fossil fuels has severe implication on increase in the amount of CO_2 in the atmosphere. Although, methane, nitrous oxide, ozone, also contribute to global warming but, carbon dioxide is primarily responsible for

the rise of the Earth's temperature by trapping heat radiated from the Earth. Carbon dioxide has a long atmospheric lifetime, therefore exerting a larger overall warming influence than all of the other heat-trapping gases combined. According to ICAO, the contribution of civil aircraft to global greenhouse emissions is around 2%. The carbon dioxide is the natural by-product when hydro-carbon fuel is burned during jet engine combustion. The only way to reduce CO_2 is by burning less fuel. In the last couple of decades, innovation and technology advancement in aviation sector has helped to fuel efficient jet engines tend to produce less carbon dioxide.

2.2.3 Water vapour (H_2O)

Water vapour plays a pivotal role as a greenhouse gas. Similar to CO_2, water vapour is also a natural by-product of hydro-carbon fuel combustion. Aircraft engine at high altitude produces water vapours, under certain atmospheric conditions and condenses into droplets to form condensation trails, or contrails. Contrails are visible line clouds that form in cold, humid atmospheres and are thought to have a global warming effect though less significant than CO_2 emissions effects. Contrails are extremely rare from lower-altitude aircraft, or from propeller-driven aircraft or rotorcraft [14] .

Cirrus clouds have been observed to develop after the persistent formation of contrails and have been found to have a global warming effect over-and-above that of contrail formation alone. There is a degree of scientific uncertainty about the contribution of contrail and cirrus cloud formation to global warming and attempts to estimate aviation's overall climate change contribution do not tend to include its effects on cirrus cloud enhancement.

2.2.4 Carbon Monoxide (CO)

Carbon monoxide is colourless, odourless, and tasteless, but it is highly toxic and if inhaled, can be hazardous to one's life. It reduces the capacity of blood to absorb oxygen and if taken in high amounts, it can cause asphyxiation and eventually death [5]. Incomplete combustion in the jet engine produces carbon mono-oxide (CO).

The main reason for incomplete combustion is lower reaction temperature, pressure, inhomogeneous mixing of fuel and air in the combustor, the mean drop size of the spray, and chilling of combustion gases near wall from liner wall cooling air.

The Figure 2-3 shows, carbon mono-oxide decreases as temperature increases because carbon mono-oxide oxidises in an exothermic reaction to form carbon di-oxide. But, after 1900 K there is a rise in carbon mono-oxide production, which is due to the fact that carbon di-oxide goes into endothermic reaction to form carbon mono-oxide. As, this reaction is endothermic, it takes heat from the system therefore reducing the combustion efficiency. Therefore, careful combustor designing is done in order for the temperature to lie within the required reaction limit for the carbon monoxide to convert into carbon di-oxide and not vice-versa.

Carbon monoxide is part of the series of cycles of chemical reactions that form photo-chemical smog. Along with aldehydes (R-CHO), it reacts photo-chemically to produce hydro-peroxyl radicals (HO_2) [15]. A hydro-peroxyl radical subsequently oxidizes nitrogen oxide (NO) to nitrogen dioxide (NO_2). This creation of NO_2 is the critical step leading to low level ozone formation around airport vicinity. Simplified, reaction equation of the ozone formation from CO is given below:

$$CO + 2O_2 \rightleftharpoons CO_2 + O_3$$

Ozone gas (O_3), or trioxygen is a triatomic molecule, consists of three oxygen atoms. It is an allotrope of oxygen which is much less stable than the diatomic allotrope (O_2). Ozone formed in the airport vicinity is an air pollutant with harmful effects on the respiratory systems for inhabitants and if inhaled can cause bronchitis, asthma and heart attack [16].

2.2.5 Unburned Hydrocarbons (UHC)

UHC contains the fuel droplets or vapours that didn't burn completely during the combustion process. It is mainly formed due to bigger fuel droplet sizes and due to poor atomization, inadequate burning rate, the chilling effect or combination

of many. UHC is also toxic and hazardous for human health. Formation of UHC also signifies wastage of unburned fuel which is uneconomical for the aviation. Generally those factors that influences CO emissions also influences UHC emissions and in much the same manner.

2.2.6 The oxides of sulphur (SO_X)

It is formed due to burning of fuels with traces of sulphur which sometimes is added in order to increase the lubricity of the fuel. The sulphur in fuel reacts with air in combustion to form SO_X which is highly toxic and corrosive in nature. It causes acid rain, which reacts with the calcium present in walls of heritage monuments, disfiguring the architecture of the building. Inhaling sulphur dioxide can increase respiratory diseases and can cause death.

2.2.7 Smoke

Smoke is produced by soot or carbon particles formed in fuel rich regions in combustor which also causes coking of the fuel injector. Its formation depends on the characteristics of the fuel i.e. viscosity and volatility. The drop size plays a major part in production of smoke, so if the quality of atomization is non-uniform then the smoke will be generated, which is also toxic and can cause asphyxiation. Soot is mostly carbon particles and it can damage the combustor liner, due to its high heat radiative property which further increases maintenance cost and eventually reduces life expectancy of the engine.

2.2.8 Oxides of Nitrogen (NO_X)

Generally, most of the nitric oxide (NO) formed during combustion process inside gas turbine engine subsequently oxidizes into NO_2. Therefore, usually NO and NO_2 are lump together to express the results in terms of oxides of Nitrogen (NO_X). NO_X is pollutant from aero engine exhausts which plays a major role in disturbing the atmospheric ozone concentration.

NO_X is responsible for low level ozone formation near airport area which is toxic. If inhaled may lead to many respiratory illness, impaired vision,

headaches and, allergies. The reaction mechanism of ozone formation [5; 14; 17; 18] at lower level is explained below:-

$$NO_2 \overset{hv}{\rightarrow} NO + O, \qquad 2\text{-}1$$

$$O + O_2 \rightleftharpoons O_3 \qquad 2\text{-}2$$

Similarly, NO_X emission emitted by aircraft at high altitudes can deplete the ozone layer. The reaction mechanism of ozone` layer depletion at stratosphere is mentioned below:-

$$NO + O_3 \rightleftharpoons NO_2 + O_2 \qquad 2\text{-}3$$

$$NO_2 + O \rightleftharpoons NO + O_2 \qquad 2\text{-}4$$

It is clear from the above equation that the NO is liberated again after the reaction which then further reacts with ozone to form more oxygen.

Ozone forms a protective layer across the Earth which stops solar ultraviolet (UV) radiation. Therefore, depletion of ozone will allow increase in penetration of the UV rays which will further increase the chances of skin cancer among humans. The International Civil Aviation Organisation (ICAO) has set up landing and take-off cycle (LTO) NO_X emission standard for an aircraft and it's making it more stringent for future to have a clean atmosphere. The stationary gas turbine

It is produced by different mechanism described later on in the section 2.5. Furthermore, the factors which play a pivotal role in NO_X formation during combustion are; degree of uniformity/non-uniformity of the fuel distribution within the combustor, flame temperature, pressure, residence time and fuel atomisation. Non-uniform fuel distribution creates small pockets of fuel which burns in a diffusion mode at near stoichiometric fuel/air ratios, giving rise to many local high temperature regions in which NO_X forms in considerable quantities. Reduction in mean droplet size of fuel hampers the formation of envelope flames, so that a larger proportion of total combustion occurs in premixed mode thereby producing less NO_X.

Major part of the NO_X is generated in the higher temperature region known as thermal NO_X described in detail in section 2.5.1. As Figure 2-3 shows, NO_X formation is exponentially dependent on temperature; an obvious way of reducing NO_X emissions is by lowering the temperature in the combustion primary zone.

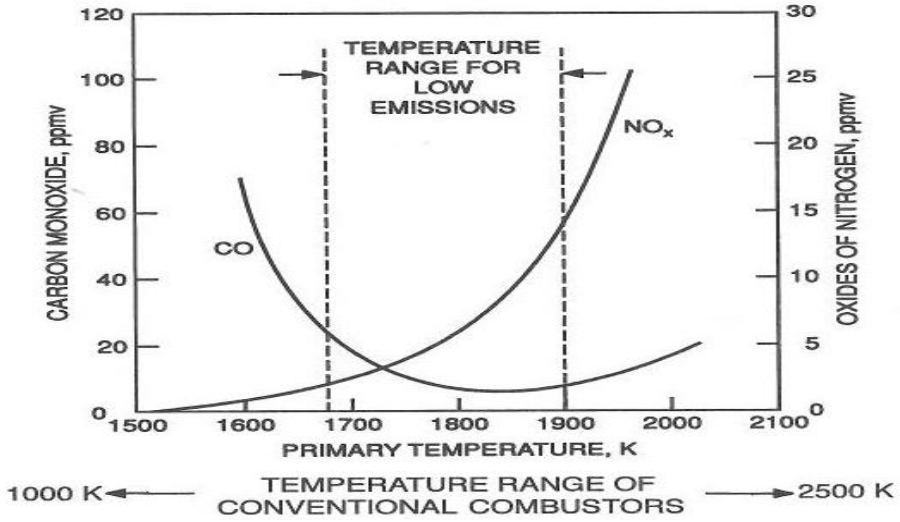

Figure 2-3: Effect of Temperature on NOx and CO formation

One way to reduce the thermal NO_X is by introducing additional air but if used in excess, it can raise the primary-zone velocity, which has an adverse effect on ignition and stability performance. An alternative way to reduce NO_X emission is to inject water or steam in the primary zone of the combustor. But, this technique is not feasible for aircraft engines as carrying large amount of water amounts to increase in weight therefore not fuel efficient. On the other hand, stationery gas turbine engines have been using water or steam injection in order to control NO_X emission to the level required by the regulations [19]. As described in section 1.1, emission regulations for stationary gas turbines tend to vary from one country to another due to different legislations and ordinances governing the size and usage of the plant under consideration and the type of fuel used. Further details about the legislations formulated by the EPA for stationary gas turbine are described in [6-8].

The stringent regulations by ICAO described in section 2.4 for the aviation NO_X in landing and take-off cycle can be fulfilled by carrying just enough water for

injection in the LTO cycle. Though there are various penalties of water injection in combustor such as; higher capital cost for treating the water before injection, potential corrosion leads to higher maintenance cost, increase in CO & UHC emissions, and increase in combustion pressure pulsation [5]. These drawbacks of water and steam injection have encouraged the development of the "Dry low-NO_X" (DLN) combustors described in section 2.9 so that it can meet the emission goals without having to resort to water injection.

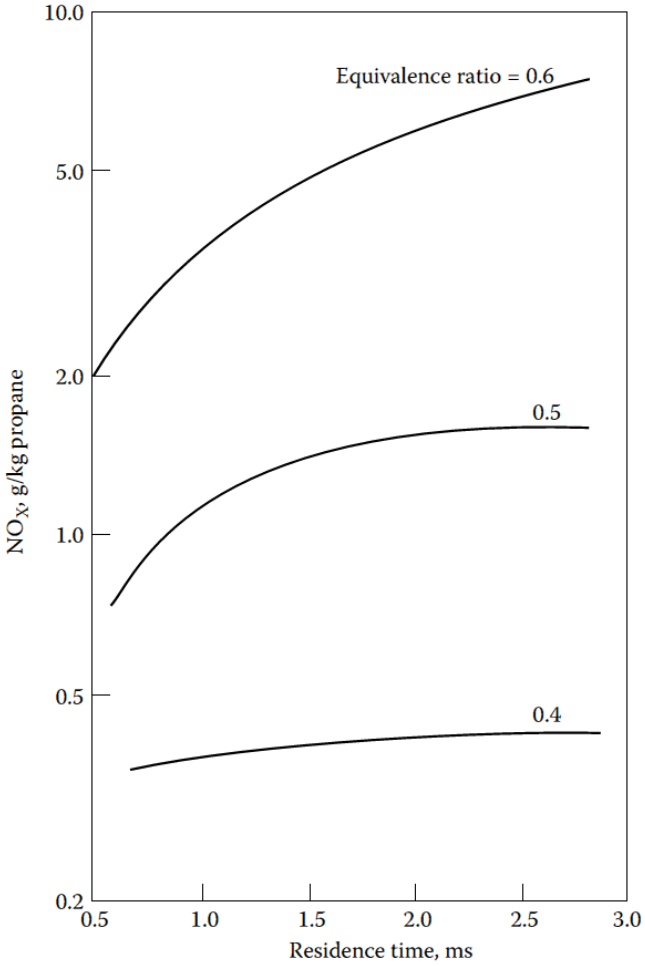

Figure 2-4: Effect of residence time on NO_X [20]

Combustor residence time influences the production of NO_X emissions; as residence time increases NO_X increases except for very lean mixtures where equivalence ratio is less than 0.4, for which rate of formation is so low that it becomes independent of time [5; 20]. Figure 2-4 shows the NO_X emission dependence on the residence time. It clearly shows in Figure 2-4 that for very

lean-premixed combustors where equivalence ratio is less than 0.5, NO_X formation is independent of the residence time.

2.3 Effect of Engine Efficiencies on NO_X formation

$$\eta_{overall} = \eta_{propulsive} \times \eta_{thermal} \qquad 2\text{-}5$$

Where, $\eta_{overall}$= Overall efficiency

$\eta_{propulsive}$= Propulsive efficiency

$\eta_{thermal}$= Thermal efficiency

The overall efficiency is defined as the efficiency with which the energy in the fuel is usefully employed in propelling the aircraft and consists of the product of the thermal efficiency and the propulsive efficiency of the engine as shown in equation 2-5. Whereas the propulsive efficiency is the proportion of the mechanical energy actually used to propel the aircraft. Lastly, the thermal efficiency is defined as; the ability of an engine to convert chemical energy of the fuel into mechanical work. For a typical aircraft, overall efficiency ranges between 20 to 40%.

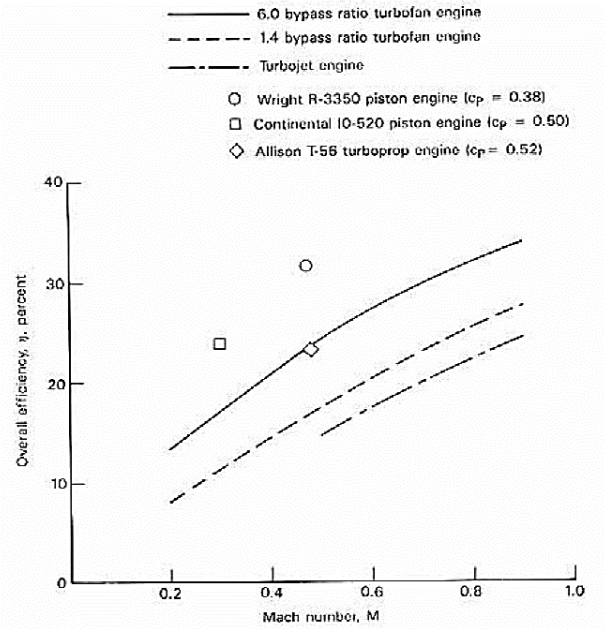

Figure 2-5 Overall efficiency of different aircrafts [21]

As from Figure 2-5, overall efficiency can be improved by increasing the jet engine exhaust velocity or by increasing the by-pass ratio. In order to improve the overall efficiency, there was a constant effort by engine manufacturers to increase the bypass ratio (BPR) (equation 2-6) of the engine for the last 40 years as it is economically viable option to save fuel cost.

$$BPR = \frac{W_B}{W_c} \qquad 2\text{-}6$$

Where, W_B=Bypass mass flow rate and W_c= Core mass flow rate

Moreover, increase in BPR reduces specific fuel consumption and thus higher bypass engines reduces CO_2 and H_2O. However, NOx formation rates rises as a result of higher combustor inlet air pressures and temperatures, explained as under.

As per the jet engine thrust equation [22] given by 2-7 :-

Nett Thrust (F_N) = Gross Thrust (F_G) – Momentum Drag (F_D)

$$F_N = WV_J + A_n(p_n - p_0) - WV_0 \qquad 2\text{-}7$$

Where, Gross Thrust (F_G) = $WV_J + A_n(p_n - p_0)$

W= Mass flow rate

V_J= Jet Velocity

A_n= Nozzle area

p_n= Nozzle Exit Static Pressure

p_0=Air Static Pressure

Momentum Drag (F_D) = WV_0

V_0= Inlet air velocity

Engine BPR shown in Figure 2-6 can be increased by two methods:

I. Reducing the engine core size and keeping the fan diameter casing constant
II. Or by keeping the engine core size constant and increasing the diameter of the bypass fan

In order to increase BPR, the first method is not practical to use, as it decreases compressor efficiency which reduces the combustor inlet pressure leading to combustion instability. The second method is the only viable method without compromising the compressor efficiency of the engine.

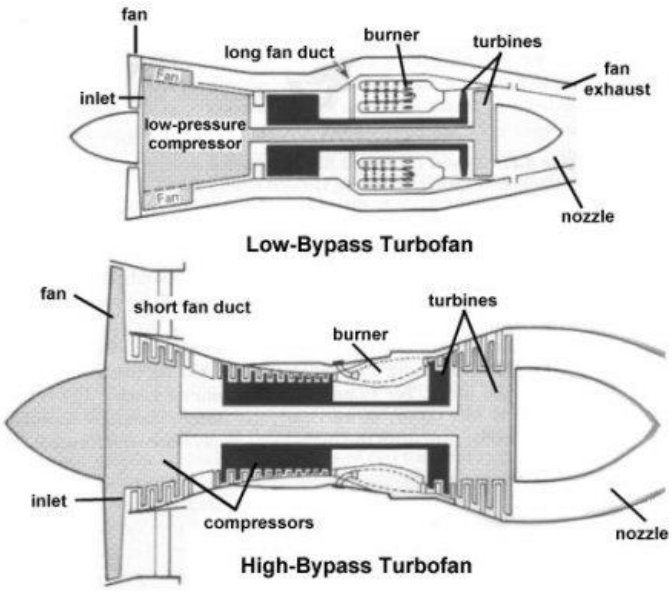

Figure 2-6: Difference between Low BPR and High BPR [23]

As the BPR increases, the fan casing diameter of the engine increases; therefore the bypass air mass flow rate increases, leading to increase in F_D in equation 2-7. Furthermore, with the increase in BPR, more work is needed to be extracted from the turbine to rotate the fan, thereby increasing the TET and hence the NO_X.

Whereas, the thermal efficiency defined as; the ability of an engine to convert chemical energy of the fuel into mechanical work and is given by equation 2-8 [24]:-

$$\eta_{thermal} = \frac{power\ to\ the\ gas\ stream}{energy\ input\ rate} \qquad 2\text{-}8$$

In order to increase the thermal efficiency of the engine, useful work has to increase thus increasing the TET or fuel flow needs to be lower for the same useful work. The increase in thermal efficiency can be achieved by higher pressure ratios across the compressor with constant fuel flow. Therefore, moving towards higher pressure ratios would be an economically viable solution for the engine manufactures to achieve higher TETs, which implies higher combustor inlet temperature. As, NO_X is a function of temperature and pressure, it increases as overall pressure ratio (OPR) increases for the engine.

Therefore, it shows how changes in efficiencies of the engine may contribute towards higher NO_X emissions in the combustor.

Now, the next section describes the ICAO objectives and the ICAO regulations for landing and take-off cycle for an aircraft.

2.4 International Civil Aviation Organisation regulation

2.4.1 ICAO Aims and Objectives

The aims and objectives of ICAO [25] are to develop the principles and techniques of international civil air navigation and to foster the planning and development of international air transport so as to:

- Ensure the growth of international civil aviation throughout the world safely and orderly
- Encourage the art of aircraft design and operation
- Encourage the development of airways, airports and air navigation facilities
- Meet the need for safe, regular, efficient and economical air transport
- Prevent waste caused by unreasonable competition
- Ensure the rights of contracting states are fully respected
- Avoid discrimination between contacting states
- Promote the safety of flight in international aviation

- Generally promote all aspect of international civil aeronautics

The Committee on Aviation Environmental Protection (CAEP) is a technical committee of ICAO council established in 1983, superseding the Committee on Aircraft Noise (CAN) and the committee on Aircraft Engine Emissions (CAEE). CAEP assists the Council in formulating new policies and adopting new Standards and Recommended Practices (SARPs) related to aircraft noise and emissions, and more generally to aviation environmental impact.

CAEP undertakes studies as and when requested by the ICAO. Its scope of activities encompasses noise, air quality and basket of measures today considered for reducing international aviation CO_2 emissions, including aircraft technology, operations improvement, market-based measure and alternative fuels. The ICAO reviews and adopts CAEP recommendations, including amendments to SARPs and in turn reports to ICAO Assembly where the main policies on environmental protection are ultimately defined [25].

CAEP meets every three years to report on the civil aviation and to recommend changes in the emission policies to be accepted by the states. In its 8th meeting held in 2010, it has recommended more stringent NO_X emission standards of up to 15 % on large engines and 5 to15 % on small engines certified after 31st December 2013.

2.4.2 ICAO Engine Emission Standards

In order to reduce the impact of aircraft emissions on environment, CAEP meets every three years to set up and review policy and emission standards by continually formatting and updating emission standards. The principal results arising from the work of the CAEP meetings is the development of the ICAO Standards and Recommended Practices (SARPs) on engine emissions and related guidance material and technical documentation. These SARPs aim to address potential adverse effects of air pollutants on Local Air Quality (LAQ), primarily pertaining to human health and welfare. Among other issues, these provisions address: liquid fuel venting, smoke, and the main gaseous exhaust

emissions from jet engines, namely; hydrocarbons (HC), oxides of nitrogen (NOx), and carbon monoxide (CO) [25].

Main concern about the LAQ is in the vicinity of an airport which is the hub for all the aircraft flying and out of any city. Therefore, ICAO emission standards focuses on the aircraft engine emissions released below 3,000 feet and emissions from airport sources, such as airport traffic, ground service equipment, and de-icing operations. The current ICAO standards for emissions certification of aircraft engines state that to achieve certification, it must be demonstrated that the characteristic emissions of the engine type for HC, CO, NO_X and smoke are below the limits defined by ICAO. The certification process is based on the Landing Take-off (LTO) cycle, as shown in Figure 2-8. The LTO cycle has four modes of operation, involving a thrust setting and a time-in mode as shown in Table 2-1.

Table 2-1: Standard LTO cycles in terms of thrust settings and time spent in operating mode [26]

Operating Mode	Thrust Setting (% of maximum sea level static thrust)	Time-in Mode (Min)
Take-off	100	0.7
Climb-out	85	2.2
Approach	30	4.0
Taxi/ground idle	7	26.0

The engine certification process is performed on a test bed where the engine runs at each thrust setting to generate the data for each of the modes of operation. The result of the engine emissions certification test includes: fuel flow (kg/s), emissions index for each gaseous pollutant (g/kg), and the measured smoke number. All of these data are stored in the publically available ICAO emissions databank [27].

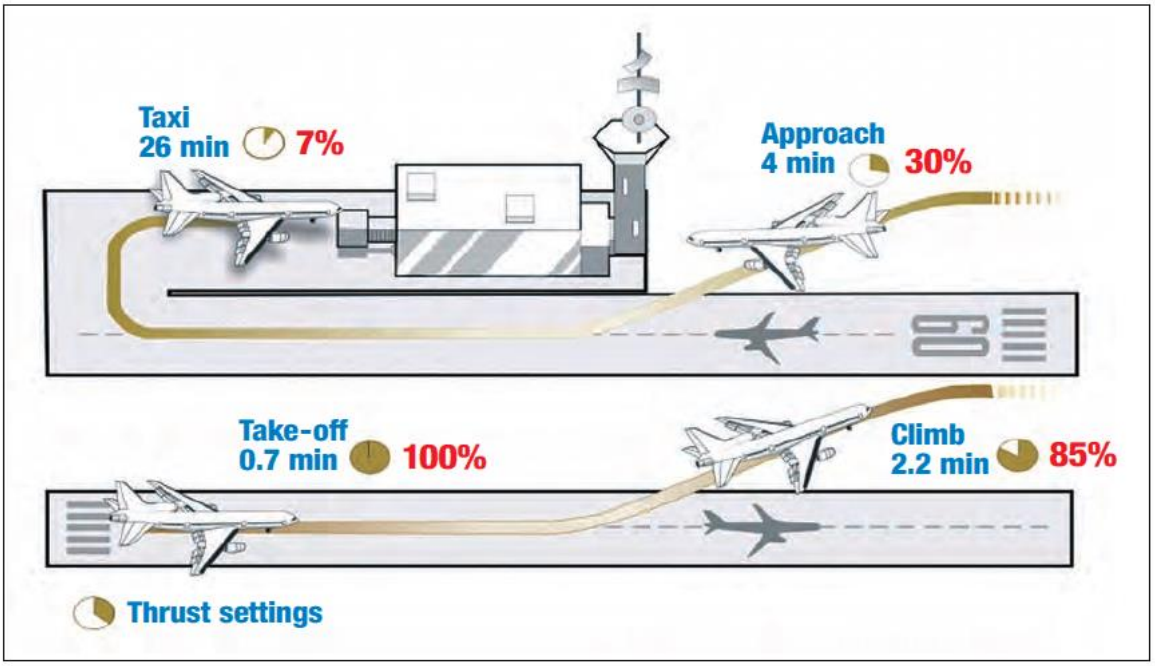

Figure 2-7: Illustration of ICAO Emissions Certification Procedure in the LTO Cycle [26]

2.4.3 ICAO NO_X Emission Standard

The Standard for NO_X was first adopted in 1981, and then made more stringent based on the recommendations of four CAEP meetings in 1993 (CAEP/2), 1999 (CAEP/4), 2005 (CAEP/6) and 2011 (CAEP/8) [25]. In addition, in 2011 a NO_X production cut-off requirement was adopted stating that individual engines produced on or after 1st January 2013 have to comply with the previous 2005 (CAEP/6) NO_X Standard. Together, these two measures will help to ensure that the most efficient NO_X reduction technologies are being employed in the production of aircraft engines [25].

Technological innovations in aviation continue to lead the way towards effective and efficient measures in support of ICAO's environmental goals of limiting or reducing the impact of aircraft emissions on LAQ. To complement the standard-setting process, CAEP developed, with the assistance of a panel of independent experts, medium and long-term NOx technology goals (10 and 20 years, respectively). Figure 2-8 depicts the graphical representation of the CAEP LTO NO_X cycle limits from 1981 up until in 2010 which was last time

CAEP conducted a NO_X technology review including the mid-term and long term goals to be achieved.

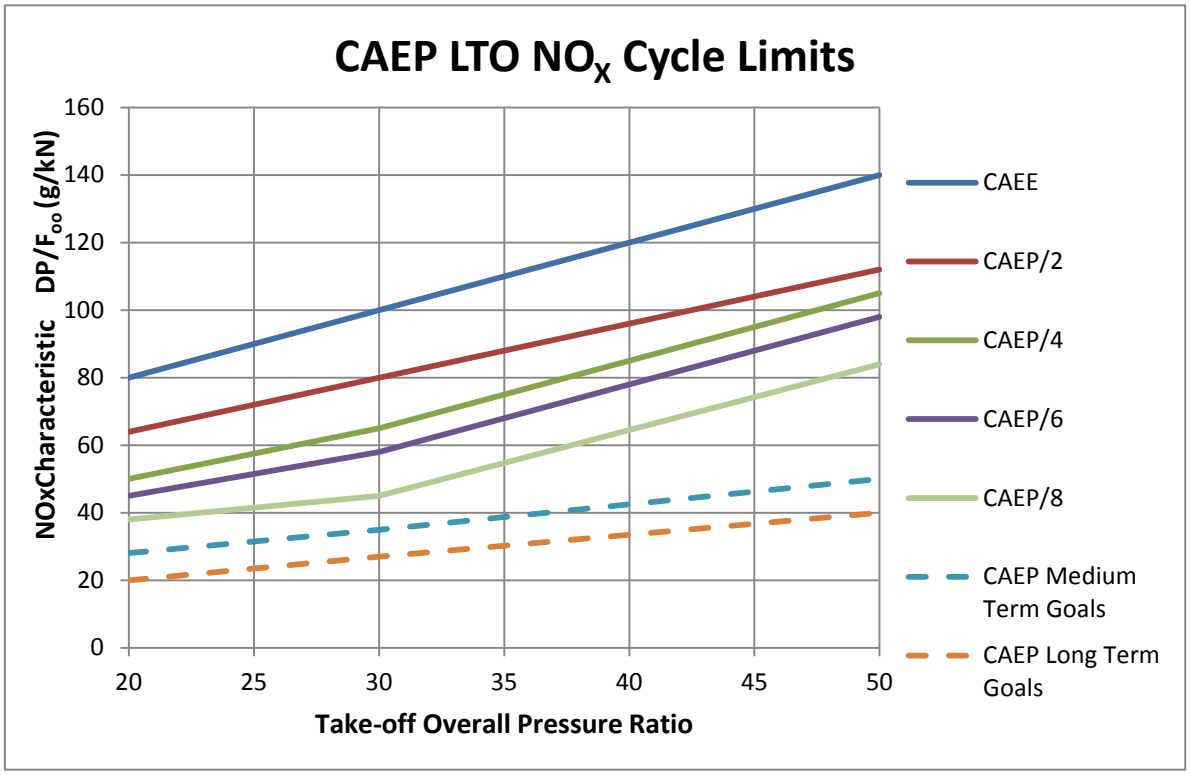

Figure 2-8: CAEP LTO Cycle Limits

Figure 2-8 shows emission standard set by CAEP for small to large size jet engines. The graph is between NO_X characteristics verses overall pressure ratio of an aircraft jet engine. DP/F_{00} represents the total NO_X emissions for the engine during the landing/take-off (LTO) cycle divided by the engine take-off thrust at sea level static, and is a parameter used for emissions regulation.

These ICAO certification limits apply only to newly certificated types and with industry standard production lives of 15+ years for most aircraft types coupled with the even longer in-service lives of 30+ years for passenger aircraft and about 45 years for freight types, total fleet NOx is slow to respond to a change in the stringency of the NO_X standard. The incorporation within these ICAO standards of a slope against OPR was in response to the characteristic for the mass of NOx emitted to increase along with increasing OPR and temperature.

These higher pressures and temperatures have been used in a drive to improve fuel and thermal efficiency of the engine. As most of the aero-engines at that time were designed with OPR of greater than thirty in order to curb down the fuel consumption and carbon dioxide emissions, it was decided at CAEP meeting to give a leeway to aircraft manufactures on that occasion by relaxing for the NO_X emissions. Hence in the Figure 2-8, there is a kink in CAEP/6 & CAEP/8 NO_X characteristics after the overall pressure ratio (OPR) of thirty. Nevertheless, CAEP/8 meeting proposed medium and long term goals with stringent NOx characteristics guidelines without giving any leeway to the engine manufactures even for overall pressure ratios greater than thirty to emit less NO_X emissions by 2030 [26] and hence no kink in the later future goals.

The ICAO legislation focuses mainly on the LTO cycle emissions whereas most NO_X are emitted in the cruise for higher bypass ratio engines, the ICAO may propose stringent legislations even for the cruise NO_X in the future.

Therefore, this has led to widespread research on reducing the NO_X emissions for the jet engine and the governmental funding bodies have started to pour money on research in order to reduce the emission footprint of aviation on environment.

In Europe, Clean Sky was born in 2008 with a funding of €1.8 billion with public private partnership between the European Commission and the industry partners from aviation industry and multiple universities across Europe with its mission to develop breakthrough technologies to significantly increase the environmental performances of airplanes and air transport; resulting in less noisy and more fuel efficient aircraft [28]. Cranfield University is also one of the partner universities in the clean sky project and is contributing through Techno-economic Environmental and Risk Analysis (TERA) framework; more detail can be found from references [29-33] .

The next section describes the NO_X emission formation during the combustion process of an aircraft engine.

2.5 Mechanism of NO_X formation

Nitrogen oxides (NO_X) are pollutant emissions which form during the hydrocarbon fuel combustion process in gas turbine engines. The primary nitrogen oxides generated from combustion systems are nitric oxide (NO), nitrogen dioxide (NO_2), and nitrous oxide (N_2O). The combination of NO and NO_2 is generally referred to as NO_X. Nitrogen oxides are a primary air pollutant linked to photochemical smog, acid rain, tropospheric ozone, ozone layer depletion, and global warming [34]. According to the journal "Atmospheric Environment", aviation cruise NO_X plays a vital role in perturbation of Ozone layer at stratosphere [18].

There are mainly five major ways of NO_X formation;

1) Thermal NO_X
2) Prompt NO_X
3) N_2O route to form NO_X
4) NNH route to form NO_X
5) Fuel Bound Nitrogen (FBN) route

2.5.1 Thermal NO_X

Thermal NO_X forms when the atmospheric nitrogen present in the air enters the combustion chamber and due to the high flame temperature, it oxidises with the oxygen present in the air. This is an endothermic chemical reaction which occurs when temperature exceeds 1850K. The set of reaction proposed by Zeldovich also known as Zeldovich mechanism [35] is detailed below:-

$$O_2 \rightleftharpoons 2O \qquad \text{2-9}$$

$$N_2 + O \rightleftharpoons NO + N \qquad \text{2-10}$$

$$N + O_2 \rightleftharpoons NO + O \qquad \text{2-11}$$

$$N + OH \rightleftharpoons NO + H \qquad \text{2-12}$$

Nitrogen Oxide (NO) is produced when nitrogen reacts with oxygen atoms via reaction 2-10 at high temperature (>1800K). This reaction initiates a chain of

chemical kinetics process in reaction 2-11 & 2-12, where molecular nitrogen formed at 2-10, reacts with atmospheric oxygen (O_2) and (OH) to form nitrogen oxide and O and H free radical. As, the concentration of atomic oxygen in the flame front is largely an exponential function of temperature, NO formation via the Zeldovich mechanism has a similar relationship with flame temperature. Therefore, as shown in Figure 2-3, as the flame temperature increases, the NO_X increases exponentially due to post flame thermal NO_X production.

The rate of production of NO_X via the Zeldovich mechanism can be estimated through the equilibrium concentration of oxygen in the post-flame zone below mentioned in equation 2-13 by Bowman [36]:-

$$\left(\frac{d[NO]}{dt}\right) = 6 * 10^{16} T_{eq}^{-0.5} \exp\left(-\frac{69{,}090}{T_{eq}}\right) [O_2]_{eq}^{0.5} [N_2]_{eq} \left[\frac{moles}{cm^3 sec}\right] \qquad 2\text{-}13$$

2.5.2 N_2O route

An alternative way of NO formation is by the N_2O route. The reaction mechanism via N_2O is described below:-

$$N_2 + O \rightleftharpoons N_2O \qquad 2\text{-}14$$

$$N_2O + O \rightleftharpoons NO + NO \qquad 2\text{-}15$$

$$N_2O + H \rightleftharpoons NO + NH \qquad 2\text{-}16$$

However, N_2O can react with alternative way given as under:-

$$N_2O + O \rightleftharpoons N_2 + O_2 \qquad 2\text{-}17$$

$$N_2O + H \rightleftharpoons N_2 + OH \qquad 2\text{-}18$$

But, N_2O route has less significance at most conditions, except under fuel-lean, low-temperature conditions. For gas turbines engines that operate under lean-premixed conditions at higher pressures, one of the major chemical pathways of NO formation is via the N_2O route.

The change of NO mass fraction in the gas turbine combustor due to the thermal NO and N_2O mechanisms can be derived from the reactions 2-10 to 2-18 [2; 37], assuming that:-

- Reaction is mixing controlled,
- O, O_2, OH, H and N_2 are in equilibrium
- N is in a steady state.

The NO mass fraction rate of change is given by equation 2-19 [2; 37]:-

$$\left(\frac{dY_{NO}}{dt}\right) = \left(\frac{2\bar{M}_{NO}}{\rho}\right)(1-\alpha^2)\left\{\frac{R_1}{1+\alpha K_1} + \frac{R_6}{1+K_2}\right\} \qquad 2\text{-}19$$

Where mass fraction of NO is denoted by Y_{NO}, molar weight of NO is $\bar{M}_{NO}$, ρ is the density, α is defined by $\alpha = [NO]/[NO]_{eq}$, R_1, R_6, K_1 and K_2 are constants defined as follows [37]:-

$$\mathrm{R}_1 = k_{1f}[N]_{eq}[NO]_{eq} \qquad 2\text{-}20$$

$$\mathrm{R}_6 = k_{6f}[O]_{eq}[N_2O]_{eq} \qquad 2\text{-}21$$

$$\mathrm{K}_1 = \frac{R_1}{R_2 + R_3} \qquad 2\text{-}22$$

$$\mathrm{K}_2 = \frac{R_6}{R_4 + R_5} \qquad 2\text{-}23$$

Where,

$$\mathrm{R}_2 = k_{2f}[N]_{eq}[O_2]_{eq} \qquad 2\text{-}24$$

$$\mathrm{R}_3 = k_{3f}[N]_{eq}[OH]_{eq} \qquad 2\text{-}25$$

$$\mathrm{R}_4 = k_{4f}[H]_{eq}[N_2O]_{eq} \qquad 2\text{-}26$$

$$\mathrm{R}_5 = k_{5f}[O]_{eq}[N_2O]_{eq} \qquad 2\text{-}27$$

Where k_{1f} to k_{6f} are the forward reaction constants and the $([\ ])_{eq}$ refers to the concentration reactants species.

2.5.3 Prompt NO_X

Thermal NO and N_2O reaction sets were driven by the interaction between nitrogen and an O atom, whereas, prompt-NO formation is an attribute of hydrocarbon flames in which hydrocarbon radical CH reacts with molecular N_2 [38].

Prompt-NO formation was first proposed by Fenmore [39] to explain the nitric oxide found in the thin reaction zone close to the burner surface in the experimental data obtained from CH_4, C_2H_4, and C_3H_8 flames. The thermal-NO route does not explain this observation because of the lack of atomic oxygen or nitrogen at this relatively cold location. The reaction mechanism of prompt-NO formation is shown in the respective equations below:-

$$N_2 + CH \rightleftharpoons NCN + H \qquad 2\text{-}28$$

$$NCN + OH \rightleftharpoons NO + HCN \qquad 2\text{-}29$$

$$NCN + O \rightleftharpoons NO + CN \qquad 2\text{-}30$$

Additionally, NCN further reacts with H to form N and HCN species that can lead to NO formation.

$$NCN + H \rightleftharpoons HCN + N \qquad 2\text{-}31$$

$$N_2 + C \rightleftharpoons CN + H \qquad 2\text{-}32$$

The N atoms formed in 2-31 and 2-32 can react with O_2 and OH to enhance the thermal-NO formation via reactions 2-11 and 2-12.

As concentration of CH radical is significantly small in the post flame zone, prompt-NO doesn't form in that region.

The prompt NO can be estimated by a formula based on De Soete [40], which is derived by Celis [2; 37]:-

$$\left(\frac{dY_{NO}}{dt}\right) = \left(\frac{\bar{M}_{NO}}{\rho}\right) f_{pr} k'_{pr} ([O_2]_e)^a [N_2]_e [C_2H_{23}] \exp\left(-\frac{36499.507}{T}\right) \qquad 2\text{-}33$$

Where,

$$f_{pr} = 4.75 + 0.0819x - 23.2\emptyset + 32\emptyset^2 - 12.2\emptyset^3$$

$$k'_{pr} = 6.4 \times 10^6 \left(0.0820575 \times \frac{T}{P}\right)^{a+1}$$

Where a is,

$$a = \begin{cases} 1.0 & X_{O_2} \leq 4.1 \times 10^{-3} \\ -3.95 - 0.9 ln X O_2 & 4.1 \times 10^{-3} < X_{O_2} \leq 1.11 \times 10^{-2} \\ -0.35 - 0.1 ln X O_2 & 1.11 \times 10^{-2} < X_{O_2} < 0.03 \\ 0.0 & X_{O_2} > 0.03 \end{cases}$$

2.5.4 NNH Route

It was proposed by Bozzelli and Dean [41] that NNH which is an intermediate species formed by the reaction between N_2 and an H atom, can react with an O atom to produce NO as shown in the reaction 2-34 & 2-35. This route is particularly viable at low flame temperatures. Furthermore, super-equilibrium O-atom concentration at the flame front can also increase the rate of NO formation via the NNH route as shown below.

$$N_2 + H \rightleftharpoons NNH \qquad \text{2-34}$$

$$NNH + O \rightleftharpoons NO + NH \qquad \text{2-35}$$

As per the experimental observation by Konnov [42], it has been demonstrated that NO formation via NNH is of major importance in hydrogen combustion in a stirred reactor, even for lean mixtures at 1400–1560 K.

2.5.5 Fuel Bound Nitrogen (FBN)

Fifth way for NO_X formation inside the jet engine combustor is when solid and liquid fuels which contains chemically bound nitrogen example; coal, biomass, heavy fuels combines with oxygen during combustion. Dagaut [43] has listed fuel-bound nitrogen contents in solid fuel. Generally, nitrogen contents in distillate fuels range from 0 to 0.65 wt. percent [36].

The increase in reaction rate of fuel bound NO_X depends on the amount of nitrogen contents present in the fuel; this change increases slowly as the flame temperature increases.

The reaction pathway involving the NO_X formation with FBN is complex, as it depends on the structural bonds of nitrogen with parent molecule. Below is the detailed chemical mechanism for NO formation with the reaction of HCN [38; 43] in FBN:-

$$HCN + O \rightleftharpoons NCO + H \quad \text{2-36}$$

$$HCN + OH \rightleftharpoons CN + H_2O \quad \text{2-37}$$

$$CN + OH \rightleftharpoons NCO + H \quad \text{2-38}$$

$$NCO + O \rightleftharpoons NO + CO \quad \text{2-39}$$

$$NCO + OH \rightleftharpoons NO + CO + H \quad \text{2-40}$$

As this research focuses on the aviation light fuel with almost no nitrogen present in the fuel, this process is not been taken into account while modelling NO_X prediction software.

The next section looks at the different methods that can be used to predict or calculate the NO_X emissions from a gas turbine engine.

2.6 Jet Engine NO_x Emission Predictions

2.6.1 Introduction

Preliminary combustor design and emissions prediction software tools are becoming increasingly important during the conceptual design phase of aero-engine combustors. They allow a large number of designs to be explored, in a relatively short amount of time, thereby identifying the most promising designs to consider for further development. According to Shakariyants [44] emission models can be divided primarily into three types:-

- Empirical and Semi-empirical correlation models
- Physics or reactor based models
- CFD models

2.6.2 Correlation Based Methods

Correlation based emission prediction models are widely used to predict NO_X and CO for combustors for which experimental data is available in the public domain. These models are mainly dependent on experimental data measured for particular combustor. They depend on parameters such as combustor geometry, design features, operating conditions; fuel type and fuel spray characteristics. Furthermore, novel combustor's geometry and requirement is different from a conventional combustor which limits the use of empirical correlation to conventional combustors only. Some of the empirical correlations have been briefly illustrated here.

2.6.2.1 **Lefebvre correlation**

$$NOx = 9 \times 10^{-8} * P^{1.25} V_c * \exp\left(\frac{(0.001 T_{st})}{\dot{m}_A T_{pz}}\right)\left(\frac{g}{kg}\right) fuel \qquad 2\text{-}41$$

All the values of the constant and variables used in Equation 2-41 were obtained from analysis of experimental data on NO_X emissions from several different aero-engine combustors [5; 45]. It is the stoichiometric flame temperature(T_{st}) that determines the formation of NO_X and not the average flame temperature in the combustion of heterogeneous fuel–air mixtures. However, for the residence

time in the combustion zone, which is also significant to NOx formation, the appropriate temperature term is the average value(T_{pz}), as indicated in the Equation 2-41.

$$CO = 86\dot{m}_A T_{pz} exp - (0.00345 T_{pz})/(V_c - V_e)(\frac{\Delta P}{P})^{0.5} P^{0.5} \frac{g}{kg} fuel \quad 2\text{-}42$$

The formation of CO in the PZ (primary zone) takes longer than the time required in producing NO_X. Where V_e is volume employed in fuel evaporation, T_{pz} is average temp throughout the PZ, V_c is combustor volume, which depends on initial mean drop size, that's why good atomization is important for low CO emissions.

2.6.2.2 **Rizk and Mongia Correlation**

$$NO_x = 15.10^{14}(t - 0.5t_e)^{0.5} exp - \left(\frac{71{,}00}{T_{st}}\right) P^{-0.05} \left(\frac{\Delta P}{P}\right)^{-0.5} \frac{g}{kg} fuel \quad 2\text{-}43$$

Here, t_e accounts for the influence of fuel evaporation on NO_X. According to equation 2-43, a reduction in mean drop size should increase NOx emissions by reducing the time required for fuel evaporation. However, if combustion takes place under conditions where the evaporation time is negligibly small in comparison with the total combustor residence time, for example, at high combustion pressures, NOx emissions can actually go down with a reduction in mean drop size [46].

1 EI (g/kg of fuel) is roughly = 12 ppmv (parts per million by volume)

$$CO = 0.18 \times 10^9 \exp\left(\frac{7800}{T_{pz}}\right) / \left(P^2 (t - 0.4t) \left(\frac{\Delta P}{P}\right)^{0.5}\right) g/kg \quad 2\text{-}44$$

This equation [46] shows lower dependence on combustion temperature. It has slightly higher dependence on pressure.

2.6.2.3 **Odgers and Kretschmer Correlation**

$$NO_x = 29 \exp -(21{,}670/T_c) P^{0.66} \times [1 - \exp -(250\tau)] \text{g/kg fuel} \quad \text{2-45}$$

Time of NO_X formation varies for different atomizers for aircraft combustors. For example, 0.8ms (air blast atomizers) and 1.0ms (pressure atomizers) and NO_X formation times for industrial combustors burning liquid fuels are in range of 1.5 to 2.0 ms [47].

2.6.2.4 **G. D Lewis correlation**

$$NO_x = 3.32 \times 10^{-6} \exp(0.008 T_c) P^{0.5} \text{ ppmv} \quad \text{2-46}$$

The amount of NO_X which forms in lean and homogeneous combustion depends on post combustor temperature and pressure according to this equation [5]. This correlation has independence of residence time (as relevant time is relaxation time instead). It has good prediction of experimental data as the residence times of roughly all the aero-engines are few milliseconds.

2.6.2.5 **The Boeing Fuel Flow 2 Model**

The Boeing Fuel Flow 2 (BFF2) model was developed specifically to calculate the aircraft emission NO_X, CO and UHC. The BFF2 method first establishes correlation between emission indexes of gaseous pollutants and fuel flow for the corresponding known emission information from ICAO emission databank for that engine [44]. BFF2 model is able to calculate emissions at different atmospheric conditions such as, temperature, pressure, humidity. This model also provides a fuel flow correction factor for the engine for the same. As, the ICAO databank emissions data is based on the information from engine manufacturer who tests the engines un-mounted, this correction is required. This method led the user to calculate emissions at any altitudes for an aircraft engine.

2.6.2.5.1 Steps to calculate emission using BFF2 method

This method uses the following equations [48]:

$$EIHC = REIHC\left(\frac{\theta_{amb}^{3.3}}{\delta_{amb}^{1.02}}\right) \quad 2\text{-}47$$

$$EICO = REICO\left(\frac{\theta_{amb}^{3.3}}{\delta_{amb}^{1.02}}\right) \quad 2\text{-}48$$

$$EINO_X = REINO_X\, e^{H}\left(\frac{\delta_{amb}^{1.02}}{\theta_{amb}^{3.3}}\right)^{\frac{1}{2}} \quad 2\text{-}49$$

Where $H = -19(\omega - 0.0063)$ 2-50

$Where, H\ is\ humidity\ factor\ and\ \omega\ is\ specific\ humidity\ given\ by$:

$$\omega = \frac{0.62198\ \varphi\ P_v}{P_{amb} - 0.37802\varphi P_v} \quad 2\text{-}51$$

Where φ is relative humidity

P_v is saturation vapour pressure

P_{amb} is inlet ambient pressure

$$P_v = (0.014504)10^{\beta} \quad 2\text{-}52$$

Where β is given by:

$$\beta = 7.90298\left(1 - \frac{373.16}{T_{amb}}\right) + 3.00571 + 5.02808\log\left(\frac{373.16}{T_{amb}}\right) + (1.3816 \times 10^{-7})\left[1 - 10^{11.344}\left(1 - \frac{373.16}{T_{amb}}\right)\right] + (8.1328 \times 10^{-3})\left[10^{3.49149}\left(1 - \frac{373.16}{T_{amb}}\right) - 1\right]$$

Where EI, REI is Emission index and reference emission index in g/kg, H is the factor accounting for the moisture content in air. δ and, Θ are ratios between free stream and ISA sea level static pressures and temperatures, given below:

$$\delta_{amb} = \frac{P_{amb}}{101325} \text{ and } \theta_{amb} = \frac{T_{amb}}{288.15} \quad \text{2-53}$$

Step 1:

The correction factor for the fuel flow on four ICAO points are shown in Table 2-2 from [48]

Table 2-2: Fuel Flow correction factor

ICAO Point	Take-Off	Climb-Out	Approach	Idle
Correction Factor	1.010	1.013	1.020	1.100

Step 2:

After step 1, once the corrections are done, the emission indices (EI) are plotted against the corrected fuel flows on log scale as shown in Figure 2-9.

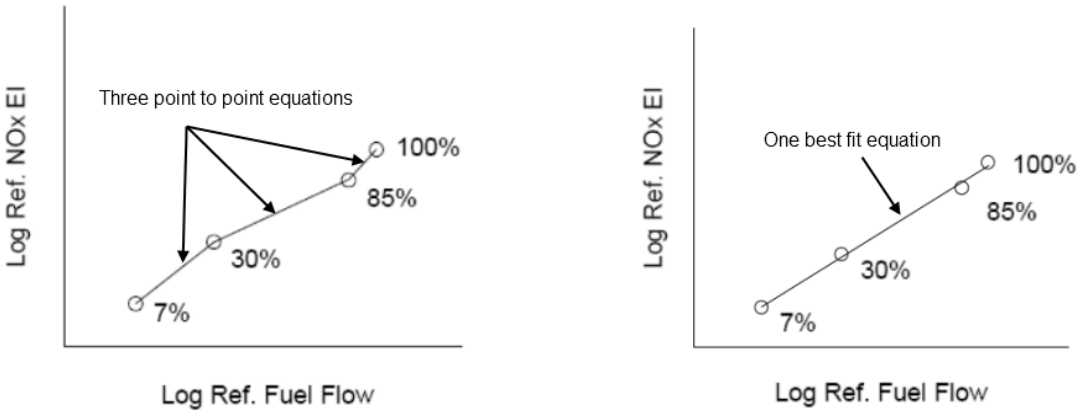

Figure 2-9: Log Ref. EINOx vs Log Ref Fuel Flow- point to point fitting method

The data points are curve fitted to show trends of EI for different fuel flows. There are two approaches possible, either defining a single best fit equation for the whole set of points or defining an equation between each ICAO reference

point (called point to point fitting) leading to the creation of 3 equations. The latter option is said to lead to more accurate results. Each method is illustrated in Figure 2-9.

Step 3: Fuel Flow Factor

The fuel flow factor, W_{ff} is given by:

$$W_{ff} = \frac{W_f}{\delta_{amb}} \theta_{amb}^{3.8} e^{0.2M^2} \quad \text{2-54}$$

Where M = Mach number.

Step 4: Compute EI

The new emission indices are calculated by the equations 2-47, 2-48, 2-49, and 2-50:

Where *REIHC, REICO, REINO$_X$,* = intersection of corresponding curves and W_{ff}.

2.6.2.6 **P_3T_3 Method**

The P3T3 method [49; 50] classifies as a semi-empirical method as it is based on engine condition parameters such as pressure and temperature at combustor inlet instead of just the fuel flow like BFF2. As a consequence, this method is considered more advanced compared to BFF2. The similarity between P3T3 and BFF2 method is the use of the ICAO emissions databank as the reference emissions index to start with.

The principle of the method is to plot the $EINO_X$ at ground level (GL) against the combustor inlet temperature (T_3GL) for the four ICAO emission points. Two other plots are also initially constructed for the ground level reference, that is, the combustor inlet pressure (P_3GL) against combustor inlet temperature and the overall fuel-air ratio (FARGL) against the combustor inlet temperature. Temperature and pressure at the combustor inlet and the fuel-air ratio at ground level are not information given by the ICAO emissions databank and thus need to be computed by engine simulation software. The level of accuracy of this simulation software will therefore have a significant impact on the accuracy of

the P_3T_3 method. For each plot, similarly to the BFF2 method, a second order polynomial fit is obtained. One main difference compared to BFF2 method is that the plots are not in a log-log scale.

Once the three plots and the three equations are set, it is possible to compute the NO_X at altitude using Equation 2-55.

$$\mathrm{EIN}O_{X_{ALT}} = EINO_{X_{GL}}\left(\frac{P_{ALT}}{P_{GL}}\right)^{n}\left(\frac{FAR_{ALT}}{FAR_{GL}}\right)^{m}\exp(H) \qquad 2\text{-}55$$

In order to use equation 2-55, it is necessary to know the engine condition at altitude (using the engine model). The parameters are pressure ($P3_{ALT}$) and temperature ($T3_{ALT}$) at combustor inlet and overall fuel-air ratio (FAR_{ALT}) at altitude.

$EINO_{X_{GL}}$, P_{GL}, and FAR_{GL} are interpolated using their respective polynomial equations given $T3_{ALT}$. P_{ALT} and FAR_{ALT} are directly taken from the engine model.

Finally, similar to the BFF2 method, the humidity correction factor (H) is added to take into account of NO_X at altitude for the calculation of the emission indices. The disadvantage of this method is that it needs proprietary information of an engine like P3, T3, FAR at reference conditions, and the engine-specific exponents. It is observed from [50] that pressure exponent *n* of 0.4 and FAR exponent *m* of zero are the best ones to use if the engine-specific exponents are not known in the equation 2-55.

2.6.3 Stirred Reactor Based Model

The process of combustion inside a gas turbine engine constitutes of chemical kinematics reaction, turbulent mixing and evaporation. These processes happen simultaneously, in a real time, in a three dimensional aspects with a transfer of air/fuel, mass and energy. The most simplified approach to account for such a complex process is by using partial differential equations to solve for mass, energy and momentum conservation.

The stirred reactor method assumes finite rate chemistry inside the combustor using simplified chemical kinetic models. The basic concept of the reactor-based method is to split the combustor into a number of reactors to compute the overall emissions. The stirred reactor method breaks down the combustor into a number of smaller regions and calculates, within each reactor, the production or elimination of pollutants of interest [2]. According to [51; 52], stirred reactor or physics based model is of two types:-

Single reactor models: Such models treat the engine combustor as a single thermochemical reactor characterized by averaged performance parameters based on the inlet properties and overall equivalence ratio. Emission production is then related to those parameters. Alternatively, only the primary zone can be considered instead of the whole combustion chamber. Depending on the available information, it would be characterized by mean adiabatic flame temperature, equivalence ratio, residence time, etc. The downside of using single reactor model is; it can average out the various parameters, therefore, not capturing the micro level chemical kinematics inside the combustors.

Multi reactor models: This model simulates engine combustor as a network of thermochemical reactors standing for combustor zones, either combination of or part(s) thereof. Herein, the geometry and performance variables are either calculated with simplified flow solutions and correlations or assumed on the basis of engineering judgement and generic knowledge. Emission formation is simulated in the model reactors with either empirical or simplified kinetic algorithms. Multi-reactor model is preferred over the single reactor model because it can capture the chemical kinematics within the combustor fairly well.

The physics based approach constitutes a compromise between empirical correlations and CFD calculations. It has some desired features of both of them, whereas at the same time it avoids main disadvantages of empirical correlations; which doesn't include all the complex processes that take place inside the combustor and it is based on the specific combustor test rig experiment results.

Furthermore, in order to predict emission for the novel combustors, experimental data and the combustor geometry in most cases are in the preliminary stages of research. So, it is not readily available in public domain. Due to the absence of experimental data, it is not possible to calculate emission using empirical correlation methods.

As it is described in [37], the stirred reactor theory is based on the turbulent chemical mixing of compounds within the designated combustor area rather than on the minute details of spatially-varying velocities and turbulence fields within a combustor [53]. So, two modes of continuous flow mixing is defined as: (1) 'stream mixing', which occurs between fuel and air streams, and is required to achieve local flammable mixture proportions; (2) 'Backmixing' is achieved for partially or wholly burned gases to mix with fresh reactants to self-sustain ignition. Backmixing is represented by stirred reactors.

There are three generic reactor models which were utilised in this study, they are; reactor model consists of perfectly-stirred reactors (PSR), reactor model consists of partially-stirred reactors (PaSR), and lastly a reactor model consists of series of perfectly-stirred reactors (PSRs). They are described in the next section.

2.6.3.1 **Perfectly-Stirred Reactor (PSR)**

The perfectly stirred reactor (PSR) is a backmixing process which is assumed to be infinitely fast and homogeneous. But, PSR approach on its own is not suitable for gas turbine combustors [53], as it does not represent the macroscopic in-homogeneities in the chemical kinetics of the combustor. In PSR approach, two streams enter the combustor; one is the air or combustion gas products with specific temperature, pressure, mass flow and the second is fuel stream. Series of Perfectly-Stirred Reactors (PSRS) Model

2.6.3.2 **Series of Perfectly-Stirred Reactors (PSRS) Model**

Hammond and Mellor [54; 55] during the early 1970s proposed and developed this type reactor. The idea is to place number of perfectly stirred reactors in series to discretise the air and fuel mixture in that region. The number of series

of reactors is user-defined and depends on the level discretisation required in the volume of any particular combustor region. Generally, the number of reactors is increased until the emission output is independent of the number of perfectly stirred reactors.

2.6.3.3 **Partially-Stirred Reactor (PaSR) Model**

The PSR approach is not a very appropriate model to be used wholly because it does not represent macro-level in-homogeneities inside the combustor. Therefore, a partially-stirred reactor (PaSR) model was developed by Fletcher and Heywood [56] that can statistically describe the variations in gas composition, temperature and residence time, which influences the rate of pollutant formation, especially NO_X in the primary zone. However, only gross flow at the reactor exit is predicted.

2.6.4 CFD Modelling

The third method which is used to study the fundamental combustion process and heat transfer inside the jet engine combustors is CFD modelling. Currently, engine manufacturers use CFD simulation to design and predict the emission characteristics of novel jet engine combustors before testing it experimentally in a rig. This is a powerful method with abilities to predict emission fairly well for a well-defined combustor.

Firstly, the flow properties of the modelling combustor are obtained and then it can be modelled in 2D or 3D. Generally, it is preferred by engine manufactures to use 3D combustor model for the combustor. It requires detailed 3D combustor geometry to calculate the chemical kinetics mechanism for combustion. Therefore, it divides the combustor into grids with millions of nodes, so that, it can capture the chemical kinetics well [57].

As, some information such as pressure and temperature is critical for emission estimation in the flow, CFD solver includes energy terms when resolving the Navier-Stokes equations. It applies the chemical kinetic relationships of emission at each node of the model. For example, in order to predict NO_X

emission, the NO_X formation equation using Zeldovich and prompt NO_X mechanisms can be used described in section 2.5.

CFD simulation also requires extensive validation. In case of modelling existing combustors technology, the results can be validated with the empirical/semi-empirical correlation method and ICAO data which is available in public domain [58]. Whereas, it is difficult to get the geometry information of a novel combustor design for CFD simulation because data in public domain is not made readily available by engine manufactures.

Zhang [59] carried out a CFD study of NOx emission for a model aircraft engine combustor. The NOx formation was modelled by the concept of post-processing, which resolves the NOx transport equation with the assumption of stationary temperature distribution inside the combustor. The test rig studied in this paper was called low emission stirred swirl (LESS) combustor, a two-stage model combustor, fuelled with liquid kerosene and designed by Beihang University (BUAA). The main stage of LESS combustor employs the principle of lean pre-mixed and pre-vaporized (LPP) concept to reduce pollutant, and the pilot stage depends on a diffusion flame for flame stabilization. Numerical prediction of NOx emission showed a good agreement with test data at both idle condition and full power condition of LESS combustor. The computational time for CFD calculation was 10 hours for 1.0 million grid and 16 hours for a 2.5 million grid for that LESS combustor.

Further details about the NOx formation in a combustor using CFD based modelling has been carried out in some papers mentioned in [57; 59-66].

Cranfield University has a trajectory optimisation tool which estimates best possible fuel efficient and low emission trajectory for an aircraft. The stirred reactor NO_X emission prediction model is aimed to be integrated with the trajectory optimisation framework to compute an optimised trajectory for lowest NO_X emissions for an aircraft.

As, the stirred reactor modelling approach provides a reasonably good compromise with respect to computational time and robustness relative to

correlation and CFD based methods. Therefore, after careful consideration, stirred reactor approach is selected for the development of the NO_X emission prediction model for the novel combustor.

The next section briefly describes the background of the gas turbine combustor and discusses the combustor sizing concept.

2.7 Gas Turbine Combustor Background

The combustor is the component in the gas turbine engine where fuel is added to the high pressure air entering from the compressor to subsequently burn. Figure 2-10, shows combustion chambers in its simplest form.

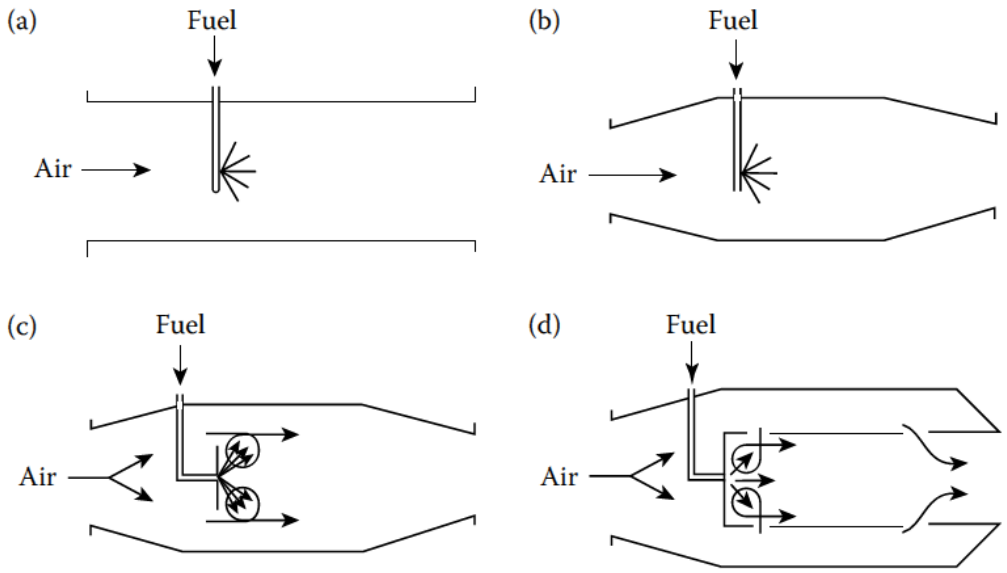

Figure 2-10: Derivation of the conventional combustor configuration [5]

Figure 2-10(a) shows the simplest form of combustor; a straight duct connecting the compressor with turbine. But, this very simple arrangement is not suitable to use as the pressure losses would be excessive.

In order to reduce this pressure loss to an acceptable level, a diffuser can be used to lower the air velocity, as shown in Figure 2-10(b). After, the diffuser is installed, a flow reversal is necessary to be created to provide low-velocity region to anchor the flame and this is shown by installing a baffle in Figure 2-10(c). But, still this arrangement is not suitable as, in order to produce the

desired temperature rise, the overall chamber air/fuel ratio is required to be in a range of flammability limits.

The combustion is sustained by a re-circulatory flow of burned products that can provide a continuous source of ignition for the incoming fuel/air mixture. The air which is not required for combustion is admitted downstream of the combustor zone to mix with the hot burned products, to reduce the temperature to a value which is acceptable to the turbine as shown in Figure 2-10(d).

Therefore, Figure 2-10, illustrates the logical development of the conventional gas turbine combustion chamber in its most widely used form. There are many variations on the basic pattern, but, generally, all chambers incorporate an air casing, diffuser, liner, cooling holes and fuel injector as key components of a combustor as shown in Figure 2-11.

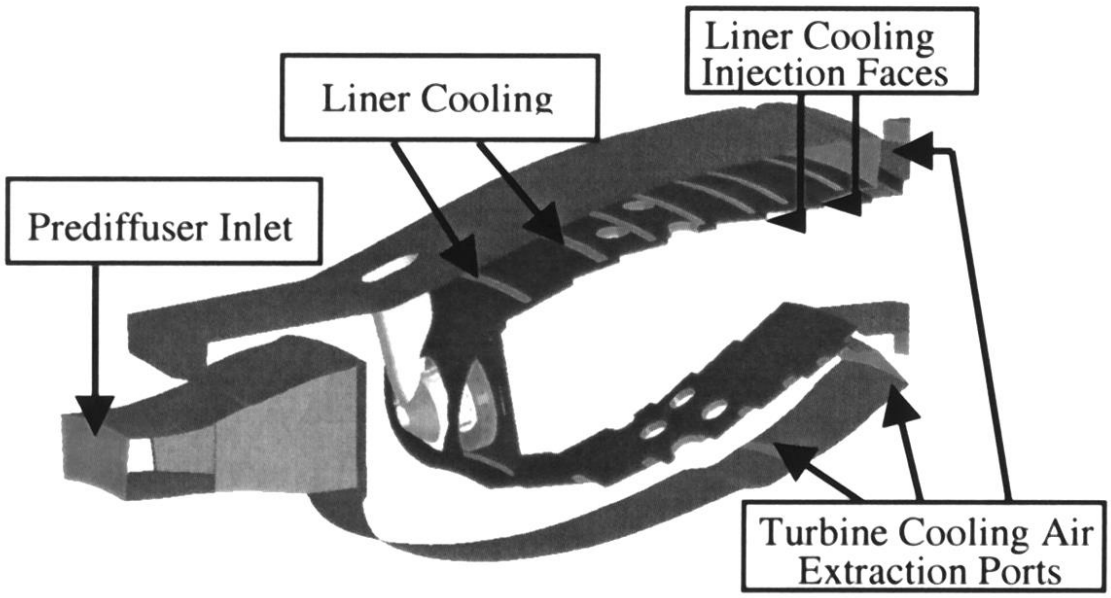

Figure 2-11: A Conventional Combustor layout [5]

2.7.1 Combustor Performance Requirements

A combustor must satisfy a wide range of performance requirements whose relative importance may vary depending on the engine type and specific application. The basic requirements are stated below:

- *Pollutant Emissions*: The pollutant emissions of a combustor should be minimal. Pollutants are particulates, NOx, CO, UHC, Soot, Smoke or SO_X, generated in the combustion process. Emissions of these products are legally limited for civil aero-engines by the ICAO regulations as explained in section 2.4.

- *Pressure Drop*: The pressure loss inside the combustor can be segregated in terms as cold loss and hot loss or fundamental loss. The cold loss consists of pre-combustor diffuser losses and liner loses. It is almost 3% pressure loss across the nozzle guide vane leading edge for film cooling. Overall pressure loss in the combustor is in the range of 4-5%. There is always a pressure loss associated with heat release and whenever there is addition of heat there is a reduction in density which results in an increase in velocity (mass flow continuity) and this requires a pressure loss for the momentum change [81]. Therefore, in order to allow maximum performance of the gas turbine, the pressure drop within the combustor is required to be minimal. However, for proper mixing of the burning gases within the combustor and to drive the cooling flow of the nozzle guide vanes (NGV), some pressure drop is required. So, a compromise has to be made between an acceptable pressure drop level and combustion performance.

- *Wall cooling flow*: The wall cooling flow is taken from the liner flow and dipping it, is beneficial as it provides extra dilution air which can be burnt downstream of combustor to either operate leaner thereby reducing NO_X and CO or to generate better exit temperature profile for turbine.

- *Ignition*: Reliable and smooth ignition is required, both on the ground (especially at very low ambient temperatures) and, in the case of aircraft engines flameout, at high altitude.

- *Efficiency*: Very high combustion efficiency close to 100% is required to convert all the chemical energy into heat. This is an important factor to minimize the specific fuel consumption of the aircraft engine.

- *Stability Limits*: The combustor should be able to operate within wide ranges of pressure, air/fuel ratios (AFR), velocities; covering the whole operating range of the gas turbine including windmilling and relight.

- *Temperature Distribution*: The combustor is required to provide outlet temperature distribution that is tailored to maximize the lives of the turbine blades and nozzle guide vanes.

- *Cost*: It is required that the combustors are designed for maximum performance with minimum cost associated with it along with ease of manufacturing.

- *Durability*: The life of a combustor has to be compatible with that of the aircraft engine and the intervals between compulsory repairs required should be maximal. It should not be having any life limiting component which requires a complete overhaul. Size and shape has to be compatible with the engine envelope and to have multi-fuel capability based on petroleum, synthetic, and biomass.

Size and weight are more important considerations especially for aircraft engines, whereas for industrial engines more emphasis is placed on long operating life and multi-fuel capability. Low fuel consumption and low pollutant emissions are paramount for all types of engines.

The next section gives an insight into the basic constraints posed to a combustor during design phase.

2.7.2 Gas Turbine Constraints on Combustor

The gas turbine imposes constraints on the combustor due to its size, shape, technology and operating conditions.

The constraints are in terms of:

- *Mass Flow*: The operating conditions of a gas turbine engine require a wide range of mass-flow rates. The combustor has to be designed in order for it to work efficiently throughout the whole mass-flow range.

- *Length:* The shaft connecting compressor and turbine design limits of torsion and vibrations, poses a restriction in having longer combustor. This length constraint has an important effect on the shape of the combustor.

- *Turbine Entry Temperature (TET) T4*: The design of the turbine (material used, blade cooling technique) limits the combustor exit temperature and is fixed by the cycle requirement. As, the gases exiting the combustor are directly fed to the turbine therefore the temperature of those gases must meet the required turbine entry temperature.

- *Exit Temperature Traverse:* In order to aid turbine to reach its expected life, it needs to be given a defined temperature profile. The temperature profile is generated within the combustor by the non-perfect mixing of the cold cooling flow with the hot core. The combustor temperature traverse needs to be close to the optimal temperature profile limited by the turbine cooling capability and stress profile to achieve maximum turbine life.

- *Combustor Inlet Pressure P_3*: The gas turbine engine experiences a wide range of operating pressure. Therefore, the combustor has to be designed to work efficiently within this whole range of pressures. Especially, for re-lighting condition at very high altitude where the pressure is at its lowest and ignition is difficult.

- *Combustor Inlet Temperature T_3*: The engine pressure ratio of the compressor and inlet air temperature defines the combustor inlet temperature. It varies with the operating pressure. So, the inlet

temperature is high at the highest pressure ratio. It has an effect on the fuel burn as well. The increase in combustor inlet temperature has a significant effect on the cooling performance and pollutant emissions because; the inlet compressor delivery air which is used as cooling flow is hotter.

The next section explains the functionalities of a typical conventional combustor.

2.7.3 Conventional Combustor

The choice of a combustor type and layout is determined by the overall engine design and the need to utilize the available space as effective as possible. There are three types of combustor as illustrated in Figure 2-12

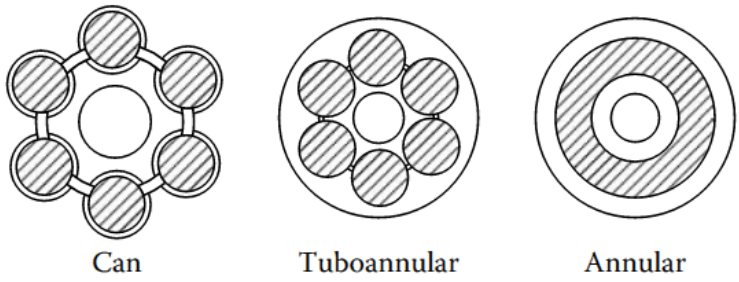

Figure 2-12: Depiction of combustor types [5]

A tubular (or “can”) combustor shown in Figure 2-12 comprised of a cylindrical liner mounted concentrically inside a cylindrical casing. Almost all the early jet engines, such as the Whittle W2B, Jumo 004, and the RR Nene, Dart, and Derwent, featured tubular combustors, usually in numbers varying from 6 to 16 per engine [5]. Weight issue and length is the main disadvantage of tubular combustor which prohibited it to be used in aircraft engines

A tubo-annular or can-annular combustor is a group of tubular liners, usually from 6 to 10, when arranged inside a single annular casing, as illustrated in Figure 2-12. This concept combines the compactness of the annular chamber with the mechanical strength of the tubular chamber.

When an annular liner is mounted concentrically inside an annular casing it is known as annular combustor illustrated in Figure 2-12. In many ways it is an ideal form of chamber, because of its clean aerodynamic layout which results in a compact unit of lower pressure loss than other combustor types. Its main drawback is from the heavy buckling load on the outer liner [5].

Most of the gas turbines manufactured in Europe use tubular or single-can combustors as these combustors have a simple design and a long life and can be up to 3m in diameter and 12m high.[67]. These combustors are easy to maintain and their temperature distribution is better than single-can combustors and hence lower emissions. They can be a straight-through or reverse-flow design. Most industrial gas turbines use the reverse-flow types. Due to the larger surface areas they require more cooling air compared to the annular combustor. Thus, annular combustors are popular in high-temperature applications e.g. Aircraft engines. However, the maintenance of annular combustors is relatively more difficult, and their temperature and flow profiles are less favourable than tubo- annular combustors. Due to high temperature applications in annular combustor and less flexibility in fuel, these combustor tends to produce more NOx compered to tubular or tubo-annular combustors.

Figure 2-13 shows the main components of a typical conventional combustor. The Combustion zone is divided into three zones; primary, intermediate and dilution zones respectively as shown in Figure 2-12.

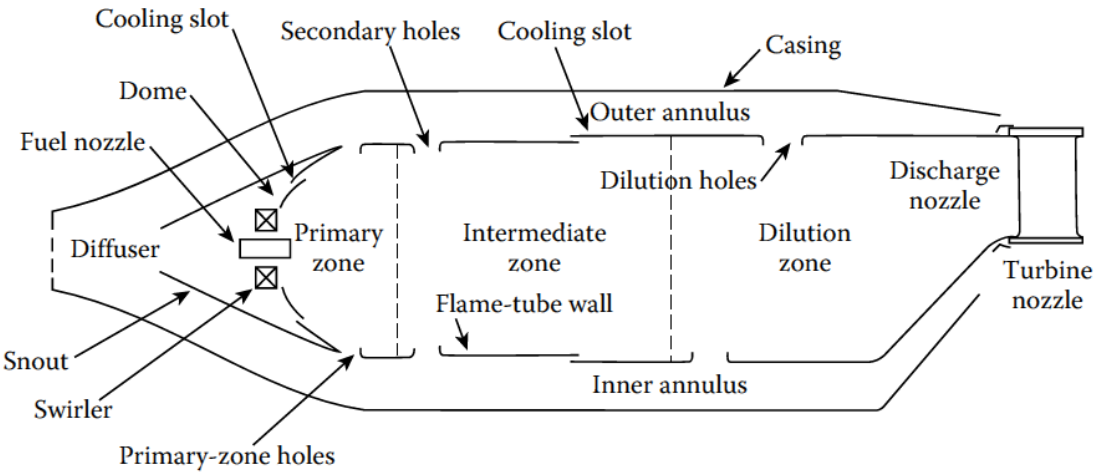

Figure 2-13: Main components of a conventional combustor [5]

The main role of primary zone of the combustor is to anchor the flame and provide sufficient temperature, time, and turbulence to achieve complete combustion of the air/fuel mixture. The creation of a toroidal flow reversal in primary zone entrains and recirculates a portion of the hot combustion gases to provide continuous ignition to the incoming air and fuel.

The temperature in the primary zone reaches more than 2000K which leads to dissociation reaction of CO_2 to CO and formation of hydrogen H_2 gases. If these gases pass directly to the dilution zone and rapidly cooled by the addition of cooling air, the gas composition would froze leading to exhausts of unburnt CO which signifies combustion inefficiency. Hence, intermediate zone is required to drop the temperature to an intermediate level by addition of some air encouraging in the oxidation of CO, soot and UHC; thus enhancing the combustor efficiency.

The role of the dilution zone is to allow the remaining air after the combustion and wall-cooling requirements to provide an outlet stream with a temperature distribution that is acceptable to the turbine design. This temperature distribution is usually described in terms of “pattern factor” or “temperature traverse quality” [5]. Generally, 20-40% of total combustor air-flow enters the dilution zone.

2.7.4 Combustion Efficiency

Combustion efficiency is defined as the ratio of heat released in combustion to total heat supplied in the system given by equation 2-56 [5].

$$\eta_c = \frac{heat\ released\ in\ combustion}{heat\ supplied} \qquad 2\text{-}56$$

Combustion efficiency depends on airflow rate, evaporation rate, mixing rate and reaction rate of the combustion given by equation 2-57 [5].

$$\eta_c = f(airflow\ rate)^{-1}\left(\frac{1}{evaporation\ rate} + \frac{1}{mixing\ rate} + \frac{1}{reaction\ rate}\right)^{-1} \qquad 2\text{-}57$$

The maximum rate of heat release under any given operating conditions are governed by evaporation, mixing, or chemical reaction rate in a combustion systems but rarely by all three at the same time.

This study concentrates on the aero engine combustor where high combustion efficiency (~100 %) is governed by the reaction rate controlled system. Therefore, it is assumed to have infinitesimally fast evaporation and mixing of fuel in the combustor. So, the equation 2-57 can be rewritten as equation 2-58 given by:

$$\eta_c = f(airflow\ rate)^{-1}\left(\frac{1}{reaction\ rate}\right)^{-1} \qquad 2\text{-}58$$

According to Lefebvre's [68], reaction rate controlled combustion efficiency can be defined by equation 2-59. This led to equation 2-60, which is known as θ parameter and used to define the combustor designing. As, θ parameter depends on the combustor inlet size, pressure, temperature and mass flow, it helps in designing novel combustors. Thus, reduces the initial rig test experimental cost for testing novel combustor design ideas [5].

$$\eta_c = f(\theta) = f\left[\frac{P_3^{1.75} A_{ref} D_{ref}^{0.75} exp\left(\frac{T_3}{300}\right)}{\dot{m}_A}\right] \quad 2\text{-}59$$

Where,

$$\theta = \left[\frac{P_3^{1.75} A_{ref} D_{ref}^{0.75} exp\left(\frac{T_3}{300}\right)}{\dot{m}_A}\right] \quad 2\text{-}60$$

Where,

P_3 = Combustor inlet pressure

T_3 = Combustor inlet temperature

A_{ref} = Reference Area of the combustor

D_{ref} = Reference diameter or height of the combustor inlet

$\dot{m}_A$ = Air mass flow rate

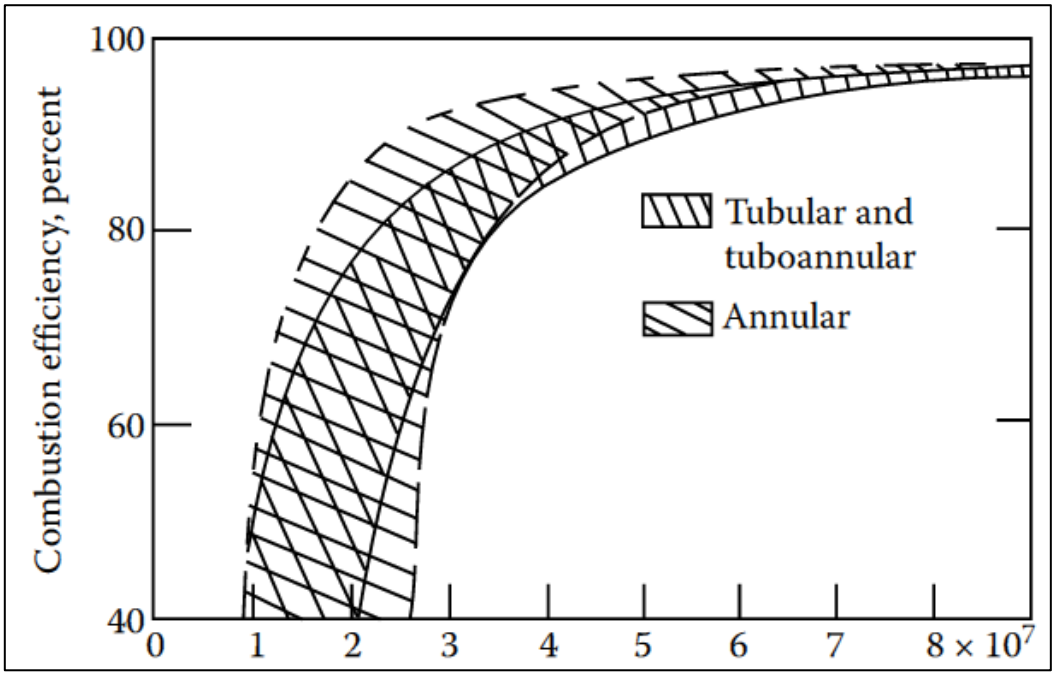

Figure 2-14: Design chart for a conventional combustor [5]

The θ parameter can be used to design the geometry of a combustor. But, any new chamber design must be based to a large extent on previous experiences. Figure 2-14 by Lefebvre [5] summarises the past combustion efficiency data from all known systems and correlated against all the relevant variables.

The most demanding operating conditions for all types of engines are at the minimum inlet pressure P3 which usually corresponds to the engine windmilling for aircraft engines after a flameout at high altitude.

According to Lefebvre [5] *"At flameout in flight, the engine rotational speed falls rapidly to its windmilling value. The relight sequence is first to use the ignition system to relight the combustor. When this has been accomplished, the next step is to accelerate the engine up to its normal rotational speed. This normally calls for a minimum combustion efficiency of around 80%".*

In order to attain the values of A_{ref} and D_{ref} from Figure 2-14, a value of θ is selected where the combustion efficiency is 80% at a point along a horizontal line within the shaded area, and then substituting into it the values of P3, T3, and $\dot{m}_A$ corresponding to the engine windmilling at maximum guaranteed relight altitude. The selected actual point within the marked area represents a balance between the contradictory need of high efficiency combustor, small combustor size, and low development cost.

The Figure 2-15 by Lefebvre [68] shows the influence of primary zone mixture strength on shape of the theta curve. Three curves displaying the influence of rich, stoichiometric and lean burn primary zones on the theta parameter and efficiency are shown in Figure 2-15.

Both burning velocity and combustion are at maximum with stoichiometric mixture that's why the curve begins to flatten out at about combustion efficiency of 80% but, has a steep decline in the left hand curve of the theta due to lower combustion efficiency. In case of weak primary zone, the left hand portion of the curve starts at a higher value of theta than the stoichiometric mixture and due to its lower burning velocity has a shallower slope.

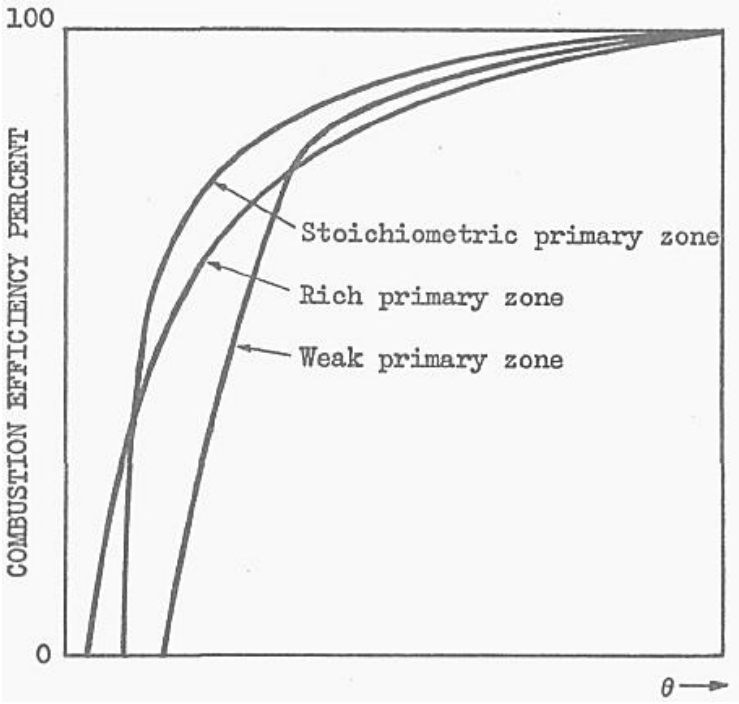

Figure 2-15: Influence of primary zone mixture on the theta parameter [68]

The weaker primary zone path rises to a higher level of efficiency due to the lower dissociation loss and at almost 85 % efficiency, terminates fairly in a “knee” bend. For rich mixtures, the theta curve starts closer to the origin and has a lower initial slope due to relatively low burning velocity. In case of rich mixture primary zone, most of the heat release takes place in the secondary zone which reduces the distinction between the roles of both and it shows clearly in the theta curve which flattens out gradually with increase in theta.

As per the observation of Lefebvre [68] *“The ability of the right hand portion of the theta curve to attain hundred percent combustion efficiency depends partly on the length of the flame tube but to a greater extent on the amount of air employed in the film-cooling the walls”*. Unburned or partially burned fuel can be entrained in this air and be conveyed along the flame tube from one layer to another before being discharged from the combustor. As, the temperature of the cooling-air is low, the chemical reaction rates are lower. Thus any unburned fuel which is entrained in the mixture will not combust and be wasted. Generally, the lower the amount of air employed in the film-cooling, mainly in the primary zone,

better is the prospect of achieving hundred percent combustion efficiency at the chamber outlet.

Now, the next section describes the previous work on the emission prediction model “Hephaestus” at Cranfield University.

2.8 Development of “Hephaestus” for Conventional Combustor model

The *“Hephaestus”* is the mythological name for the “*Greek God of Fire”* and it is given to the in-house gas turbine combustor emission prediction software at Cranfield University which has a capability to predict CO, NO_X and UHC emissions. This model has been coded using the programing language *Fortran 90*. This model was first developed by Celis [37] for the emission prediction for a conventional combustor and further modified by Pervier [2], specifically for NO_X prediction.

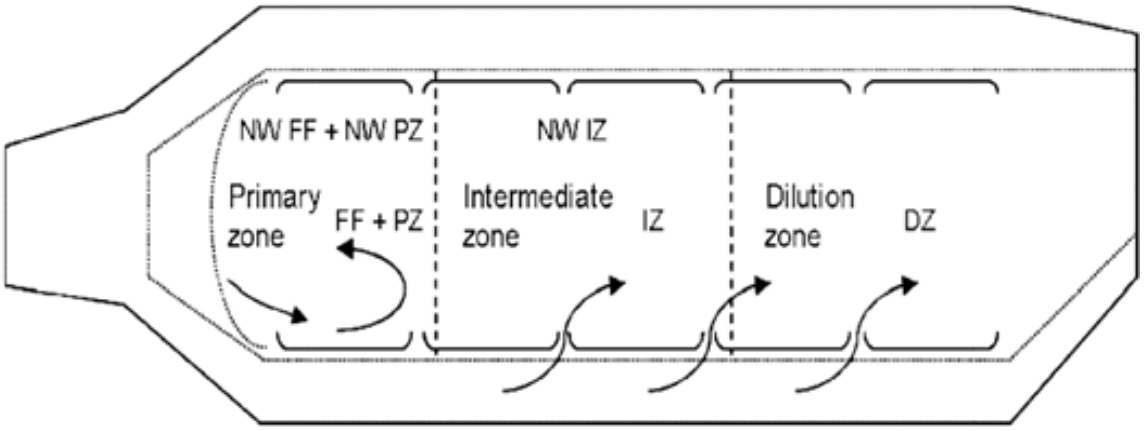

Figure 2-16: Conventional Combustor interior representations [37]

The schematic of the conventional combustor interior representation is shown in Figure 2-16. It is divided into four zones; Flame-Front (FF), Primary-Zone (PZ), Intermediate-Zone (IZ) and Dilution-Zone (DZ) respectively. The air flow in the combustor is divided in two parts. One flow is towards the core and the other is towards the Near-Wall (NW) region. The model is based on the stirred reactor method.

Three generic reactors are developed for this approach; perfectly-stirred reactor (PSR), a series of perfectly-stirred reactor (PSRS) and partially-stirred reactor model and they are explained in section 2.6.3. The arrangement of the reactors inside the conventional combustor developed by Celis [37] is shown in Figure 2-17. As it is illustrated from Figure 2-17, configuration of the reactors are placed as perfectly stirred reactor (PSR), partially stirred reactor (PaSR) and a series of perfectly stirred reactor (PSRs). PSR are assumed to be homogenous instantaneous mixture of air and fuel where as PaSR is non-uniform mix of air and fuel. PSRs are the series of many small PSR in the combustor chamber.

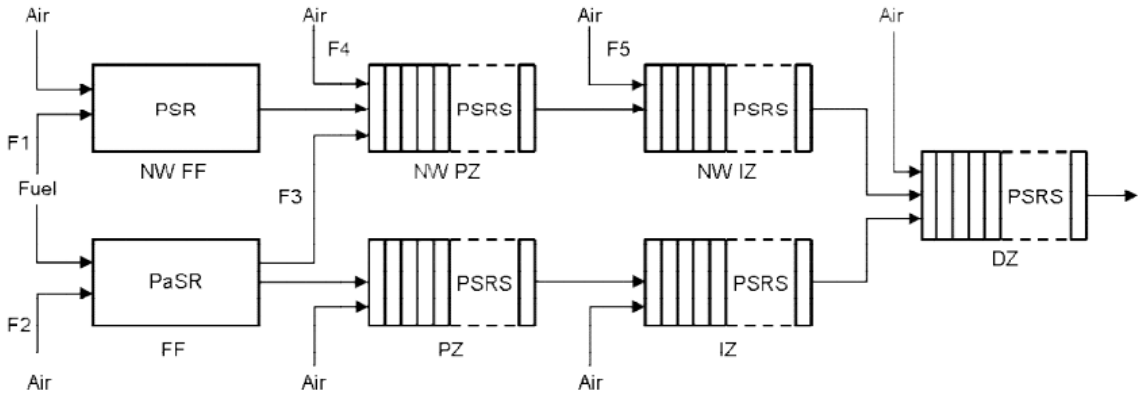

Figure 2-17: Multi-reactor model for conventional model by Celis [37]

From Figure 2-17, “F” is the fluid flow in the different reactors given by F1, F2, F3, F4 and F5. Here F1 is the fraction of fuel reaching the Near-Wall mixing zone at Flame Front (NW FF) modelled with PSR and the rest in the FF core, F2 is the proportion of the swirler and dome air that goes into the PaSR reactor at Flame Front (FF), F3 is the fraction of the burning gases admitted into the second Near-Wall PSRS reactor at Primary Zone (NW PZ), F4 is the fraction of air initially assigned for primary zone entering the NW PZ PSRS reactor and F5 is the fraction of air initially assigned to the intermediate zone that goes into the Near-Wall PSRS reactor of intermediate zone (NW IZ). Furthermore, rest of the air or gas left after entering the NW of the reactor enters the core of the reactor for that particular zone.

The model developed by Celis [37], underestimated the NOx production at all power setting for the CF6-80E1A3 type engine shown in Figure 2-19. The reason behind that was not considering the recirculation or residence time distribution in the model. This model was later on modified by Pervier [2] with a different reactor arrangement as shown in Figure 2-18. The number of reactor is reduced to focus on the NOx predictions only. As, the most important zones with high temperatures where significant amount of NOx is produced are the flame front and the primary zone, emphasis is given to these zones to predict NOx emissions.

Moreover, reducing the number of reactor significantly reduced the computational time in the modified model.

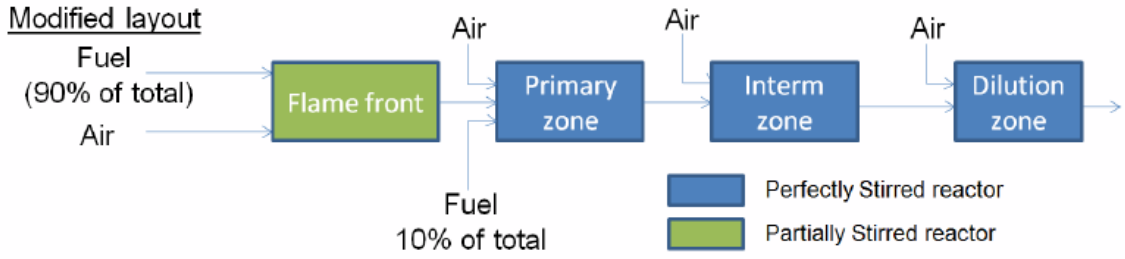

Figure 2-18: Arrangements of Reactors in conventional combustor [2]

Another modification in the model is the amount of fuel that is entering in the different reactors. In the Celis model, it was assumed that 100% of the total fuel flow is entering in each combustor zone separately. It means, all the fuel which is entering the flame front zone split between core and near wall region is again entering into the primary zone and then again subsequently in intermediate and dilution zone.

This way of distributing fuel was inaccurate for the combustion in Celis model as it assumes the air and fuel reaction to take place multiple times in different reactor even downstream of the combustor again in a similar fashion; whereas, the actual fuel and air combustion takes place in the flame front zone mainly, and to the lesser extent in combustor downstream zones.

In the modified model it is assumed that 90% of fuel enters and combusts in the flame front zone and the rest 10% burns in the primary zone. The other

modifications brought to the model comprises of reduction in the number of reactors by using a perfectly stirred reactor (PSR) models instead of series of perfectly stirred reactors (PSRS) to reduce calculation time. Modifications were made in the flame front partially stirred reactor to improve the computational speed by calculating the clipped Gaussian elements entirely using FORTRAN code instead of calling a Matlab program externally in the original model. Furthermore, the CEA program was integrated internally in the model to calculate the equilibrium conditions rather calling it externally as in the original model.

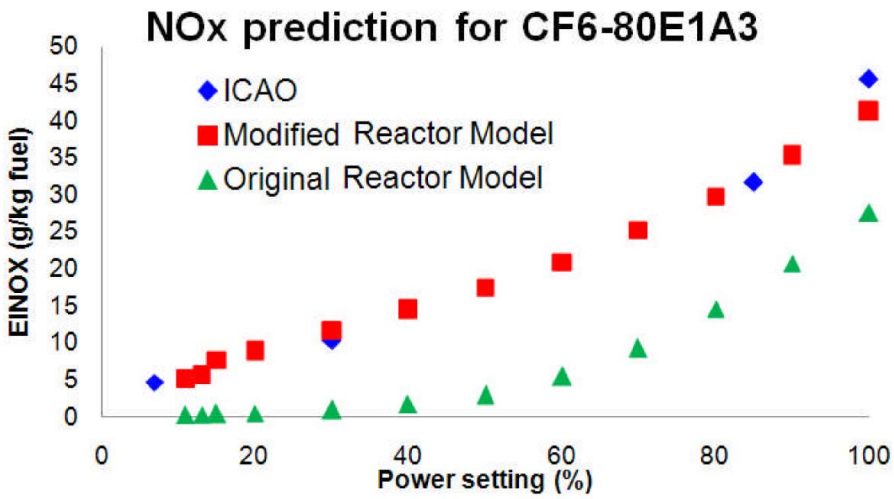

Figure 2-19: Comparison of both models [2]

Figure 2-19 shows the comparison of the results for NOx emission for both models for CF6-80E1A3 type engine. The ICAO emission points are taken at sea level with engine power setting of 100%, 85%, 30% and 7% of engine max thrust at sea level.

Currently, the Hephaestus is able to predict emissions for the conventional combustors which can be verified with the ICAO emission databank. The next section is going to describe some of the novel gas turbine low NO_X emission combustor concepts and is assessed according to availability of data and suitability to be modelled using stirred reactor method.

2.9 Dry Low NO_X Emission (DLN) Combustors

This section describes some of the DLN combustors which can reduce NO_X emission substantially without water injection and hence the name Dry Low NO_X combustors. The requirements for DLN combustors are; high system operability to achieve stable combustion at all operating conditions, good system response to rapid load changes, acceptable levels of combustion noise and, if required (stationary gas turbine), capability for switching smoothly from gas to liquid fuel, and vice versa.

Some of the DLN concepts are briefly discussed below.

2.9.1 Variable Geometry Design

The variable geometry combustors are designed such that the air flow into the combustion chamber can be varied. At high power settings, large quantities of air is allowed to the primary zone to reduce its temperature and hence, reduction in formation of NO_X. Whereas, at lower power settings or with reduction in engine power, the large part of air is partially diverted towards dilution zone to maintain the temperature in the primary zone thus reducing CO and UHC emissions. As, research conducted by several authors, including study done by NASA [69-72], variable geometry reduces not only NO_X drastically but, it improves altitude relight performances because of this air distribution capability from primary zone to dilution zone. Figure 2-20 is a pictorial representation of a variable geometry combustor.

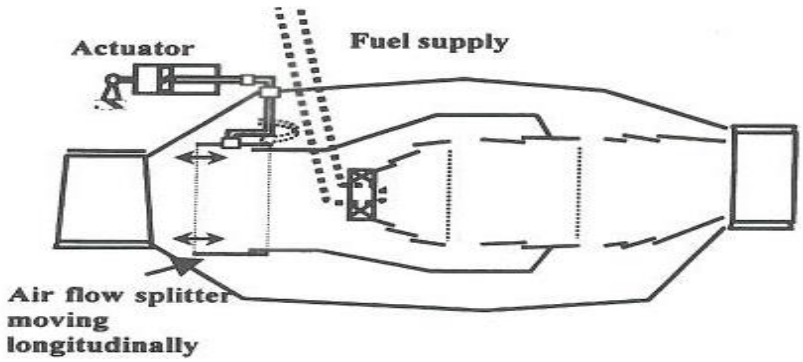

Figure 2-20: Variable Combustor Geometry [5]

The main drawback of this design is its complex control mechanism and the complex feeding of air into the zones which tend to increase cost, weight and reduce reliability. Furthermore, if the pressure drop across liner is allowed to vary too much, then achieving desired temperature pattern in the combustor efflux gases could be a problem. The variable geometry combustors have the potential of reducing almost all major pollutant without reducing performance because of the temperature flexibility within the different flame zones. Also, the temperature can be adjusted in such a way that it will never fall below a minimum of 1670 K at which chemical reaction rates are relatively high. This property enables the combustion zones to be made smaller thus, reducing the combustor size leading to cost and weight benefit. Ideally, the variable geometry combustors should be used in conjunction with premix-prevaporize fuel-injection systems. This avoids the local high-temperature, high NOx-forming regions, created by the presence of fuel droplets in the combustion zone [5].

2.9.2 Staged Combustors

As with variable geometry combustor, the combustor flame temperature is controlled within limits by varying air flow from one zone to another with changes in engine power settings. Whereas, in staged combustors the airflow distribution remains constant, the fuel flow is switched from one zone to another in order to maintain the combustor temperature [5]. One of the methods of fuel staging is “selective fuel injection”; in this method, fuel is supplied to combinations of fuel injectors at different power requirement conditions. The idea of this type of technique is to raise the equivalence ratio and hence the temperature at localized zones at low-power operation. This approach reduces the CO and UHC emissions and extends the lean blowout limit to lower equivalence ratios. There are two ways for staged combustion; in “series or parallel”. The former combustion is also termed as “Axially Staged” and the latter approach is called “Radial Staged”. The next section described both ways starting with the Radial staging first.

2.9.2.1 **Radial Staging**

Figure 2-21 shows the radially staged Dual Annular Combustor (DAC) where the combustor domes of the inner and outer stages are arranged radially or parallel to each other. The fuel injector tips for both the pilot and main stages are amounted on a common feed arm.

GE DAC is used in GE CFM 56-5B for A320 and A321 aircraft as shown in Figure 2-21. The pilot stage is optimized for starting at low power settings and is designed to operate lightly loaded and provide the entire temperature rise needed at startup, altitude relight, and engine idle conditions. At idle, the equivalence ratio of the combustion zone is selected to minimize the emissions of CO and UHC. The other annular combustor is specifically designed to optimize the combustion process at high-power settings. It features a small, highly loaded combustion zone of short residence time and low equivalence ratio to minimize the formation of NO_X and smoke.

The main advantage of radial staging is that it allows all the combustion performance goals to be achieved, including low emissions, within roughly the same overall length as a conventional combustor. This short-length feature is attractive from the standpoints of low engine weight and reduced rotor dynamics problems [5]. Due to design of combustor, GE has achieved 35% reduction in CO and UHC and 45% reduction in NOx emissions for the DAC shown in Figure 2-21.

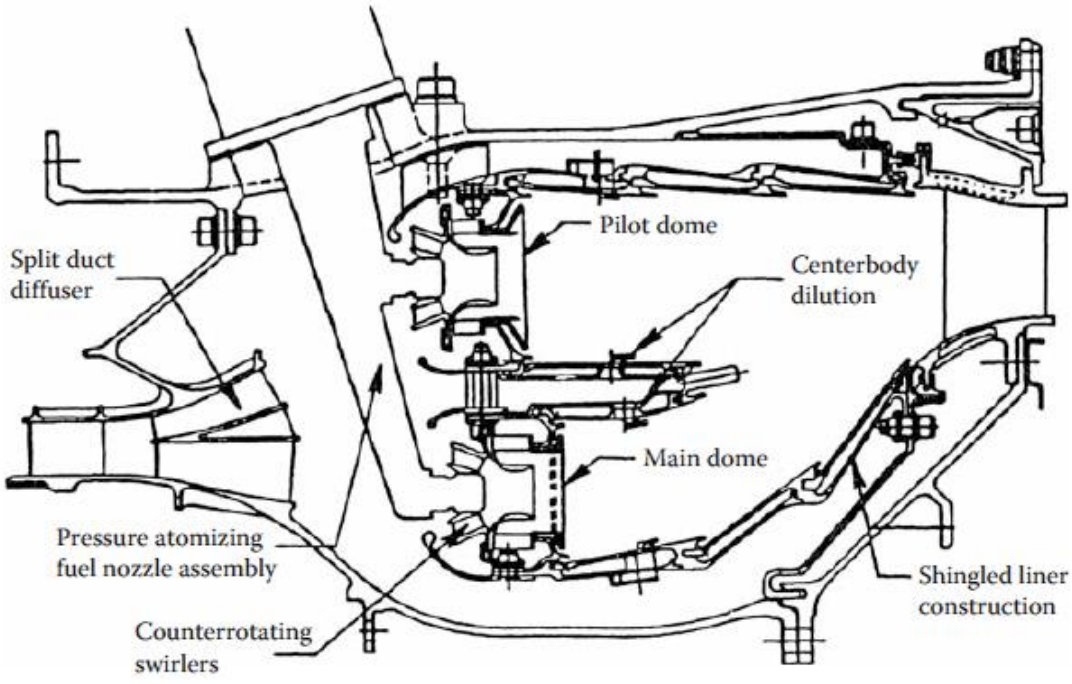

Figure 2-21: GE Dual Annual Combustor [5]

This combustor has many drawbacks as well. One basic drawback is that as, pilot and main dome are placed parallel to each other, all the zones are in the common region of air supply from compressor outlet temperature, so all the regions will have same relatively poor lean blow out limit [5]. Furthermore, due to fuel staging in parallel, the peaks of the temperature profile could shift in radial position, with potential adverse effects on the hot sections downstream of the combustor.

Moreover, in order to aid turbine to reach its expected life, it needs to be given a defined temperature profile. The temperature profile is generated within the combustor by the non-perfect mixing of the cold cooling flow with the hot core. The combustor temperature traverse has to be very close to the optimal temperature profile limited by the turbine cooling capability and stress profile to achieve maximum turbine life. In case of radially staged combustion, temperature profile could be generated in such a way that it has an adverse effect on the turbine blade downstream. Radial staging combustors can reduce pollutants substantially but on the cost of complex designs and increased number of fuel injectors

2.9.2.2 **Axial Staging**

In axial staging, the secondary stage is situated downstream and it operates at lower equivalence ratios to reduce NOx. The primary stage provides heat to initiate rapid combustion at maximum power setting. It has wider stability limits and high combustion efficiency. But the design increases the length of the combustor and requires a separate feeding arm for fuel.

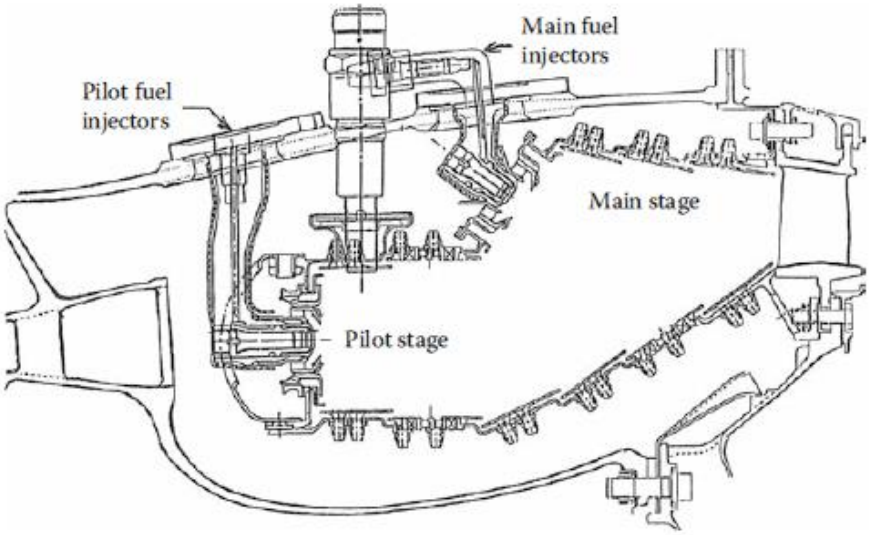

Figure 2-22: Axial staged combustor for P & W V2500-AS engine [5]

The main combustion zone is supplied with hot air from primary zone at high-power settings, providing rapid ignition, high combustion efficiency and wider stability limits than DAC. Axial fuel staging ensures more uniform radial and circumferential temperature distribution which contributes to longer nozzle guide vanes life. Nevertheless, this concept is associated with additional length that increases overall engine weight. Pratt and Whitney have successfully applied the axial staged combustor in P&W V2500-AS engine Figure 2-22 overcoming the length penalty problem by shifting the pilot zone inboard. The idea of staged combustors has led to a substantial development of liner wall cooling techniques as it requires a great amount of air to cool the large liner surface [5].

2.9.3 Catalytic combustors

The catalysts used in this combustor design oxidizes the fuel at very low temperatures and the fuel which is injected upstream of the reactor, vaporizes and mixes with the inlet air easily. This mixture brings down the maximum temperature by 1000K and reduces NOx drastically. Firstly, fuel air mixture passes over catalytic bed or reactor which consists of series of different kind of catalysts. Figure 2-23 illustrates the schematic diagram of a catalytic combustor.

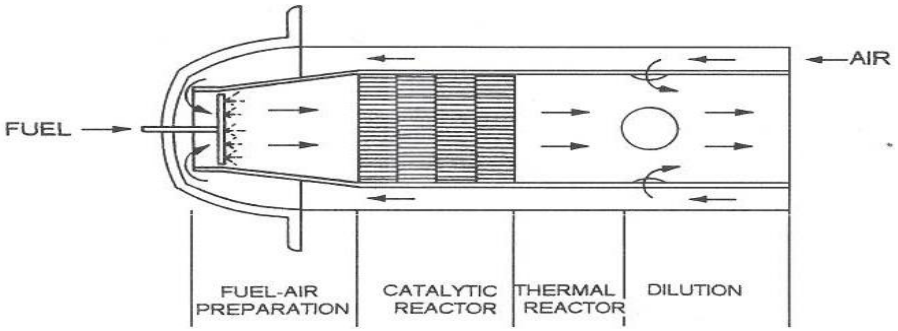

Figure 2-23: Schematic representation of catalytic combustor [5]

Ideally the first set of catalysts is highly active at low temperature to oxidize the mixture well and subsequently later on, the mixture passes through other types of catalysts which are being chosen according to the oxidizing efficiency needed. In the end a thermal reactor or catalytic bed increases the temperature to the required turbine entry temperature, thus reducing CO & UHC as well. The drawback of catalytic combustor is mainly due to the catalytic chemical properties. It may auto ignite sometime if the temperature is not coherent, so it requires highly stable catalysts at high temperatures. Also, according to Lefebvre [5] there is minimum temperature requirement to excite the catalyst; otherwise the reaction would not start. Generally, 700K is required minimum for catalyst light-off. The other problem is maintenance and durability of the material.

2.9.4 Lean Premix Pre-vaporize combustors (LPP)

As, NO_X increases exponentially as flame temperature increases, in LPP combustor the fuel is first premixed with air and pre-vaporized to make a

homogeneous mixture before entering the combustion chamber. The catch is to operate in an equivalence ratio which is close to lean blow out limit. Figure 2-24 shows a pictorial representation of GE LPP combustor.

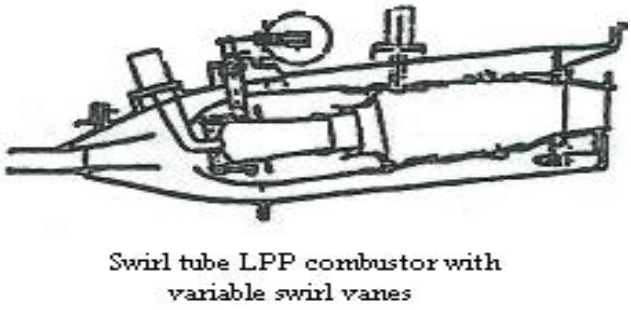

Figure 2-24: GE LPP combustor [5]

A typical LPP combustor can be divided into three main sections. The first section is for fuel injection, fuel vaporization, and fuel–air mixing. Its function is to achieve complete evaporation and mixing of fuel and air before combustion. It eliminates droplet combustion or formation of small pockets of fuel and supplies the combustion zone with homogeneous mixture of low equivalence ratio, which process combustion at a uniform low temperature, thereby decreasing the amount of NOx formation. The second section stabilizes the flame by creating one or more recirculation zones. Combustion is completed in this region and the resulting products flow into section three, which comprises a conventional dilution zone. This process eliminates local fuel rich zones and thus attenuates NO_X production.

One of the advantages of LPP combustion is that it is essentially free from soot or carbon formation. Especially when gaseous fuels are used, “lean premixed” or “LPM” is more appropriate because evaporation is not required. The absence of carbon not only eliminates soot emissions, but also greatly reduces the amount of heat transferred to the liner walls by radiation, thereby reducing the amount of air needed for liner wall cooling [5]. This is an important property of LPP as it means that more air is available for lowering the temperature of the combustion zone and improving the combustor temperature pattern factor.

The other advantage for this system arrangement is that the flame temperature doesn't exceed 1900 K, and the equivalence ratio is close to lean blowout limit which removes the NO_X formation dependency on residence time [20]. Thus, LPP systems can be designed with long residence times to achieve low CO and UHC, while maintaining low NO_X levels. This finding is especially significant for industrial engines, where size is less important than aero engines. As noted above, this approach leads to an LPM combustor volume that is approximately twice that of a conventional combustor [73].

The main drawback associated to LPP combustor is that; as it requires more time for fuel vaporization and fuel-air premixing upstream of the combustion zone, this may lead to have auto-ignition at high inlet temperature and pressure at high power settings. One way to avoid auto-ignition or flashback is by designing the LPP combustor, such that the sum of the fuel evaporation and mixing times exceed the auto-ignition delay time.

Pervier has modeled the LPP combustor in Hephaestus and predicted the NO_X emission [2]. The LPP combustor drastically reduces the NO_X emission, more details can be found in [2].

2.9.5 Lean Direct Injection Combustor (LDI)

LDI concept can be an alternative to LPP combustors. As, in the LDI system the fuel is injected directly into the flame zone which is different than LPP system where fuel is first mixed with the air and vaporized before entering into combustion zone. Thus by taking this different approach, LDI as shown in Figure 2-25 doesn't have the potential for auto-ignition or flashback like in LPP [74]. It is however important to achieve fine atomization and mixing of fuel-air, quickly and uniformly, so that the flame temperature is lower and NO_X formation is attenuated. Tacina [74] has proposed that the NO_X emission from an LDI combustor can reach the level as close as LPP combustor.

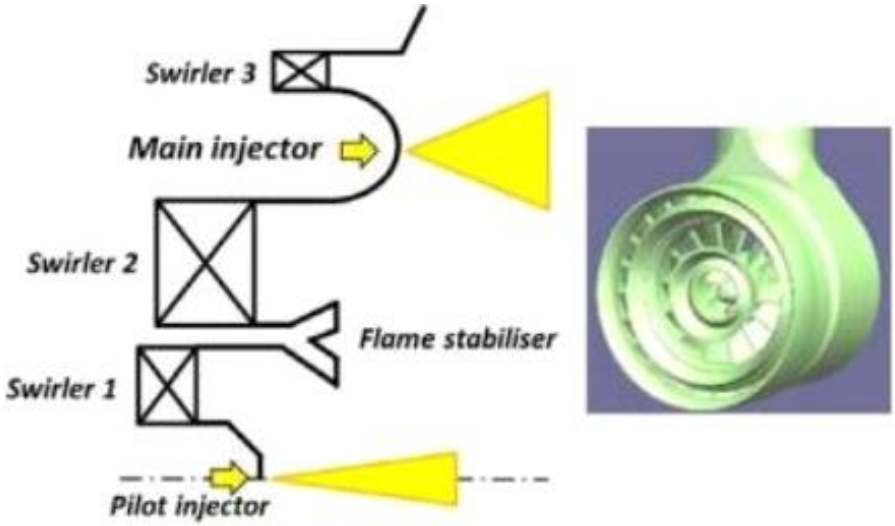

Figure 2-25: Lean Direct Injection Design [75]

The fuel is directly injected into the combustion zone making the design less complex and reducing the risk of flashback. Two concentric, internally staged high pressure fuel injectors operating at equivalence ratios close to lean blowout limit controls the mixing of air and fuel. Three axial swirlers introduce a high turbulence air to the flow and enhance the mixing process in order to decay the liquid fuel streams. To anchor the flame and ensure stable operation at wide range of power settings a flame stabilizer is located between the two first swirlers.

Another advantage of LDI concept is that it uses a simple plain orifice, fuel injector i.e an orifice at the end of the fuel tube. The use of simple fuel injectors has the potential of reducing maintenance problems such as clogging and coking, especially for the higher operating pressure ratios gas turbine engines that operate at higher compressor outlet pressure and temperature [76].

2.9.6 Partially Evaporated & Rapid Mixing Combustor (PERM)

Partially Evaporated and Rapid Mixing injector, developed by Avio Aero, is dedicated for regional turbofan engines of OPRs up to 50. The operating principle of PERM injection system is to partially evaporate the fuel within the inner duct and the rapidly mix in the combustor. Figure 2-26 illustrates a schematic of PERM concept. The fuel stream is supplied as a film over the lip

that separates two swirled airflows. Once, the fuel layer reaches the edge of the lip, primary atomization occurs in a double swirler airblast atomizer. Rapid mixing of fine droplets is greatly enhanced by the airflow from two co-rotating primary and secondary swirlers located in the centre of primary swirler. Pilot fuel injector, generates a pilot flame to support combustion stability at low-power settings. The flame generated by PERM injection system can be classified as a partially premixed flame. The combustor liners are fitted with novel effusion cooling system. Two bleeding sections are positioned downstream of the combustor liner to discharge part of the air for a better performance control [75].

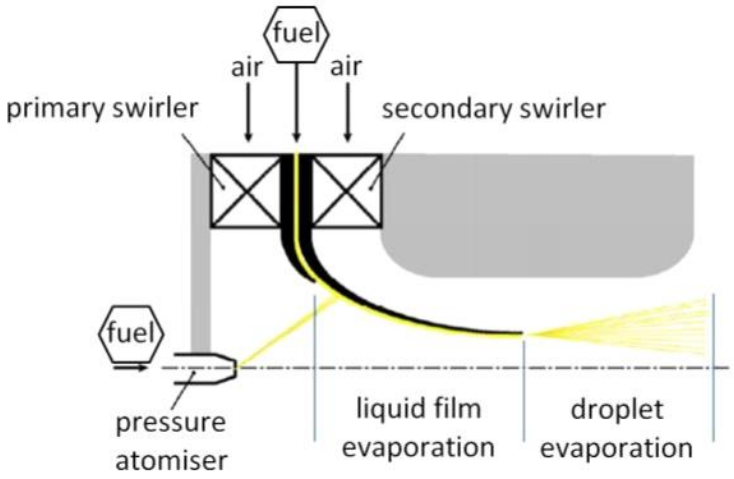

Figure 2-26: PERM Combustor [75]

2.9.7 Twin Annular Premixed Swirl (TAPS) Combustor

At present, the development of low-emission combustors is based on lean-burn technology. General Electric took a lesson from fuel staging in DAC described in section 2.9.2.1, and on this basis the Twin Annular Premixed Swirl (TAPS) combustor is evolved. It is a single annular combustor with fuel staging within the swirler. The TAPS combustor comprises two independent, swirl stabilized, annular flames for low- and high-power settings [77]. This concept is illustrated in Figure 2-27. TAPS combustor, which is going to be fitted into GEnX engine, uses the Ceramic Matrix Composite material for liner walls that significantly reduces the cooling air requirements.

This air can then be used in a mixer allowing lean burn that reduces the NOx to the level of 30% to CAEP/8 standards.

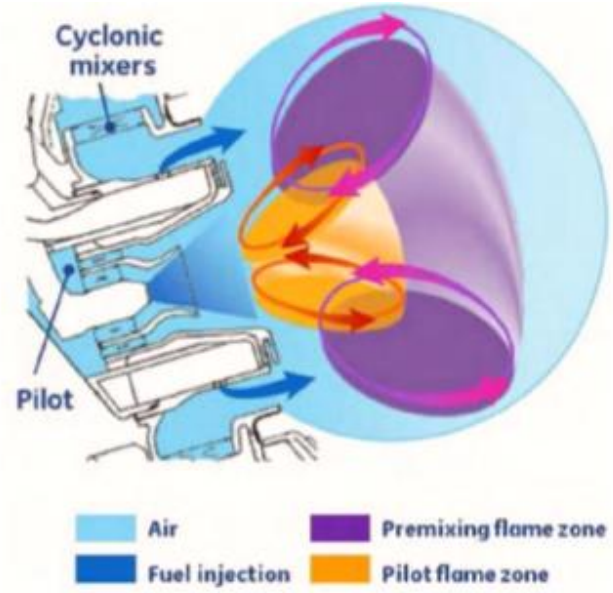

Figure 2-27: Twin Annular Premixed Swirl Combustor [77]

The pilot fuel is sprayed from the nozzle located in the centre of a larger main fuel injector. At start-up and lower-power settings only pilot fuel injector is delivered fuel to combustion zone. As the aircraft throttle settings increases in order to minimize the smoke production and maintain high combustion efficiency, the main fuel injectors are gradually raised the supply of fuel. Reaching the full-power performance, all the main injectors are operating at full capacity. A margin of 65% to CAEP/6 standards can be achieved for NOx formation with the use of this technology.

2.9.8 Rich-Burn Quick-Quench Lean-Burn combustor (RQL)

The research on Rich-Burn Quick-Quench Lean-Burn (RQL) combustor concept has been in progress since the late 1970s but it was first introduced in 1980 as a strategy to reduce NO_X emission from gas turbine engines [78].

The concept was then further developed by the National Aeronautics and Space Administration (NASA) later in the 1990's, for the reduction of NO_X in next generation High Speed Civil Transport (HSCT) aero-propulsion engines [79] described in the next section. Pratt & Whitney is currently working on the RQL

combustor technology in aero engines commercially under the name TALON (Technology for Advanced Low NOx) [80].

As shown from the combustor stability loop Figure 2-28, the RQL combustor being a rich initiated combustion has a wider flame stability limit when compared to the lean burn combustor designs. Therefore, the RQL combustor is preferred over lean premixed options in aero engine applications due to the safety considerations and overall stability throughout the duty cycle.

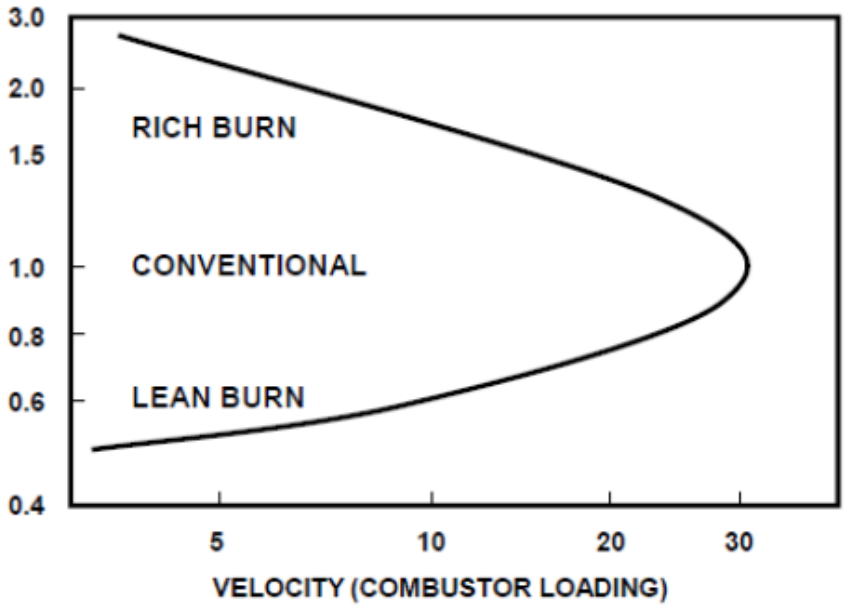

Figure 2-28: Combustor Chamber Stability Loop [81]

Whereas, in stationary gas turbine applications, lean premixed combustor technology is the standard. As safety considerations are not as severe and the duty cycle is more constrained, the reduction in NO_X emission is more substantial in contrast to RQL technology. However, RQL combustor technology is of growing interest for stationary applications due to the characteristics of (1) more effectively processing fuels with nitrogen contents, and (2) processing different types of fuels [82]. Especially, the latter characteristics of RQL is gaining importance lately, as the California Energy Commission is engaged already in RQL technology research, in cooperation with the U.S. Department of Energy, to explore the utility of RQL combustors for applications in the stationary electrical power production [82].

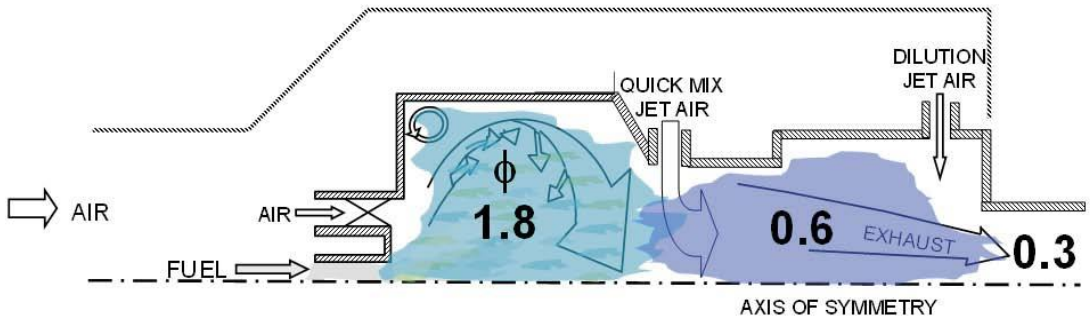

Figure 2-29: RQL combustor with equivalence ratio shown in zone [82]

In the RQL design as shown in Figure 2-29, combustion is initiated in the fuel-rich primary zone operating in the equivalence ratio of 1.2-1.8 and due to the combined effects of low temperature and oxygen depletion, the rate of NO_X formation is lower in the flame front zone.

Whereas in Conventional combustor design, a continuous admittance of air in the primary zone raises both the temperature and oxygen content, thereby greatly accelerating the rate of NO_X formation as shown in Figure 2-30, the high NO_X route. If, however, the additional air required to complete the combustion process is mixed uniformly and instantaneously with the flame front gases without the substantial temperature rise, the combustion process follows the low NO_X route as shown in Figure 2-30.

This demonstrates that in order for the rapid and effective quick-quench mixing section, its design is of critical importance to the success of the RQL concept.

After the quick-quenching of gases, the effluent originating from the rich primary zone are still high in the concentration of partially oxidized hydrocarbon species, hydrogen, and carbon monoxide. As a result, the effluent gases cannot be exhausted without further processing. In particular, the addition of oxygen is needed to oxidize the high concentrations of carbon monoxide, hydrogen, hydrocarbon intermediates. Therefore, a substantial amount of air through wall jets enters in the dilution zone to mix with the effluent gases and creates a “lean-burn” condition prior to the exit of the combustor.

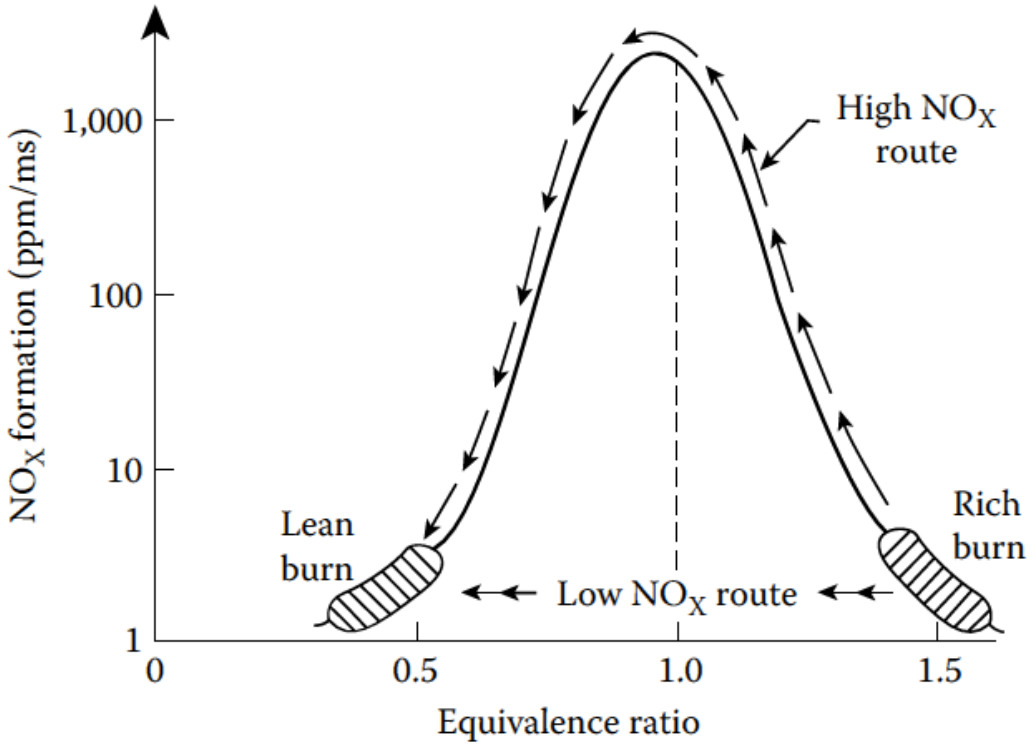

Figure 2-30: Principle of RQL Combustion [5]

RQL combustor design reduces not only thermal NO_X but due to its initial fuel-rich combustion process, it reduces Fuel Bound Nitrogen (FBN) NO_X emission by converting large amount of FBN into N_2 [83]. Nakata [84] who designed an RQL combustor for 150 MW stationary gas turbine engine found that low heating value (LHV) fuels with ammonia (NH_3) content in it when burned in initial fuel-rich stage combustion, can greatly reduce the conversion of NH_3 into NO_X. In that study the RQL combustor's rich zone was designed with equivalence ratio of 1.6 and the test was carried out at atmospheric pressure. Test confirmed a wider combustor stability limit with low NOx emissions of up to 3 ppm for combustor exit temperatures up to 1500°C.

Once the fuel-rich combustion effluent gases enter into quick-quench zone, they encounter jets of air that rapidly reduces the temperature below 1800K reducing the NOx formation substantially. As mentioned above, this transition from rich to lean zone has to take place quickly to prevent the formation of near-stoichiometric NO_X.

The temperature of the lean zone has to be high enough to consume any remaining CO, UHC, and soot left from quick-mix section. Thus, the equivalence ratio for the lean-burn zone has to be carefully selected to satisfy all emissions requirements. Generally, lean-burn combustion occurs at equivalence ratios between 0.5 and 0.7 [85].

After the requirements of combustion and liner-wall cooling have been satisfied, remaining air is used in dilution zone to tailor the exit temperature pattern for maximum turbine durability. The temperature distribution at the end of the RQL would be generally uniform due to the addition of ample air at the dilution zone.

Rizk & Mongia carried out a 3-D analysis of the RQL combustor concept [86] and it was conferred that, in addition to the equivalence ratio, the NO_x formation depends on the residence time, chemical reaction and mixing rates in each zone of the combustor. Furthermore, modification in the quick-mixing configuration can extend the range of operation for acceptable NO_X levels in RQL combustor.

2.9.8.1 **Quick-Quench Zone**

Several studies of jets in crossflow have been conducted under non-reacting conditions to produce understanding into such flow field characteristics such as the jet penetration and the flow field distributions resulting from jet mixing [87; 88]. The researches on jets in crossflow were motivated by the aerodynamics associated with [89]:

- Vertical and/or short take-off and landing aircrafts (V/STOL)
- Primary and dilution jets on conventional gas turbine combustors with a focus on jet trajectory

A single round jet entering from the quick-mix orifice in a crossflow is presented in Figure 2-31. The jet air enters the effluent gases emanating from the rich-burn region and is deflected downstream in response to the momentum of the cross flow. A recirculation zone forms in the near-wall region downstream in the wake of the jet. The radial extent of jet penetration is directed by the angle of the jet relative to the crossflow, and the entry momentum of the jet in contrast to

the momentum of the crossflow. A variety of non-reacting experiments have been used to establish empirical correlations for the maximum penetration of a single jet [82; 90]. For a single round jet injected into a circular duct, the maximum penetration is given by [5]:

$$Y_{max} = 1.15(d_j)(J^{0.5}) \sin\theta \qquad 2\text{-}61$$

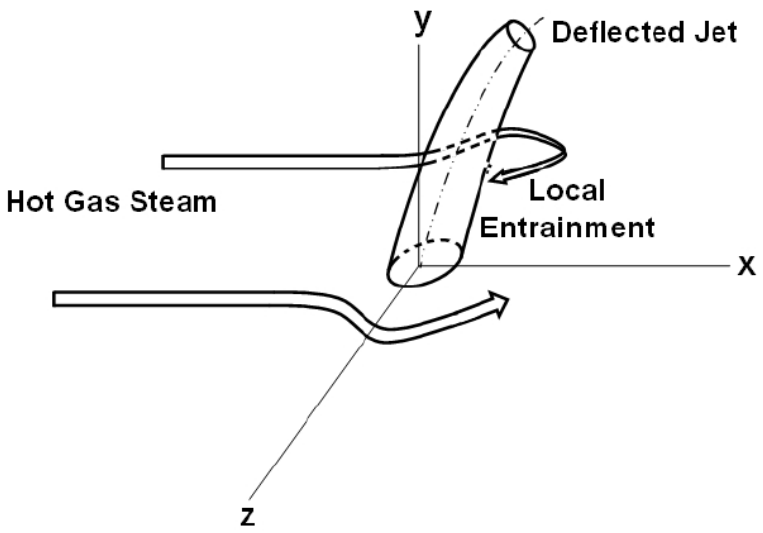

Figure 2-31: Single Jet Flow in Cross-flow in quick-quench section [88]

Where,

Y_{max} = Maximum Radial Penetration of the Jet Centreline

d_j = Diameter of the Jet Entry Orifice

θ = Entry Angle of the Jet to the Crossflow

J = Jet-to-Crossflow Momentum Flux Ratio

$$J = \frac{\rho_{jets} * {V_{jets}}^2}{\rho_{main} * {V_{main}}^2} \qquad 2\text{-}62$$

Where,

ρ = Density

$V =$ Velocity

In the gas turbine combustor, the jets are confined within the boundary of its walls. Therefore, the interaction between multiple jets is a major factor in dictating its mixing behaviour. As a result, studies have been conducted to address the mixing behaviour and optimizing the quick-quench section in the RQL combustor. For multiple jets in a tubular duct, the correlation for the maximum penetration of a single jet must account for the effects of blockage of the mass flow given by 2-63[88].

$$Y_{max} = 1.25\left(d_j\right)(J^{0.5})MR \qquad 2\text{-}63$$

Where,

$MR =$ Jet-to-Crossflow Mass Flow Ratio

In the Equation 2-63, MR is much higher for an RQL combustor (2.5) in contrast to the conventional combustor (0.25). The biggest difference between the jets in conventional and RQL combustors is orifice size for the density and momentum-flux ratios J which is same in both configurations [88].

The studies have undertaken to evaluate the orifice shape, number of orifices, and operating features such as; momentum flux ratio, density flux ratio, mass flow rate ratio with the goal of optimizing the mixing in the quick-mix section of RQL. The proposition is that the optimal mixing in the Quick-quench minimizes the production of nitrogen oxides in RQL [88].

A NASA design method developed by Holdeman [87] defined a correlation that is used to design the jet mixing section of an RQL combustor utilizing round whole jets. The correlation derived a study of jet-to-mainstream momentum-flux ratio, establishes the number of circular holes for optimum mixing given by Equation 2-64:

$$n = \frac{\pi\sqrt{2J}}{C} \qquad 2\text{-}64$$

Where:

n = Number of Circular Jet Orifices to Optimize Mixing

J = Momentum Flux Ratio

C = Empirical Constant = 2.5

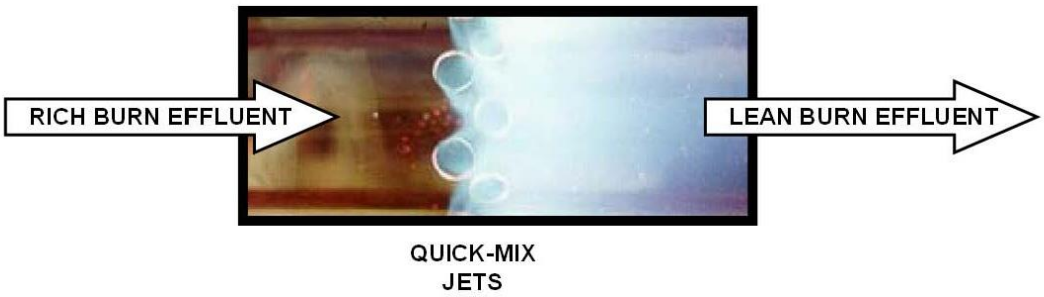

Figure 2-32: Laboratory Model of RQL Combustor [88]

Figure 2-32 shows a laboratory model of RQL combustor's quick-mixing region. Jet mixing in a crossflow has been studied in two primary mainstream geometries; the cylindrical and rectangular geometry. The cylindrical geometry has been the most extensively researched and is directly relevant to cannular combustor configurations. In contrast, the modern annular combustor configurations have procreated investigations of jets in the crossflow for rectangular geometries. For each of the two configurations, Holdeman [87; 88] has established the following procedures to design the most rapid mixing in the Quick-Mix section of the RQL combustor:

I. Cylindrical Geometry:

- Typical Mass Ratio = 2.5
- Typical Momentum Flux Ratio = 60
- Optimal Number of Orifices is given by Equation 2-64
- Orifice Size: Determined by the desired mass-flow ratio and the optimum number of orifices for the given momentum flux ratio

II. Rectangular Geometry

- Typical Mass Ratio = 2.5
- Typical Momentum Flux Ratio = 60
- Optimal Orifice Spacing:

$$\frac{S}{H} = \frac{C}{\sqrt{J}} \qquad 2\text{-}65$$

Where:

S = Orifice Spacing

H = Channel Height

An experiment was carried out by Holdeman in [87], to examine the effects of air preheat and the number of orifices on NO_X emissions in RQL combustor configurations. The facility used for the test has the capability to allow the jet air preheat to be controlled independently from the main air preheat. Mixing modules (80 mm Inlet Diameter) with a varying number of round holes but the same total area (1244 mm^2) were evaluated while maintaining a constant jet-to-mainstream momentum-flux ratio (J = 57) and mass-flow ratio (MR = 2.5).

Figure 2-33 [88] shows the NOx emission result for preheated air input and the effect of number of orifices on NOx emission in the quick-quench section of the RQL combustor for the experiment. The outcomes of the experiment are discussed below:-

- The number of orifices had a significant effect on mixing and the distribution of species. However, the overall NOx data for a constant total orifice area at a fixed momentum-flux ratio was relatively insensitive to the number of jets on the perimeter of the quick mix section, suggesting that an “optimum” mixer may not lead to the minimization of overall NOx emissions.

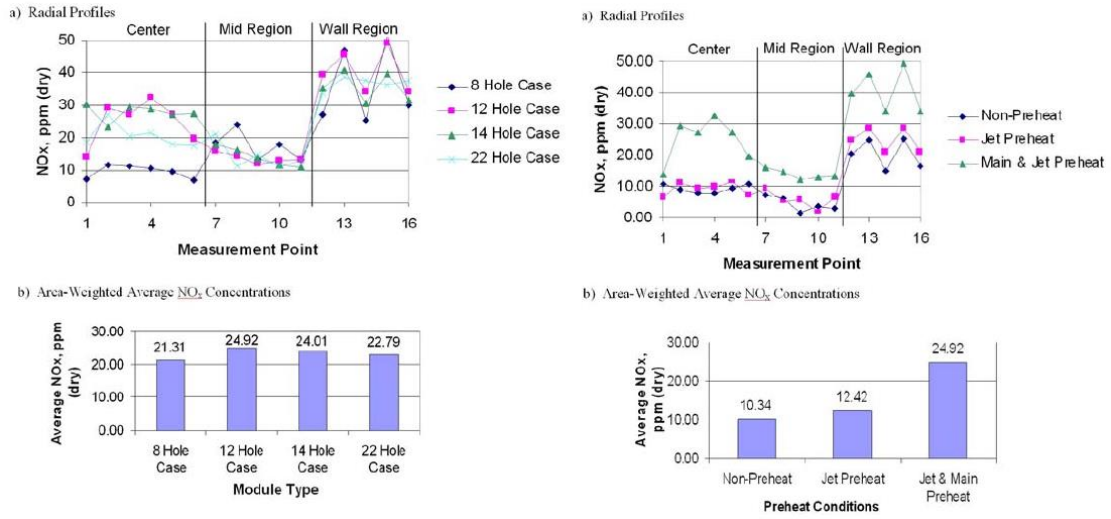

Figure 2-33: NOx emission data for number of orifice and preheat air in quick-quench section [88]

- High concentrations of NOx were observed in the wake of the jets near the wall for all modules probably because jet induced recirculation offers both high temperatures and lengthened residence times there.
- Although the jet air in the quick-mix region comprised of 70 percent of the total airflow in the RQL combustor model and it was expected that higher jet air preheat temperature would contribute significantly to higher NOx production. But, the impact of preheating quick-mix jet air alone on NOx emissions was small compared to preheating both main and jet air.
- Results from the current study do not support the assumption that an optimal mixer would lead to the minimization of NOx emissions, and shows that preheating both the mainstream and jet air has a significantly greater effect on NOx emissions than preheating only the jet air.

2.10 Conclusion

Low load or transient load events could affect the emissions performance of DLN gas turbines because of engine controls that are required to prevent combustor from flameout. In order to prevent the formation of NOx, LPP combustors are designed to operate close to engine flameout temperatures when compared to conventional combustors. If the load is reduced to a low level or increased/decreased rapidly, in order to prevent flameout, combustor

flame stability is augmented. Most manufacturers expand combustor flame stability through staged fuel distribution adjustment such as the addition of pilot fuel [5]. The addition of pilot fuel creates a diffusion flame, which increases NOx and CO emissions. Therefore, CO emissions might increase significantly if operated at sustained low load conditions due to incomplete combustion at lower temperatures.

Most of the work carried out so far on the RQL concept has confirmed its potential for ultralow NO_X combustion and low conversion of FBN into NO_X. The conversion of NH_3 into NO_X is also greatly reduced with Lower Heating Value (LHV) fuels. In comparison with conventional combustors, RQL combustors have inherently better ignition and flame blowout performances. In comparison with staged combustors, they have the important practical advantage of needing fewer fuel injectors. However, in order to fully exploit these assets, significant improvements in quench mixer designs are needed.

Literature review indicates that radical reductions in aviation NO_X emissions can be achieved by improvement of aircraft combustor designs. Especially, in the case of novel dry low NO_X combustors, RQL concept has advantages of wider combustor stability and flame blowout limits over LPP combustor. Therefore, the RQL combustor is preferred over lean premixed options in aero engine applications due to the safety considerations throughout the power requirements in a cycle.

Furthermore, stirred reactor method deemed suitable over the CFD method to predict the NO_X emission for RQL combustor in order to reduce the computation time and in enlightenment of the further development of the model which is to be integrated with the trajectory optimisation tool. The next chapter explains the preliminary development of the NO_X emission prediction model for RQL combustor using stirred reactor method and the sensitivity of the model for the input parameters such as pressure, temperature, and air flow.

3 DEVELOPMENT OF RQL NO_X EMISSION PREDICTION MODEL

This chapter explains in detail the development of the emission prediction model “Hephaestus” for RQL combustor using stirred reactor approach. Second part of the chapter explains the developed RQL combustor model’s assumptions and constraints.

3.1 Introduction

As discussed in section 2.6, there are three methods which can be adopted to predict jet engine emissions; empirical correlation method, stirred reactor based model and Computational Fluid Dynamics (CFD). In this research, Rich-Burn Quick-Quench Lean-Burn (RQL) combustor is modelled using stirred reactor approach for low NO_X prediction.

The stirred reactor approach is used to develop Cranfield’s in house emission prediction software “Hephaestus” explained in section 2.8. The next section explains the NASA RQL test rig experiment [12] on which the RQL combustor is modelled in “Hephaestus” using stirred reactor approach.

3.2 RQL Test Rig Experiment by NASA

The overall objective of the test rig programme conducted by NASA was to demonstrate the RQL combustor concept for High Speed Civil Transport (HSCT) programme [12]. That test was in support of Pratt & Whitney and GE Aircraft Engines low NOx combustor programs. The test rig was mounted in the Engine Research building at the NASA Lewis Research Centre. Figure 3-1 shows a cut away drawing from the test rig experiment [12].

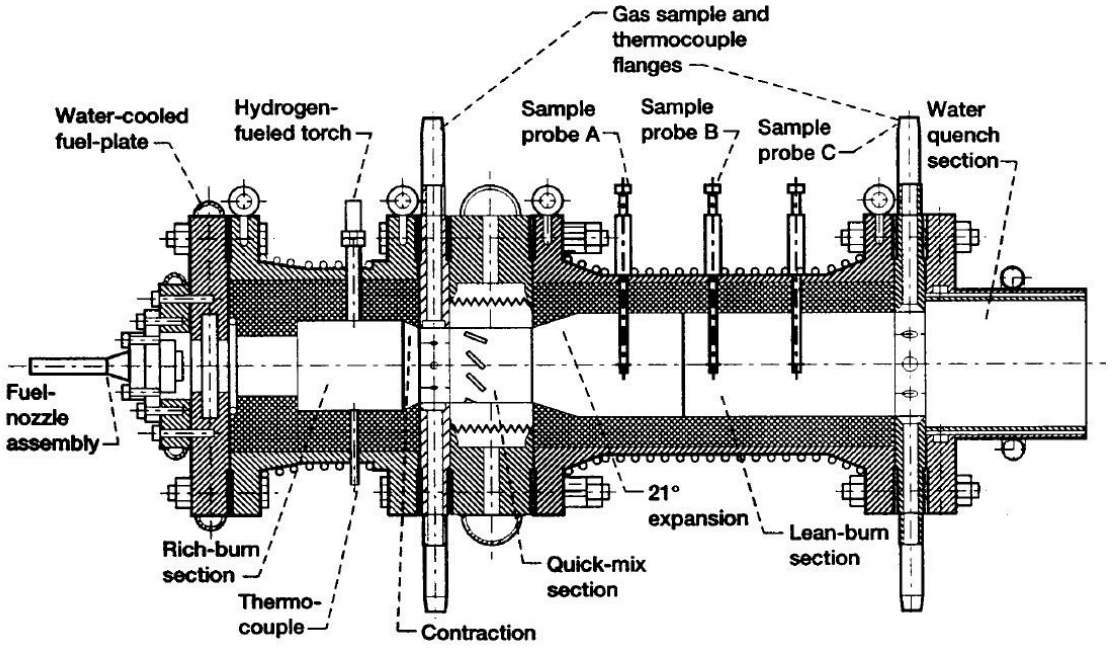

Figure 3-1 Cut-away drawing of RQL Combustor Test Rig [12]

Hot ceramic liners were used in the cylindrical flame tube rig to minimize the effects of heat loss on NO_x emission. The test rig facility could supply the combustor inlet pressure air of 16 atm at 870K. Combustion gases were sampled continuously during testing using three sampling probes A, B and C as shown in Figure 3-1. The dimensions of test rig are mentioned in the Table 3-1. Airblast fuel atomisation nozzle was utilised for the test rig.

The following was concluded from the test rig experiment:-

- The RQL test results showed low NOx and CO emissions at required conditions set for the test rig
- For this study, the test showed that the combustor inlet temperature T_3 was a dominant factor in the NO_X formation in RQL combustor. As T_3 increased from 590 K to 870K the $EINO_X$ increased three fold
- Secondary factors which influenced the NO_X formation are combustor outlet pressure, turbine inlet temperature and rich burn equivalence ratio

3.3 Development of RQL combustor model

As from section 2.9.8, RQL combustor is divided mainly into three sections. The first part is the rich-zone, where fuel and air mix and burn in fuel rich conditions

with the equivalence ratio normally in between 1.5 and 1.8. The second section is the quick-mix zone, where almost all the remaining compressor exit air mixes with the fuel-air effluent gases from the rich zone very quickly.

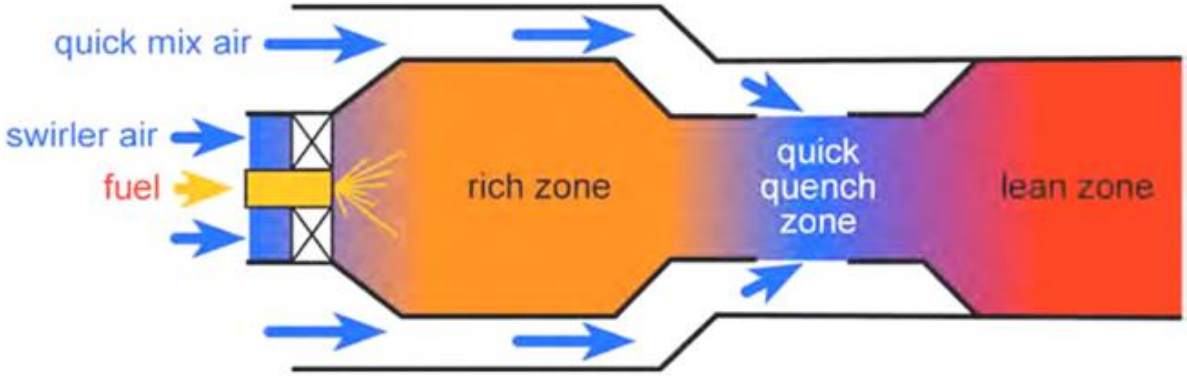

Figure 3-2: RQL Combustor Zones [91]

The equivalence ratio is in the range of 0.6-0.8 for quick quenching. Third section is the lean zone, where all the mixture blends with the remaining air and the mixture itself is lean because of highest percentage of air. The equivalence ratio is in the range of 0.3-0.4.

As in all the zones the temperature doesn't exceeds critically required for NO_X formation, the emission is considerably less compared to the conventional combustor. But, it demands careful designing to control the air flow and requires highly efficient instantaneous quick-quench mixing section.

The section 2.6.3 explains about the stirred reactor method and provides an insight into different reactors theory. As it is the Perfectly Stirred Reactor (PSR) property, the two streams of effluent gases are assumed to mix homogeneously and attain the state of chemical equilibrium instantaneously. These equilibrium conditions are assumed along all the PSR length. The calculations of chemical equilibrium are performed using the NASA Chemical Equilibrium with Application (CEA) program [92; 93] which is based on the minimisation of Gibbs free energy at constant temperature and pressure. The main aim of the NASA program is to compute combustion parameters such as equilibrium temperature, density and species mass fraction for a given reactor.

Normally, the resident time of the reactant molecule in a jet engine combustor is short and not sufficient to achieve the chemical equilibrium for all the pollutant of interest. Especially, in the present study of the exhaust pollutants NO_X and CO formed inside the gas turbine combustor are not in local chemical equilibrium. Therefore, it is necessary to include adequate kinetic model within each reactor to ensure sensible quantitative calculation of NOx and CO emissions. All the other species are presumed to be in chemical equilibrium.

Once the gas conditions such as pressure, temperature, flow rates at the inlet and exit of the PSR, and its length are known, the PSR residence time is calculated and utilised for the integration of the reaction rates of the pollutants being analysed. As, the pollutants concentrations are very low, when compared to the combustion products in chemical equilibrium, it is assumed that the heat release is not affected by their formation. Finally, the exhaust pollutant along with the combustion products in equilibrium at the exit of a given PSR are supplied as inputs to the downstream reactors utilised in a multi-reactor arrangement.

In the Partially Stirred Reactor (PaSR), the mixture fraction distribution is assumed to follow a Gaussian Probability Density Function (PDF). Celis [37] has also used a clipped Gaussian as Heywood and Fletcher [56] instead of the classical Gaussian to model the PaSR because PDF of the classical Gaussian tends to zero when the variable (here mixture fraction) tends to ±∞ However, the mixture fraction can only vary between 0 and 1 by definition

The mixture fraction f is given by [37; 94]:-

$$f = \frac{\dot{m}_f}{\dot{m}_f + \dot{m}_a} = \left(1 + \frac{1}{\emptyset . FAR_S}\right)^{-1} \qquad 3\text{-}1$$

Fletcher and Heywood [56] introduced a parameter known as ‘mixing’ (or ‘unmixedness’) parameter (S), defined as the standard deviation of the mixture fraction divided by its mean value given by:-

$$S = \frac{\sigma}{f_m} \qquad 3\text{-}2$$

Where, f_m is the mean value of the mixture fraction and σ corresponds to its standard deviation.

It is a measure of the uniformity of turbulent mixing within the reactor which implies if $S = 0$,it's completely mixed.

Sturgess [95] proposed that by matching modelling predictions to measured emissions data, the mixing parameter can be established empirically. Also, depending on combustor primary zone details, the values are expected to be different between one combustor to another in which case PaSR is to be used.

So, generally, it is expected that the mixing parameter relation would be different for dissimilar combustor design. This model also assumes that the mixing parameter is a function of the equivalence ratio based on information provided by Sturgess [95], Allaire [96], and Celis [37] as shown in Figure 3-3.

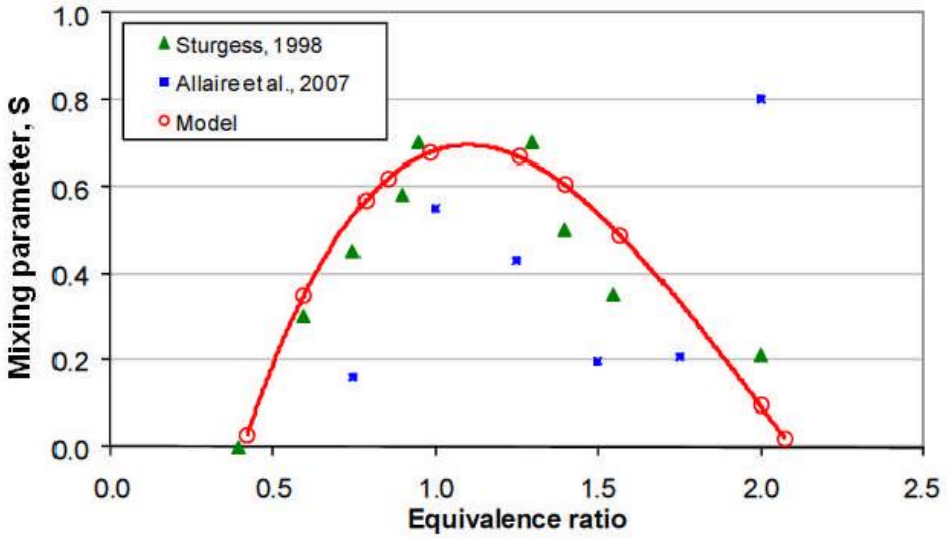

Figure 3-3: Mixing parameter versus Equivalence ratio [37]

It can be noted that this formulation of the mixing parameter limits the range of acceptable mean equivalence ratio between around 0.4 and 2.1. Therefore, the model has assumed the values of equivalence ratios between the defined values. Further to note that the NASA test rig RQL combustor Rich equivalence ratio doesn't exceed more than 2 for the experiment. Therefore, the acceptable mean equivalence ratio between 0.4 and 2.1 deemed suitable for the

development of NOx emission prediction model. The PaSR receives air and fuel mass flow as input. The mixing parameter correlation is used to calculate S. The mean mixture fraction,f_m, is determined given by the mass flow inputs and the standard deviation. The mean and standard deviation are subsequently used as input for the clipped Gaussian transformation.

Finally, in order to keep the model developed simple, and avoid an increase in the level of uncertainties in the results obtained, some processes inside the combustor such as fuel evaporation, combustion unsteadiness, have not been included in the NO_X emissions prediction model described in the present work.

3.3.1 Reactor Layout of RQL Combustor

As it can be seen from the CAD drawing of the RQL combustor in Figure 3-4, RQL combustor is divided into three regions; Rich-burn zone, quick-quench zone and lean-burn zone. The reactor layout of RQL is shown in the Figure 3-5. The rich-burn zone has one flame front reactor selected as partially stirred reactor. This assumption has been taken into account as the flame front area is fuel rich, thus the fuel/air mixture is heterogeneous with equivalence ratio of 1.8.

The second is quick-quench region and is modelled with two series of perfectly stirred reactors, one at the near wall and the other at the core. These assumptions take into account the quick mixing and abundance of air present in this zone. Eventually, both the near wall and core flow of the quick-quench zone mix together and enters the lean-burn zone. By the time the mixture reaches the lean-burn zone the mixture is assumed to be fully homogenous and hence it is assumed to be a series of perfectly stirred reactors.

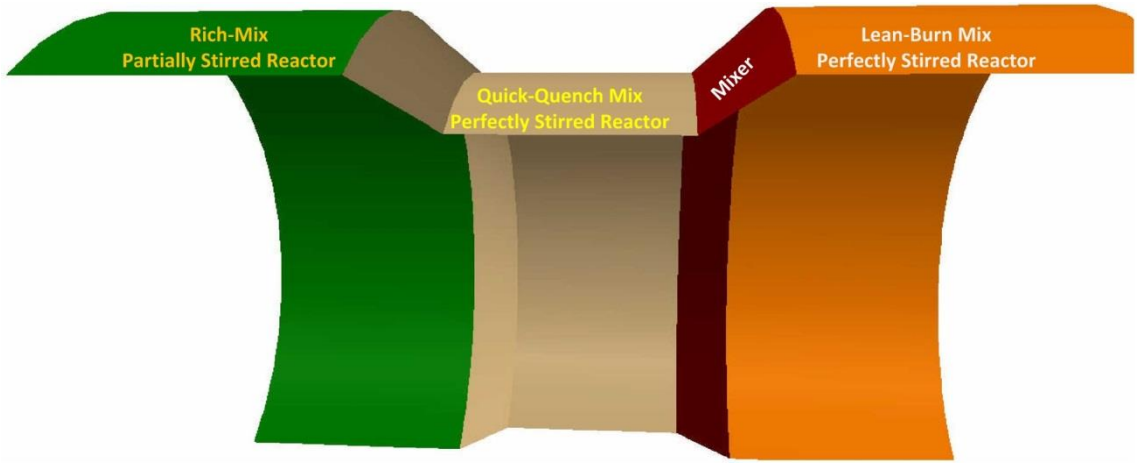

Figure 3-4: CATIA model of RQL combustor

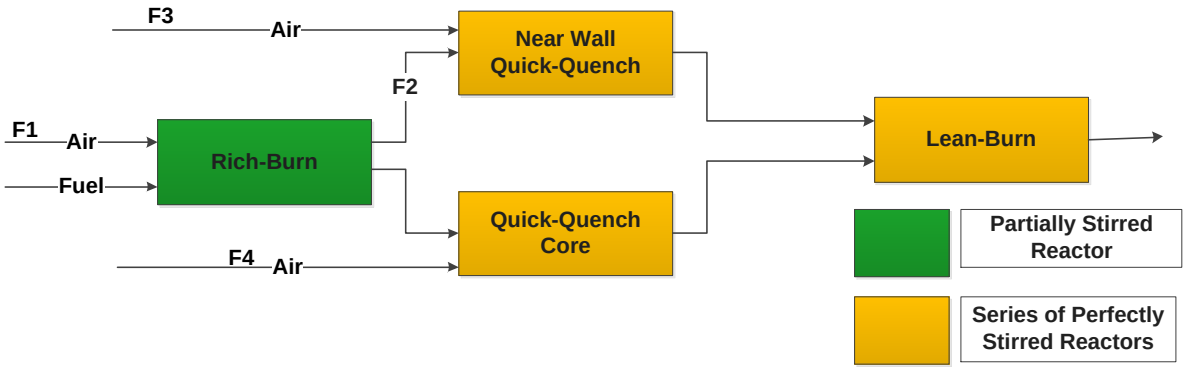

Figure 3-5: Reactor layout of RQL combustor in the model

From Figure 3-5, F1 is the fraction of air entering the flame front rich-burn zone, F2 is the fraction of the burning gases entering the near-wall reactor at quick-mix zone from rich-burn reactor and F3 is the fraction of air initially assigned for quick-mix zone entering the near wall quick mix reactor. The rest of F3 air left from near-wall quick-quench enters the quick-quench core section of the combustor denoted by F4. The reactor arrangement and the air flow inside the combustor are based on the NASA test rig combustor [12] as shown in Figure 3-1.

The RQL Combustor geometry details have been taken from the NASA test rig experiment from [12], shown in the Table 3-1.

Table 3-1: Combustor Geometry from NASA Test Rig Experiment

	Rich-Burn (RB)	Quick-Quench (QQ)	Lean-Burn (LB)
Length (m)	0.203	0.127	0.610
Diameter (m)	0.152	0.102	0.178
Area (m^2)	0.031	0.013	0.108

Based on the geometry given by the NASA test rig experiment [12], the area and corresponding length of the Rich-Burn (RB), Quick-Quench (QQ) and Lean-Burn (LB) region of the different reactors within the RQL combustor is modelled as shown in Table 3-2.

Table 3-2: RQL Reactor Geometry in Hephaestus

Inlet area RB (m^2)	Outlet Area RB (m^2)	Length RB (m)	Inlet Area QQ (m^2)	Outlet Area QQ (m^2)	Length QQ (m)	Inlet Area LB (m^2)	Outlet Area LB (m^2)	Length LB (m)
0.031	0.013	0.203	0.013	0.108	0.127	0.108	0.108	0.610

The input parameter for the model is combustor inlet temperature (T_3), pressure (P_3), combustor inlet airflow (W_A), fuel flow (W_F), ambient relative humidity and the air distribution within the different regions.

All the assumptions and constraints in modelling the RQL combustor in Hephaestus is kept same as in the NASA test rig experiment in order to verify the result with their experimental data. The assumptions which have been incorporated into the Hephaestus model from the NASA test rig experiment for NO_X prediction are explained are as under:-

- As the NASA test rig combustor is not tested with the ICAO points of take-off, ideal, cruise and approach scenario, the stirred reactor model is unable to access the suitability with the ICAO points. Hence the limitation

of the model is non-verification with the ICAO points for the NASA test rig combustor.

- As the RQL combustor is an air staged low NO_X and not fuel staged, all the fuel is fed into the flame-front rich burn zone after airblast atomization. So, 100% fuel enters the Rich burn section of the combustor.

- The air is fed into rich-burn and the quick-quench section of the RQL combustor and there is no further air input in the lean-burn section because the temperature traverse at the downstream of combustor was not the priority for the NASA test rig experiment. The emphasis of the NASA RQL combustor test rig experiment was on NO_X emission prediction. Hence, similar assumption of not ingesting air in the lean-burn section has been taken in Hephaestus for RQL NO_X emission prediction modelling using stirred reactor approach.

- The distribution of air in the rich-burn and quick-quench section is adjusted and monitored in order to achieve the required equivalence ratio in the rich-burn section of the combustor. Therefore, for different measurement points from the rig test experiment, the input air varies in the rich burn zone and hence in the quick-quench section subsequently. Therefore, the percentage of airflows into the rich-burn and quick-quench section has been calculated accordingly for the stirred reactor model.

- The rich-burn section in the NASA test rig experiment is fuel rich with heterogeneous mixture of fuel and air. The air and fuel is fed from the front section of the combustor and there are no further air intakes in the chamber which means the rich-burn section acts a single cylindrical tube with two openings; one for the intake of fuel and air and the other for the effluent gases emanating from it to go to quick-quench section. Therefore, a single partially stirred reactor is chosen to capture the chemical kinetics within the rich-burn region.

- It is assumed that the effluent gases emanating from the rich-burn section mixes quickly in the second quick-quench region and attains the state of chemical equilibrium instantaneously in the series of discrete sections. Hence, the quick-quench region is modelled with series of perfectly stirred reactors. Further, the effluent gases after attaining the equilibrium conditions in their respective near wall regions mixes with the core reactor in quick quench zone and enters into the lean burn zone.

- In the NASA test rig experiment there were three water-cooled sampling probes inserted into the lean-burn region to measure the emissions from the combustor separated from each other as shown in Figure 3-1. As, it is not possible to replicate the exact scenario in the stirred reactor model, the mass fraction of NO_X is predicted axially along the length of the RQL combustor in the Hephaestus model.

- Jet-to-crossflow momentum flux ratio (J) as explained in section 2.9.8.1 was monitored and changed for each measurement point in the NASA test rig experiment. Due to the nature of preliminary development of the stirred reactor RQL NOx emission prediction model, the number of jet orifice, the jet penetration angle and jet-to-crossflow momentum flux ratio has not been taken into account. Instead, the change in fraction of air entering into the RQL combustor F1, F2, F3, F4 somewhat compensates for the Jet-to-crossflow momentum flux ratio in this model.

The aim of developing a preliminary NOx emission prediction model for RQL combustor using stirred reactor approach is to be able to predict NO_X emission results comparative with the NASA test rig experiment and to be able to capture the chemical kinetics within the RQL combustor for predicting NO_X emissions for an aero engine. Therefore, due to aforesaid assumptions and constraints in modelling the RQL combustor, the output results might show variations from the experimental result measured from the NASA test rig.

4 RESULTS AND DISCUSSION

This chapter discusses the results from the preliminary stirred reactor model for RQL combustor and comments on the NO_X predictions output.

Table 4-1 shows the outcome of the Hephaestus for the RQL combustor and comparison of $EINO_X$ with the NASA test rig experiment. Here, the input into the RQL combustor model such as combustor inlet temperature (T3), Pressure (P3), Air mass-flow and fuel flow has been taken from the NASA test rig experiment as shown in Table 4-1.

Table 4-1: Comparison of EINOx from Hephaestus and NASA test rig

T3 (K)	P3 (atm)	Air mass flow (kg/s)	Fuel Flow (Kg/s)	$EINO_X$ (g/Kg) (NASA rig)	J (jet-to-crossflow momentum flux ratio)	$EINO_X$ (g/Kg) Hephaestus
795	7.8	2.808	0.0894	5.4	34.7	5.38
585	5.4	2.717	0.1057	1.7	16.6	1.41
797	8.0	3.048	0.0889	4.9	43.4	4.54
583	10.5	2.567	0.0984	4.5	17	4.70
583	10.0	2.784	0.0989	3.9	20.7	2.27
848	10.0	3.361	0.1048	8.6	38.9	7.02

As it can be seen from the Table 4-1, the RQL Hephaestus model has been able to predict the $EINO_X$ comparatively close to the experimental results from the NASA test rig experiment. The reason for variation of $EINO_X$ for few points is due to the assumption and constraints in model; one being not taking the jet-to-crossflow momentum flux ratio into account during the RQL combustor modelling using stirred reactor approach.

A detailed variation of different parameters in the axial direction of RQL combustor is explained in the next section.

4.1 Axial Position Results for NASA test rig combustor

This section shows the axial variation in the main parameters such as equivalence ratios, NO_X & CO mass fractions and temperature for the NASA test rig experiment combustor geometry from the Hephaestus RQL combustor model. The Figure 4-1 shows the variation of equivalence ratios in the core and near wall region of the RQL combustor axially along the length. It is inferred from Figure 4-1 that the equivalence ratio is 1.8 for the first two points in core and near wall. These points are from the flame front rich-burn region where a single partial stirred reactor for core was used to model the region and the equivalence ratio was fixed to 1.8 according to the NASA test rig experiment. Hence, the inlet and outlet equivalence ratio of the rich-burn region is unchanged.

However, the steep decline in both the near-wall and core section of the second quick-mix region is due to the addition of large amount of quenching air in the mid-section.

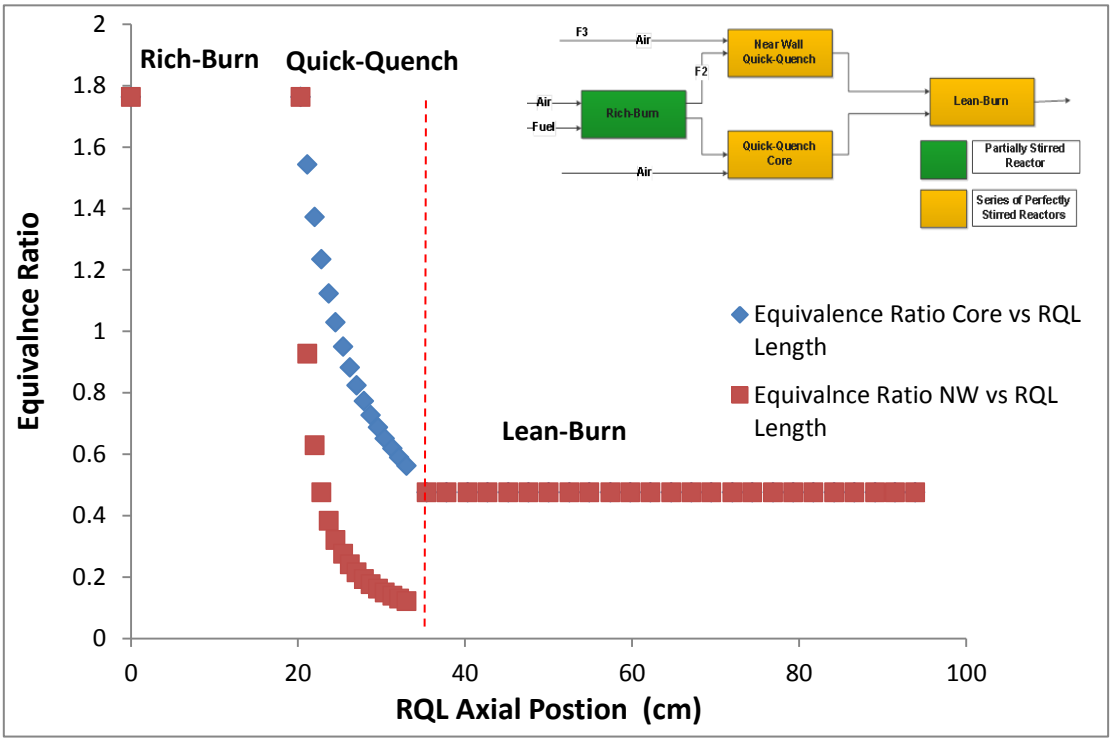

Figure 4-1: Equivalence ratio vs RQL combustor axial positions

As per the NASA test rig experiment requirement, there is no air added further in the lean-burn section. Therefore, the effluent gases emanating from the quick-quench section reaches to equivalence ratio of 0.5; it remains same for the whole lean-burn section. For real engine case, air would further be added for a uniform temperature traverse at the end of the dilution zone and hence the equivalence ratio would vary in the dilution zone.

The Figure 4-2 shows the temperature variation in the near wall and core region along the length of the RQL combustor. It is inferred from Figure 4-2 that there is a steep drop in the near-wall region temperature; this is due to the addition of abundance compressor exit air which is comparatively cooler than the combustor in the quick-quench region. When, the air first enters in the quick-mix section, it first quenches the near-wall region reducing its temperature before entering into the core section of quick-mix section.

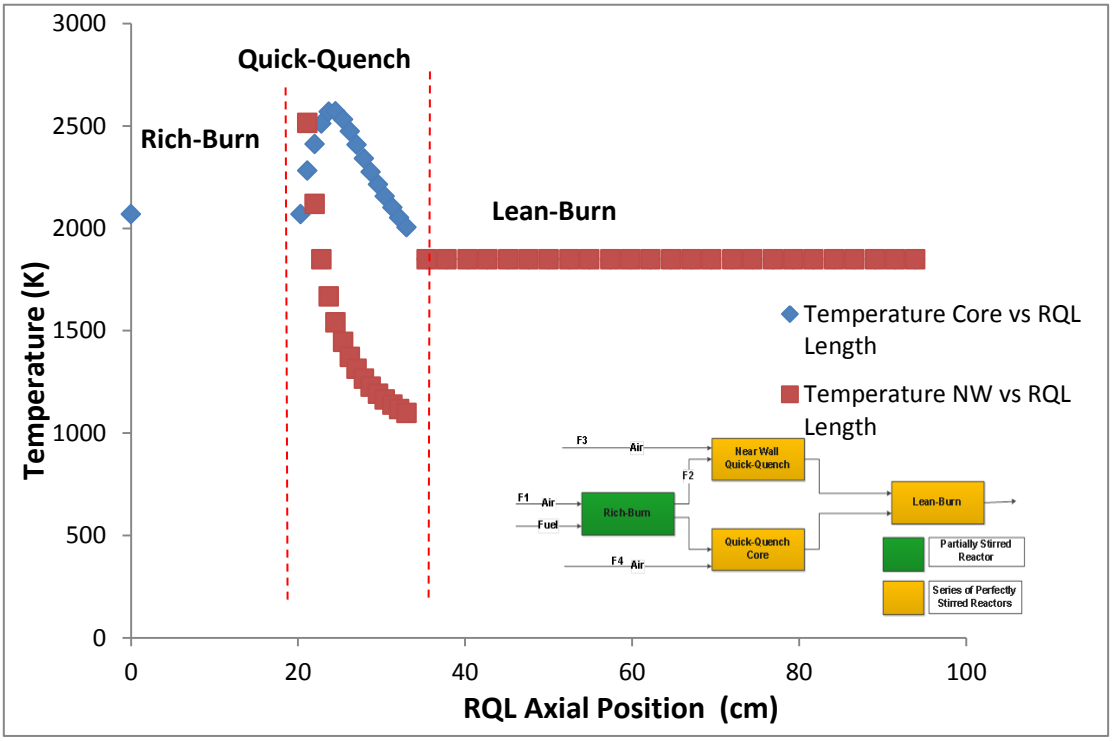

Figure 4-2: Temperature vs RQL combustor axial positions

There is rise in temperature in the core section of the quick-quench region before a sharp decline because the combustion in the core region moves towards stoichiometric ratio from 1.8 as shown in Figure 4-1 and, as further air

is added, the combustion moves towards leaner equivalence ratio of 0.5 as shown in Figure 4-1 which reduces the core temperature.

Eventually, the fuel-air mixture become homogeneous and reaches to a point of almost constant temperature which shows in the lean-burn section of the RQL combustor.

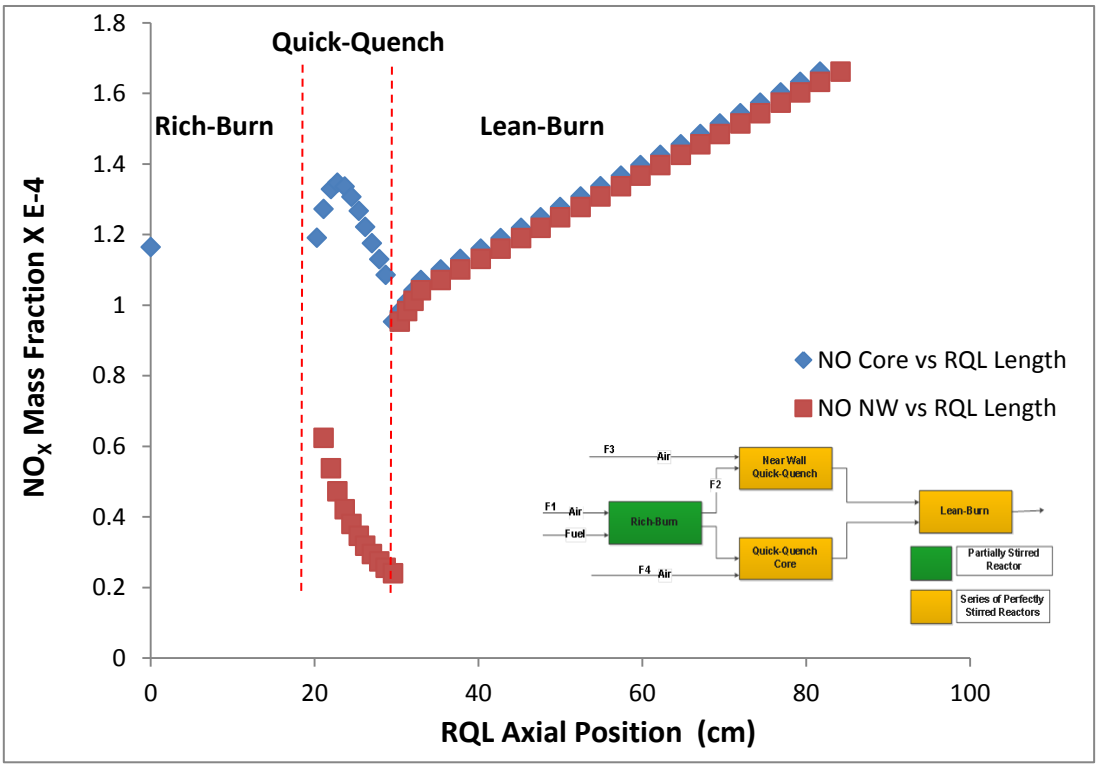

Figure 4-3: NO mass fraction vs RQL combustor axial positions

The Figure 4-3 shows the mass fraction of Oxides of Nitrogen along the length of the RQL combustor. The mass fraction is defined as the ratio of the mass of the substance to the total mass of the mixture.

The NO_X formation in a combustor is mostly thermal NOx and forms at higher temperature of more than 1800K. The Figure 4-3 of NO_X formation follows the same trend as in the Figure 4-2 of temperature variation in the near wall and core of the RQL combustor. As, most of the air is added in the quick-quench zone the mass fraction of NO_X decreases. The slight continues increase of mass fraction in the lean burn zone is due to the temperature in the range of

more than 1800 K in Figure 4-2, no further addition of air and longer residence time due to longer length of the lean burn section of the NASA RQL combustor.

The RQL combustor model Hephaestus has also predicted the Carbon Monoxide (CO) formation in form of CO mass fraction as shown in Figure 4-4.

The temperature plays a key role in the NO_X and CO formation in the combustor as from Figure 2-3 in the chapter 2. At lower temperature CO increases and at higher temperature, the CO decreases due to the oxidation reaction in which carbon monoxide reacts with oxygen to form carbon di-oxide. The result of Hephaestus for the RQL combustor shows the similar trend where the CO is in larger quantity in the rich-burn section due to the lower temperature and lack of oxygen but the amount of CO decreases as the air starts entering in the quick-mix section of the RQL combustor as shown from Figure 4-4.

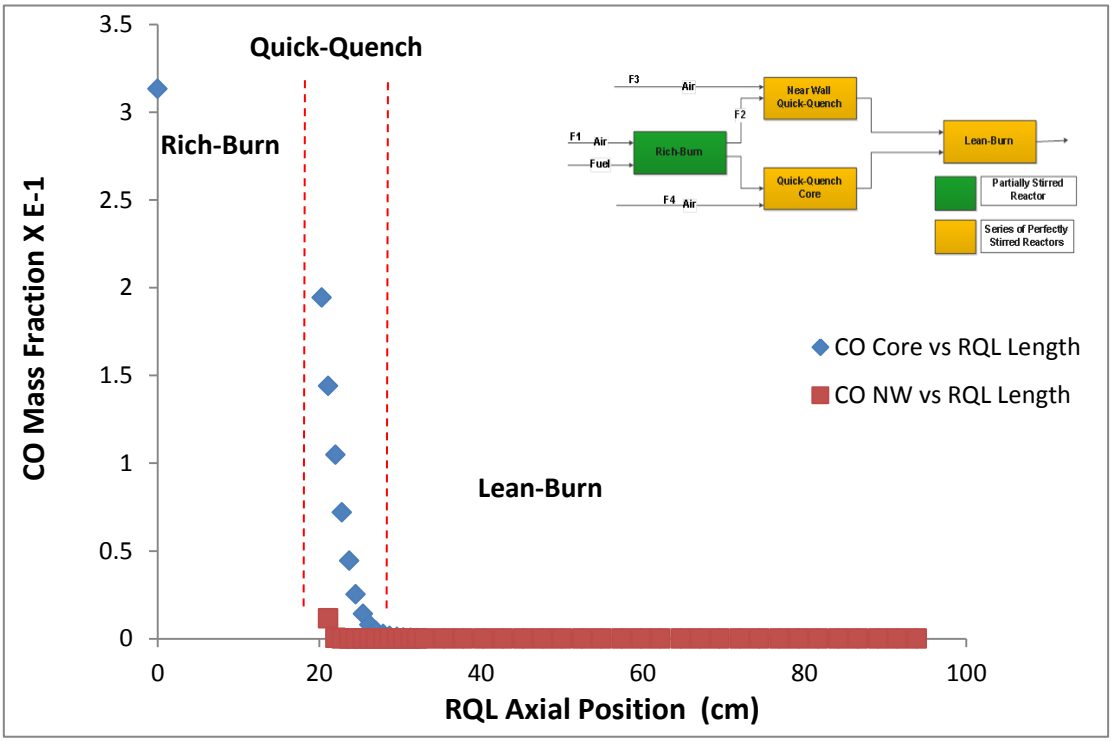

Figure 4-4: CO mass fraction vs RQL combustor axial positions

The next section carries out a case study to look at the impact on NO_X emission for CFM56 type engines when the conventional combustor has been replaced with the RQL combustor.

4.2 Case Study: CUTF1 engine with RQL

In order to compare the NO_X prediction trends between conventional and RQL combustor, an aero-engine from CFM variants is chosen. The engine has been modelled in Turbomatch [97] in-house gas turbine engine performance software at Cranfield University. It's been tested and verified by the data available in public domain.

Therefore, in order to predict NO_X in an aero-engine fitted with the RQL combustor, CFM56-5B2 type engine has been chosen, modelled and verified in Turbomatch for design and off-design point. After carrying out the engine performance calculation for take-off and cruise, various off-design calculations for different TET (Turbine Entry Temperature), the CF56-5B2 type engine is renamed as CUTF1 (Cranfield University Turbofan 1).

CFM56-5B2 engine is a two-shaft turbo-fan engine, with by-pass ratio of 5.6, pressure ratio of 31.3 and rated output thrust of 137.9kN [98]. This engine comes with two variants of combustor; one is the conventional combustor and the other is the fuel staged low NO_X dual annular combustor (DAC). For the comparative study of RQL in this engine, the conventional combustor model of CFM56-5B2 has been chosen. Table 4-2 shows the ICAO emission indices for NO_X, fuel flow, time for different power settings and total fuel burn and NO_X emission for LTO cycle [98]

In order to predict emission from Hephaestus, input parameter such as inlet pressure, temperature, fuel flow, mass flow at combustor inlet, are required which is fed from the Turbomatch engine performance calculation for CUTF1.

As the engine performance model TurboMatch couldn't converge for 7% idle condition for the CUTF1, comparison with the same is not taken into account.

Table 4-2: ICAO emission data for CFM56-5B2 engine [98]

Power Setting (%)		Time in Mode (Minutes)	Fuel Flow (kg/s)	$EINO_X$ (g/kg fuel)
Take-off	100	0.7	1.426	37.8
Climb out	85	2.2	1.158	28.5
Approach	30	4	0.376	11
Idle	7	26	0.119	4.7
LTO Total fuel (kg) or emission (g)			489	8485

The result of NO_X emission prediction for CUTF1 is shown in Figure 4-5. It is obtained from the Hephaestus model for the conventional and RQL combustor for CUTF1 engine. It clearly shows that the model is able to predict NO_X for the conventional combustor of CUTF1 and the same is verified with the data from ICAO engine emission databank [98].

In order to run the 2nd case for RQL, all the combustor input parameters such as temperature, pressure, air mass flow and fuel flow are kept same as the CUTF1 conventional combustor. First the Hephaestus model is run to predict the NO_X formation in conventional combustor and then it is verified with the ICAO emission databank. Secondly, the comparison is made with the RQL combustor prediction. It is inferred from Figure 4-5 that the NO_X formation reduces drastically in RQL when compared to the ICAO NO_X formation data of CUTF1 conventional combustor.

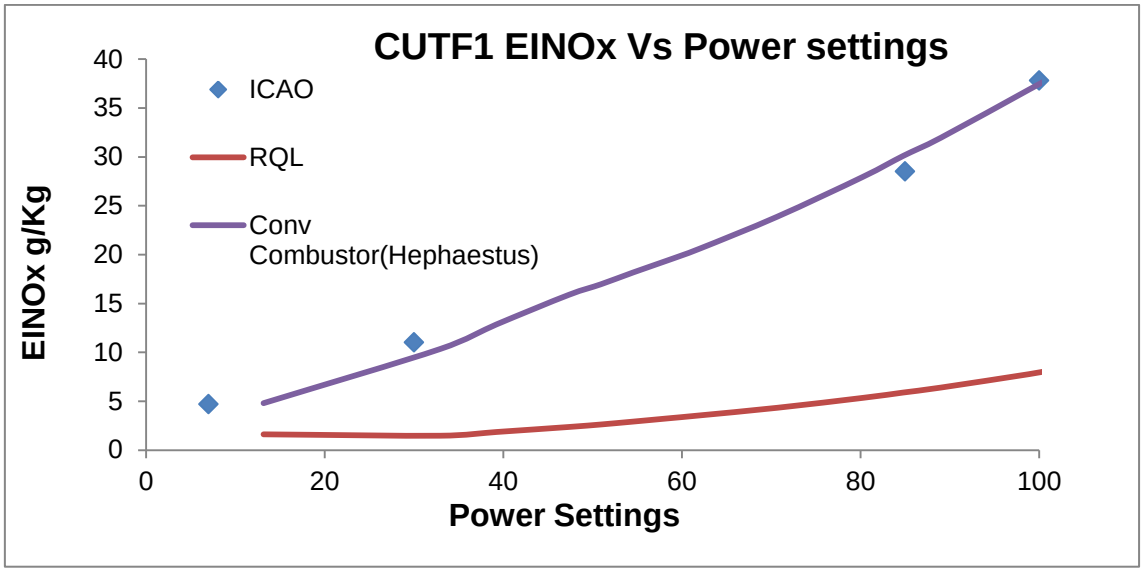

Figure 4-5: CUTF1 EINOX vs Power Settings

4.2.1 Axial Position Results: CUTF1

This section follows the same principle as in section 4.1 to predict the axial variation of the main parameters i.e. equivalence ratio, NO_X & CO mass fractions and temperature for CUTF1 engine with the NASA test rig experiment combustor geometry in the Hephaestus RQL combustor model.

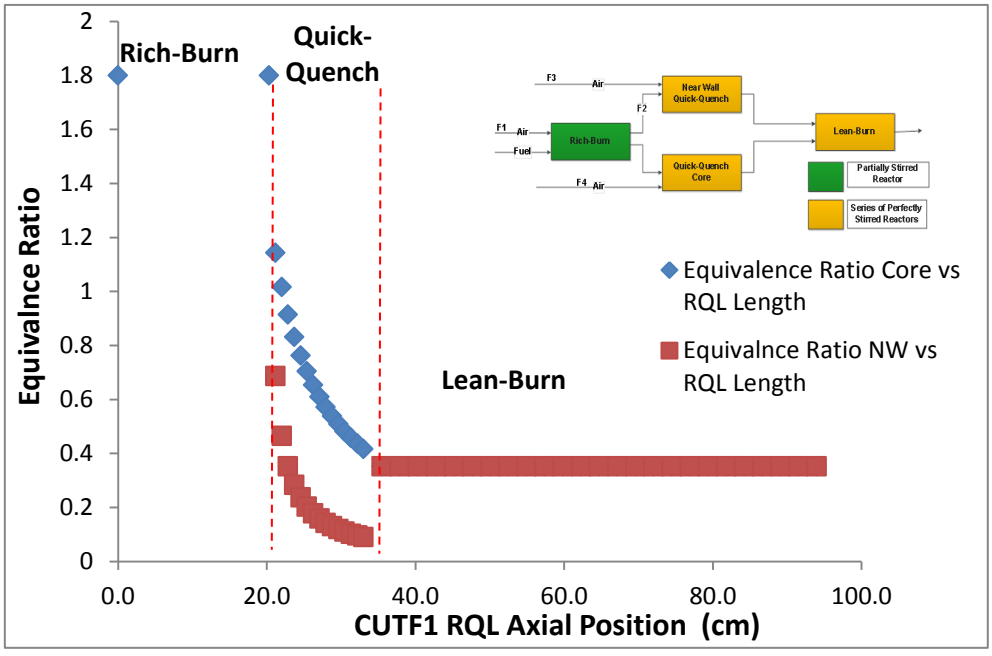

Figure 4-6: Equivalence ratio vs CUTF1 RQL combustor axial position

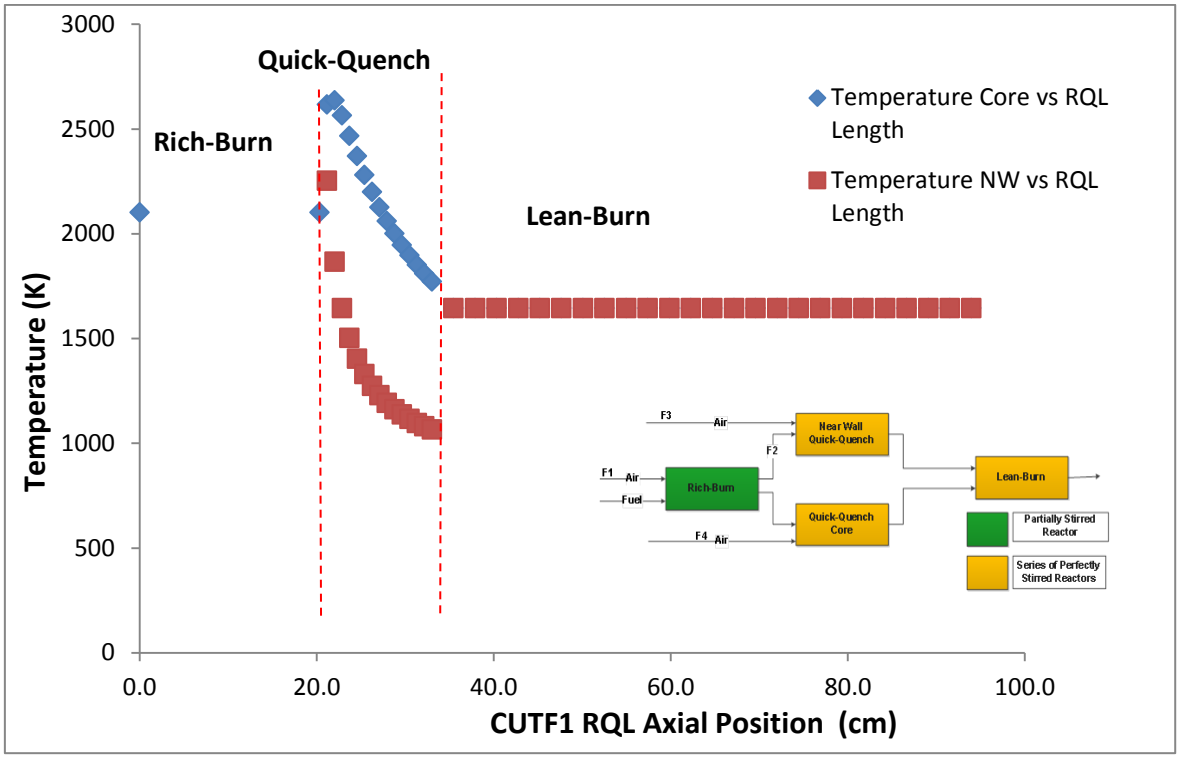

Figure 4-7: Temperature vs CUTF1 RQL combustor axial position

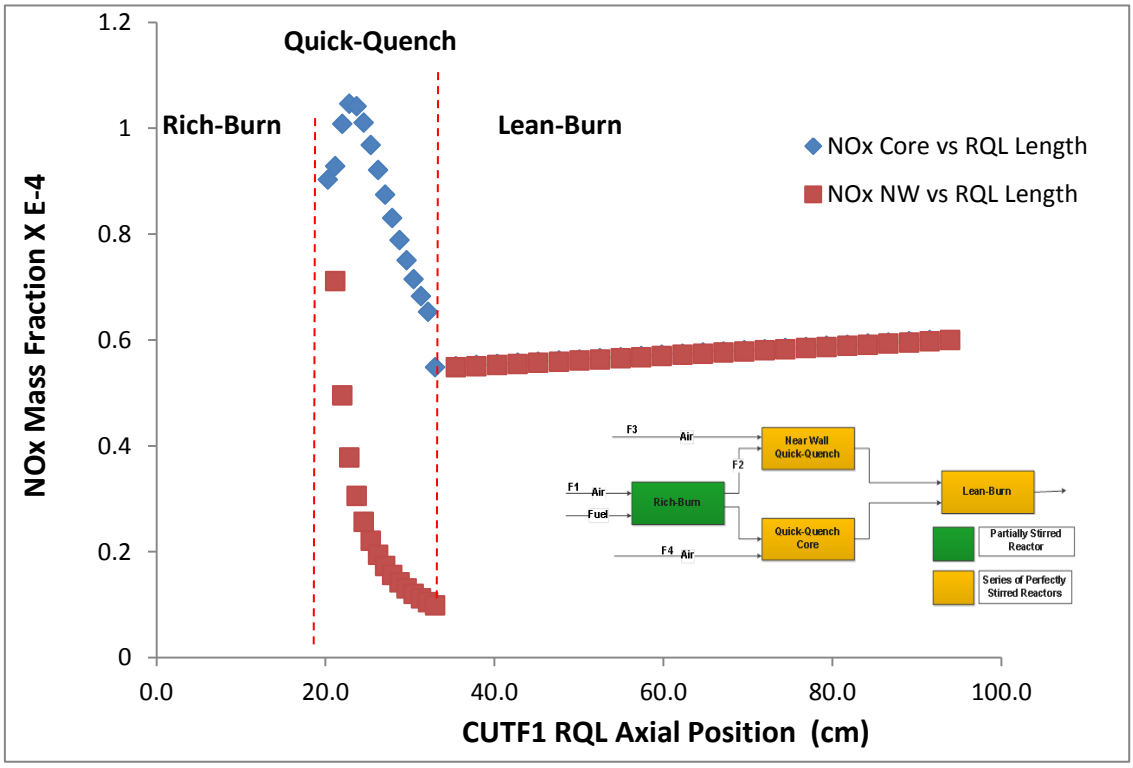

Figure 4-8: NOx mass fraction vs CUTF1 RQL combustor axial position

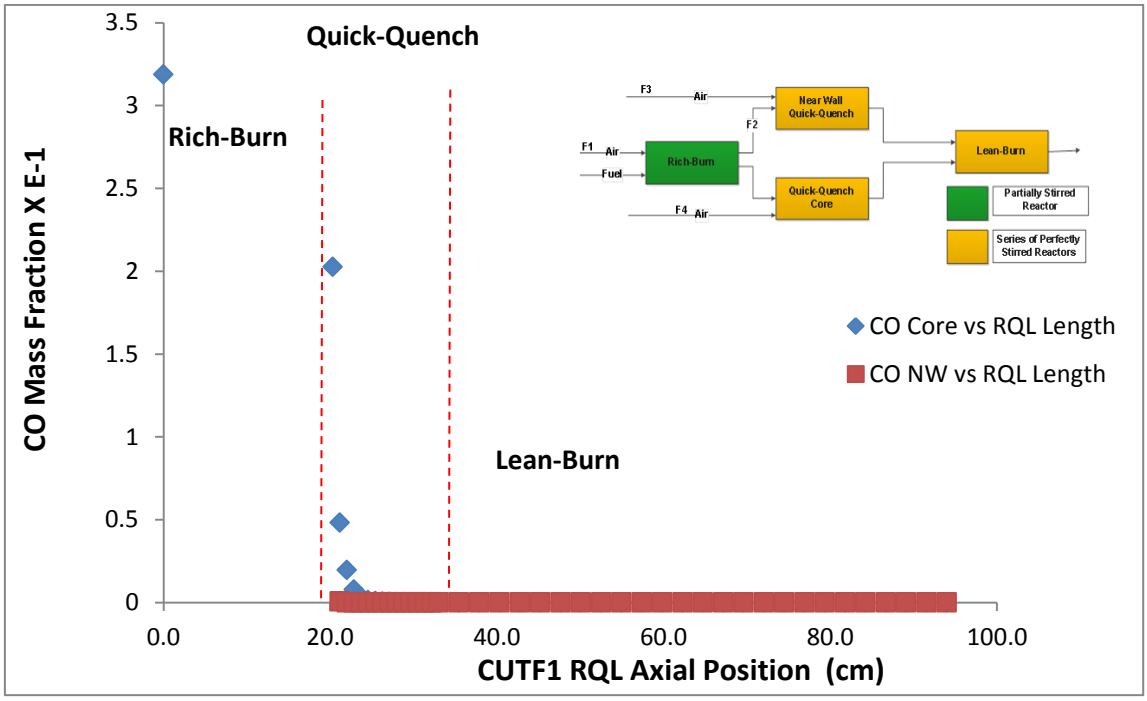

Figure 4-9: CO mass fraction vs CUTF1 RQL combustor axial position

The results from Figure 4-6 to Figure 4-9 shows same trends as shown in Figure 4-1 to Figure 4-4.for equivalence ratio, mass fraction and temperature for CUTF1 when RQL combustor geometry from NASA test rig is utilised in the stirred reactor model. Now the next section looks into the sensitivity analysis of the model by varying the model parameters in the Hephaestus for RQL combustor using CUTF1 combustor input constraints.

4.2.2 Sensitivity Analysis: CUTF1 RQL Model

There are three model parameters F1, F2, and F3 which guide the air or fuel-air mixture in the stirred reactors of the RQL combustor model (see Figure 3-5). The F4 is another parameter which is the percentage of air left from F3 and enters the quick-quench core given by equation 4-1:

$$\mathrm{F4} = [100 - (\mathrm{F1} + \mathrm{F3})]\% \qquad 4\text{-}1$$

The following analysis describes the impact of these parameters on the emission indices, equivalence ratio and temperature in the combustor zones.

All, the results are for CFM56-5B2 type engine CUTF1 at 100 % power setting for RQL combustor. Therefore, for a given prediction point, F1 to F3 varies while keeping all other combustor input parameters such as combustor inlet temperature, pressure, fuel flow and air mass flow constant.

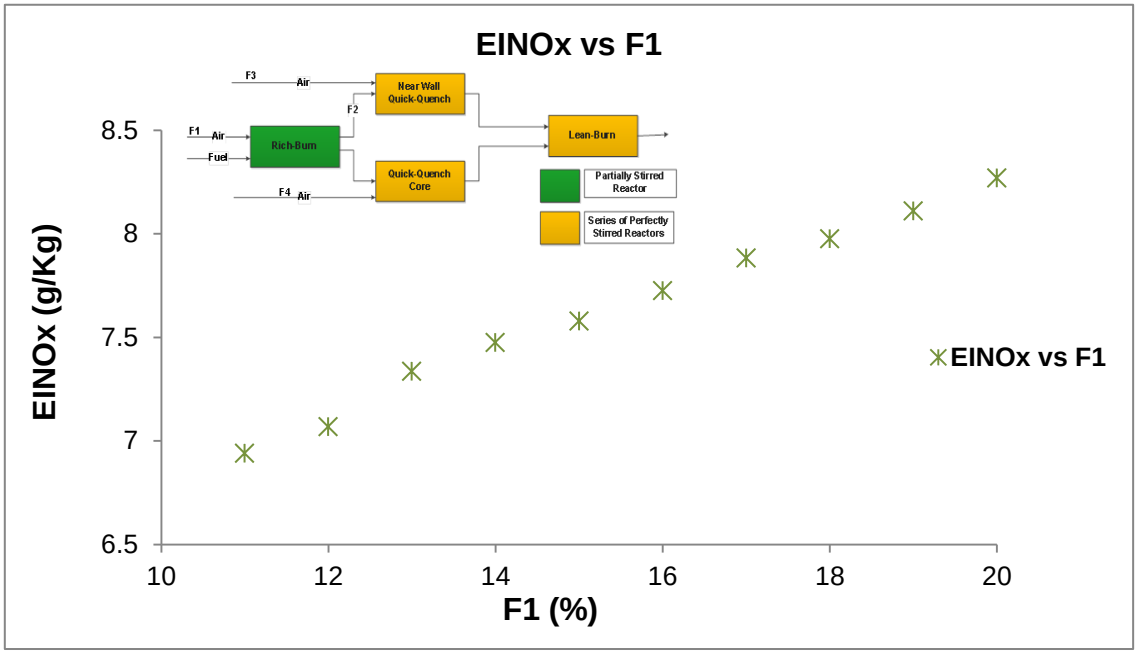

Figure 4-10: $EINO_X$ vs F1 (F2, F3, T3, P3, WA, Wff is constant)

The modelling factor F1 is the air mass flow input in the rich-burn section of the RQL combustor. As from the Figure 4-10, increase in air fraction inside the rich-burn section of RQL combustors provides abundance of oxygen molecule creates local stoichiometric regions within the rich-burn zone raising temperature and therefore increase the NO_X emission.

Whereas in Figure 4-11, increase in oxygen molecule start the oxidation reaction of carbon monoxide which is formed in rich-burn section of RQL combustor due to lack of oxygen. The oxidation reaction is an exothermic reaction releasing more energy in the system than it absorbs which further raises the temperature and accelerates the oxidation process. Due these processes carbon monoxide content reduces in the output of RQL combustor as the fraction of air F1 increases in the rich-burn section of RQL combustor.

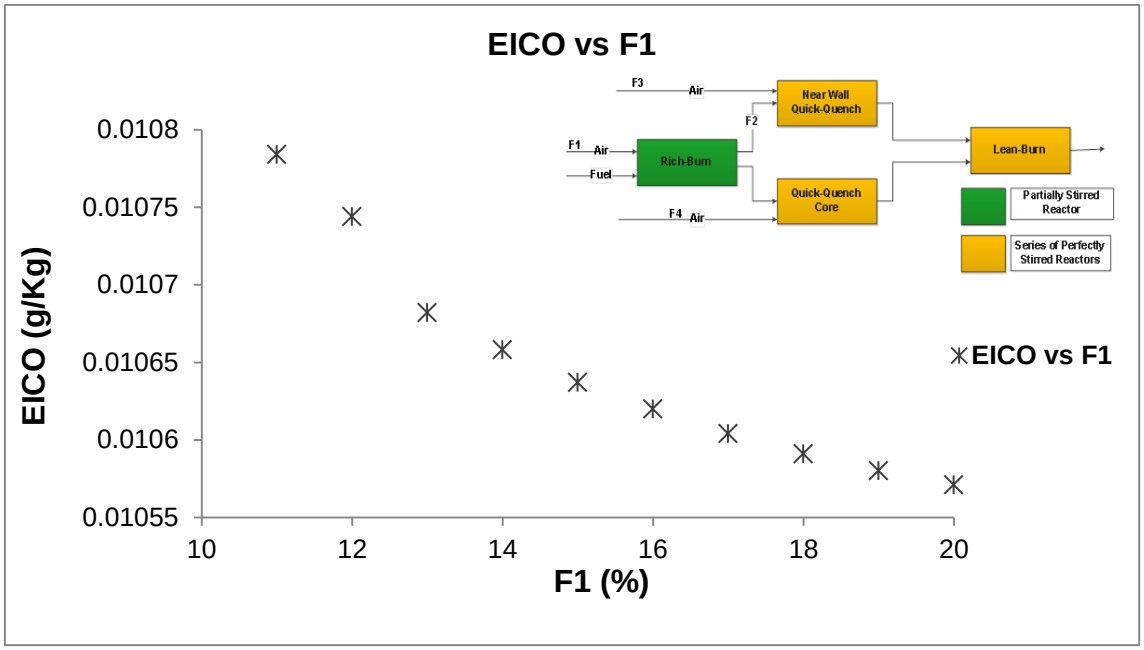

Figure 4-11: EICO vs F1 (F2, F3, T3, P3, WA, Wff is constant)

There are two series of perfectly stirred reactors which is used to model the quick-quench region of the RQL combustor; one is for the core section and the other for the Near-Wall (NW) as shown in Figure 4-12.

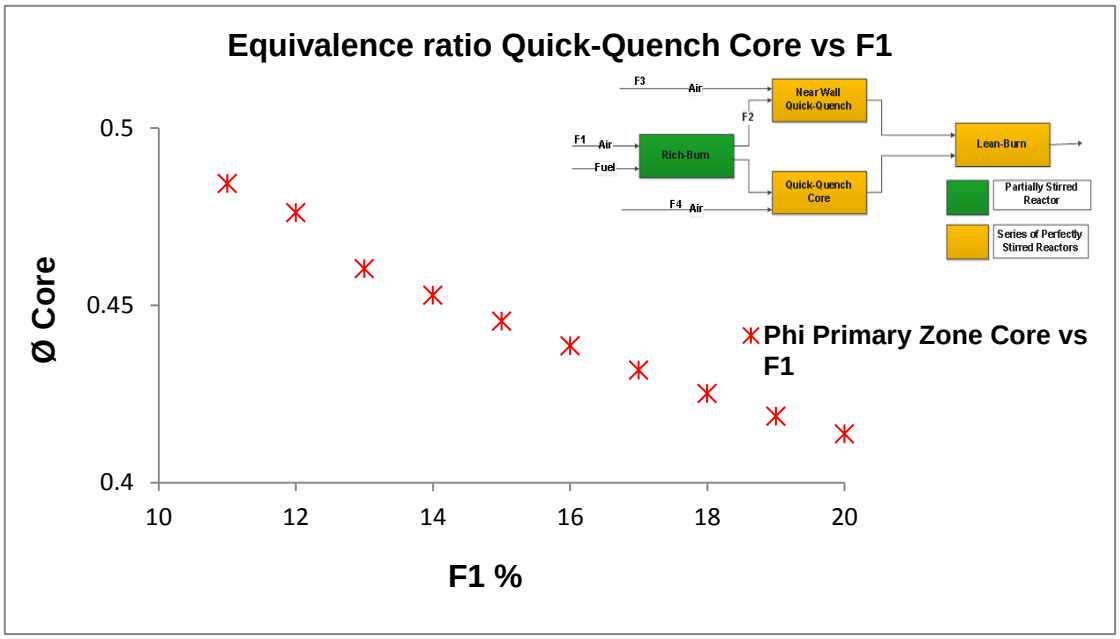

Figure 4-12: Equivalence ratio QQ Core vs F1 (F2, F3, T3, P3, W_A, W_{ff} is constant)

As more air enters the rich-burn section of the RQL combustor, more air is allowed to enter the quick-quench core section thereby reducing the

equivalence ratio in Figure 4-12. Whereas, in Figure 4-13, once more air is allowed to enter in the quick-quench core section, less air is available for the near-wall region thereby increasing the equivalence ratio of near-wall for a constant total airflow input to the RQL combustor.

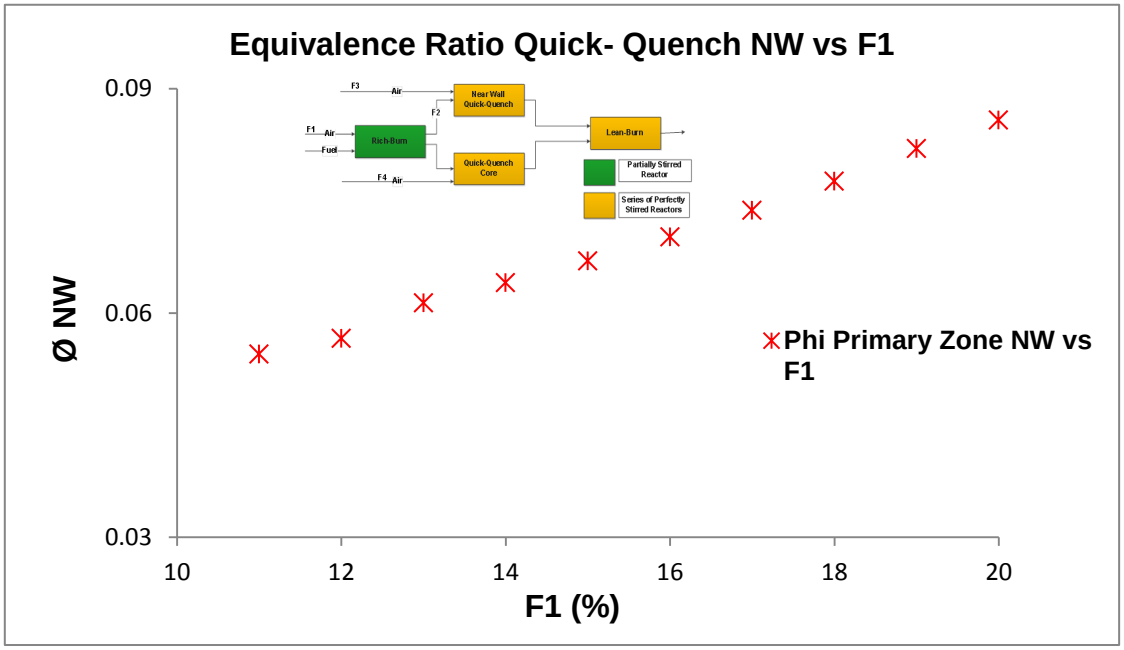

Figure 4-13: Equivalence ratio QQ NW vs F1 (F2, F3, T3, P3, W_A, W_{ff} is constant)

The modelling parameter F2 is the flow of effluent gases from rich-burn zone to the quick-quench which can't be governed in a real case scenario. Therefore, it is kept constant for a specific point for other modelling parameters sensitivity study. The stirred reactor model has the capability to vary the F2 parameter and comprehend the implication of it on the output. Therefore, just for a theoretical aspect, the result of sensitivity study on varying the F2 is presented here.

The Figure 4-14 -Figure 4-16 shows the effect of F2 on the emission indices and equivalence ratio. F2 is the percentage of effluent fuel-air rich mixture or burned gases in the rich-burned section of the RQL combustor entering into the near-wall region of quick-quench section. The left rich-burn effluent gases enter into the core section of quick-quench region of RQL combustor.

The Figure 4-14 shows that the NO_X emission decreases as F2 increases. The reason behind the increase is due to the lower temperature at the near-wall

region of quick-mix section because of cold compressor air addition at the near-wall of the RQL combustor. Therefore, as the rich burn gases enter the near-wall section of the quick-mix region, lower temperature attenuates the formation of NO_X. Whereas, this lowering of the temperature reduces the required temperature for oxidation reaction of carbon monoxide to carbon dioxide, leading to a slight increase in carbon monoxide as shown in Figure 4-15.

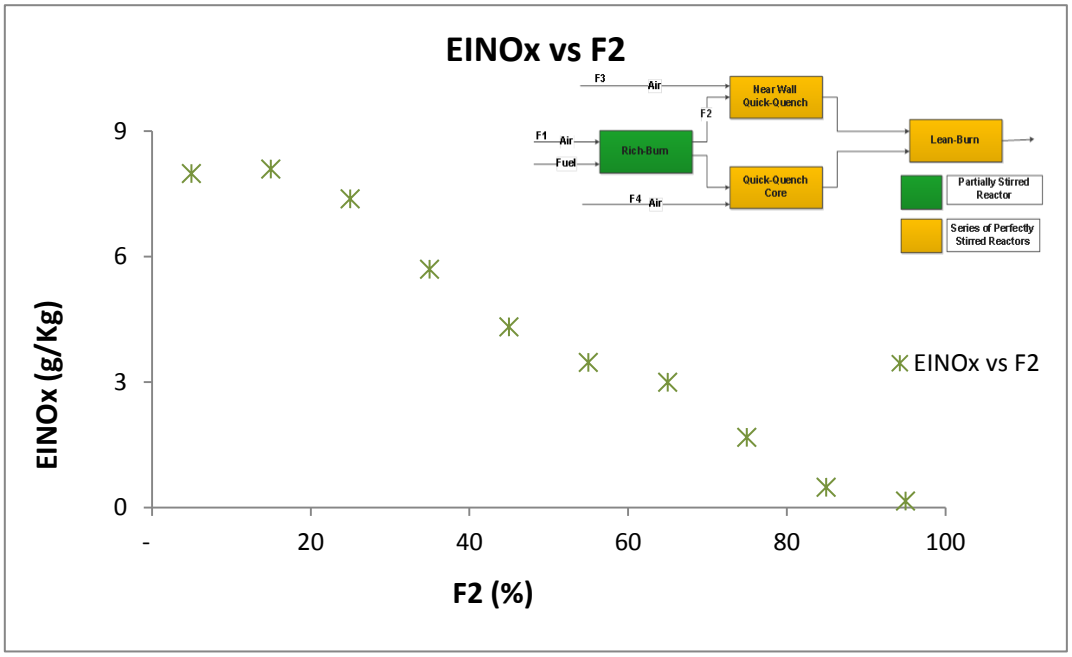

Figure 4-14: Comparison of EINOX with F2 when, F1, F3, T3, P3, W_A and W_{ff} is constant

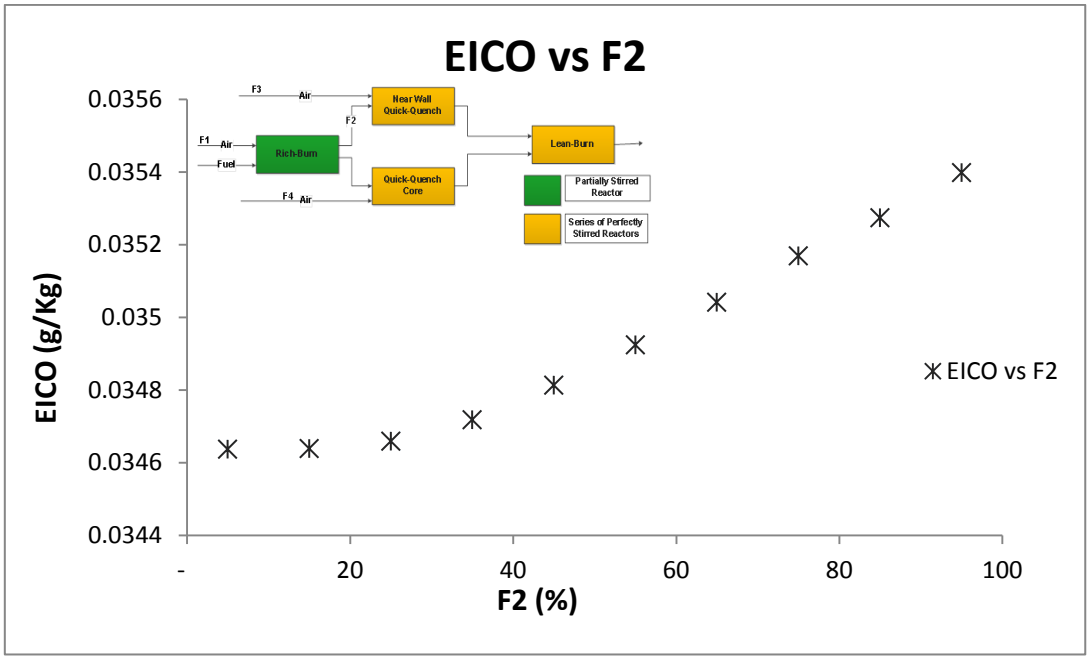

Figure 4-15: Comparison of EICO with F2 when, F1, F3, T3, P3, W_A and W_{ff} is constant

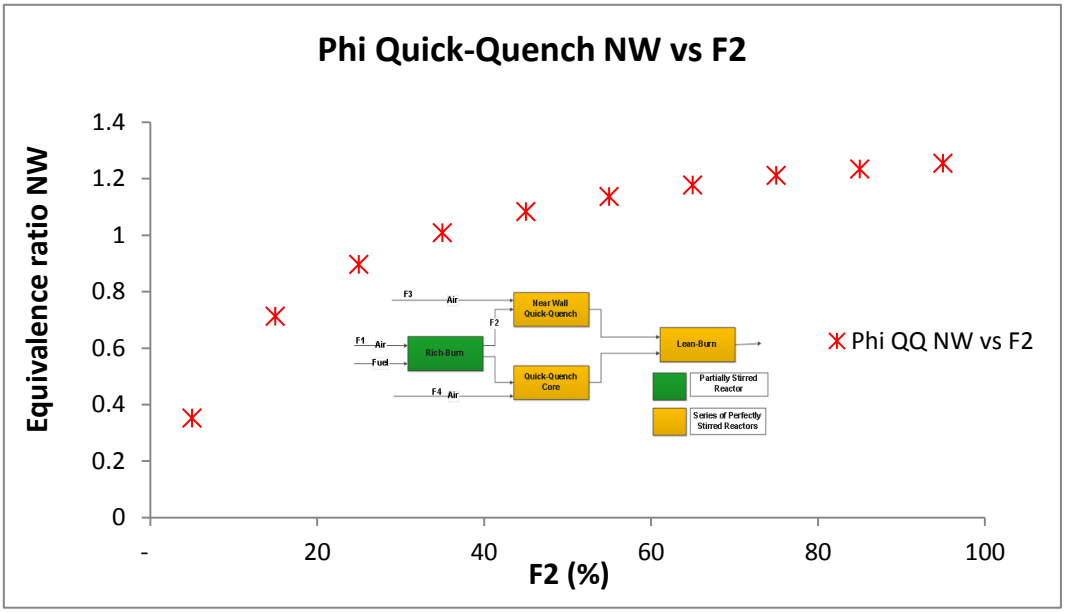

Figure 4-16: Comparison of PHI QQ NW with F2 when F1, F3, T3, P3, W_A and W_{ff} is constant

It is inferred from the Figure 4-16, that the equivalence ratio of the quick-quench near-wall increases as F2 increases. The reason behind the increase is the addition of fractions of gases into the near-wall section which are emanating

from the rich-burn section; hence, the amount of fuel droplets increases in the near-wall increasing its equivalence ratio.

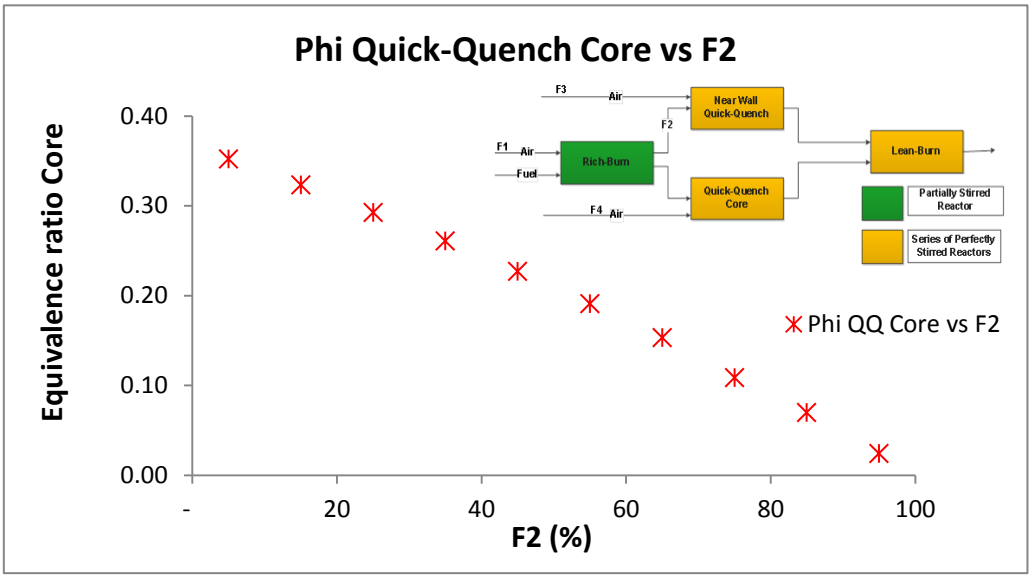

Figure 4-17: Comparison of PHI QQ Core with F2 when, F1, F3, T3, P3, W_A and W_{ff} is constant

Whereas in Figure 4-17, equivalence ratio of quick-quench core decreases because the fuel-rich effluent gases emanating from the rich-burn section with fuel droplets are accumulating in the near-wall region and less fuel droplets go in the quick-quench core section; reducing its equivalence ratio.

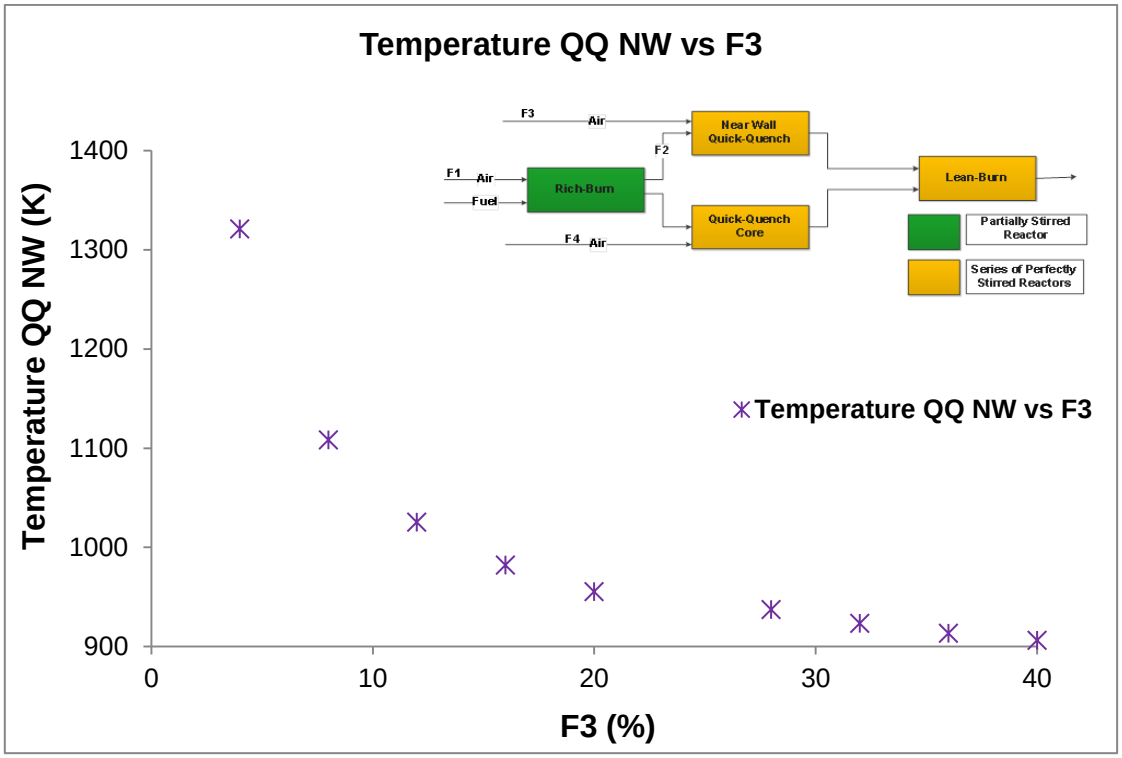

Figure 4-18: Quick-Quench Near-Wall temperature vs F3 (F1, F2, T3, P3, W_A, W_{ff} is constant)

The Figure 4-18 and Figure 4-19 describes the effect of air intake F3 into the near-wall section of quick-quench region in the RQL combustor. In this case, it is assumed in the model that 95% of effluent gases from the rich-burns section enter into the core of quick-quench region and only 5% enter into the near-wall region. Therefore, the majority of combustion reaction takes place in the quick-quench core section for this case.

It is observed from Figure 4-18 and Figure 4-19 that the temperature and equivalence ratio decreases at near-wall of quick-quench region, as F3 increases. This decrease in equivalence ratio and temperature is due to the addition of cooler air from the compressor, which enters the quick-quench section at the near-wall first, thereby reducing its equivalence ratio and temperature. The second reason is less fuel rich gases (5%) are available in the near wall section for the combustion and more in the core (95%).

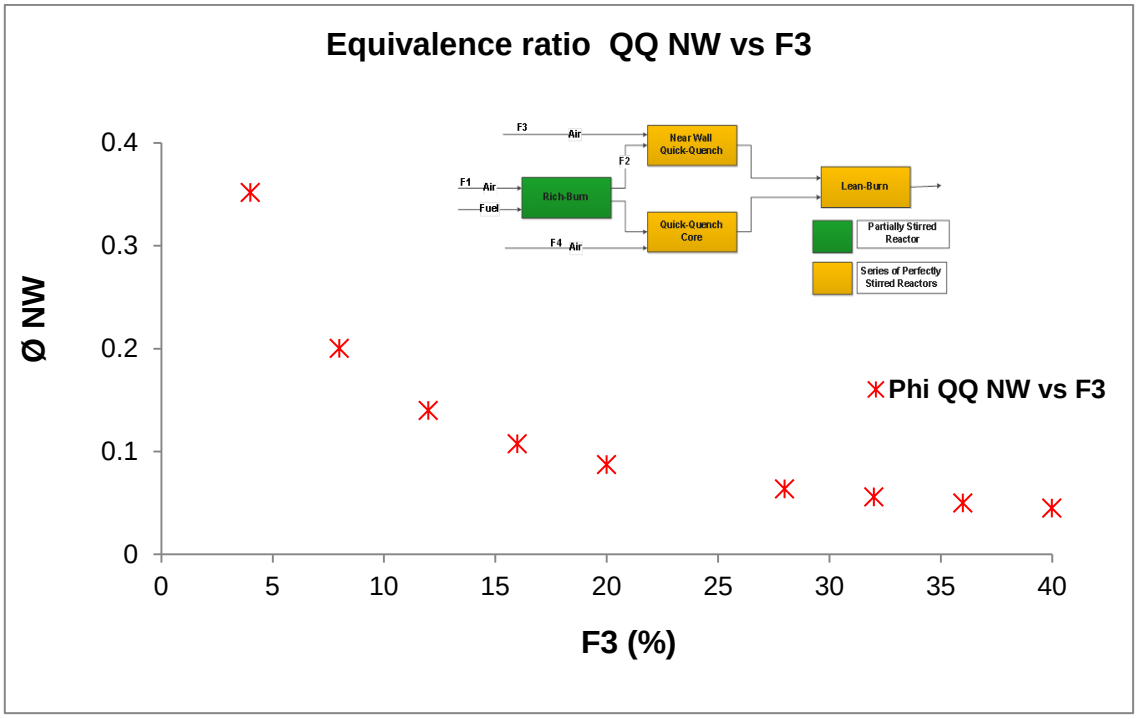

Figure 4-19: Equivalence ratio Quick-Quench NW vs F3 (F1, F2, T3, P3, W_A, W_{ff} is constant)

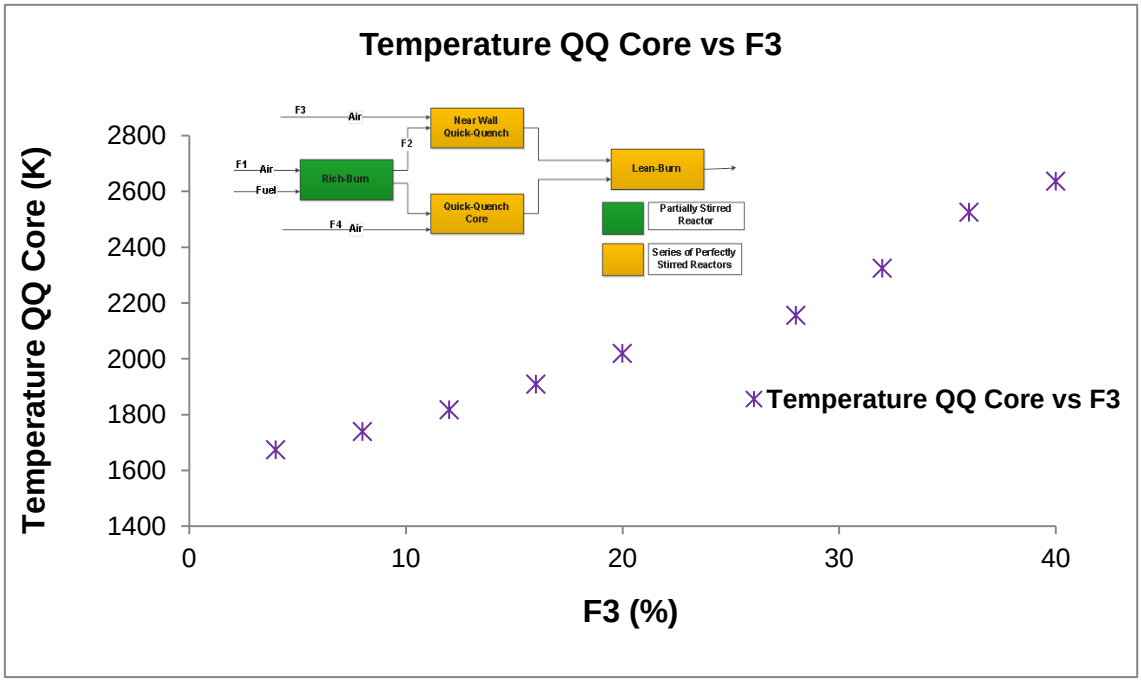

Figure 4-20: Quick-Quench Core temperature vs F3 (F1, F2, T3, P3, W_A, W_{ff} is constant)

Whereas, in Figure 4-20, temperature of the quick-quench core section increases as 95% of rich-burn gases are available in the core section for the combustion thereby increasing the temperature to more than 1850 K.

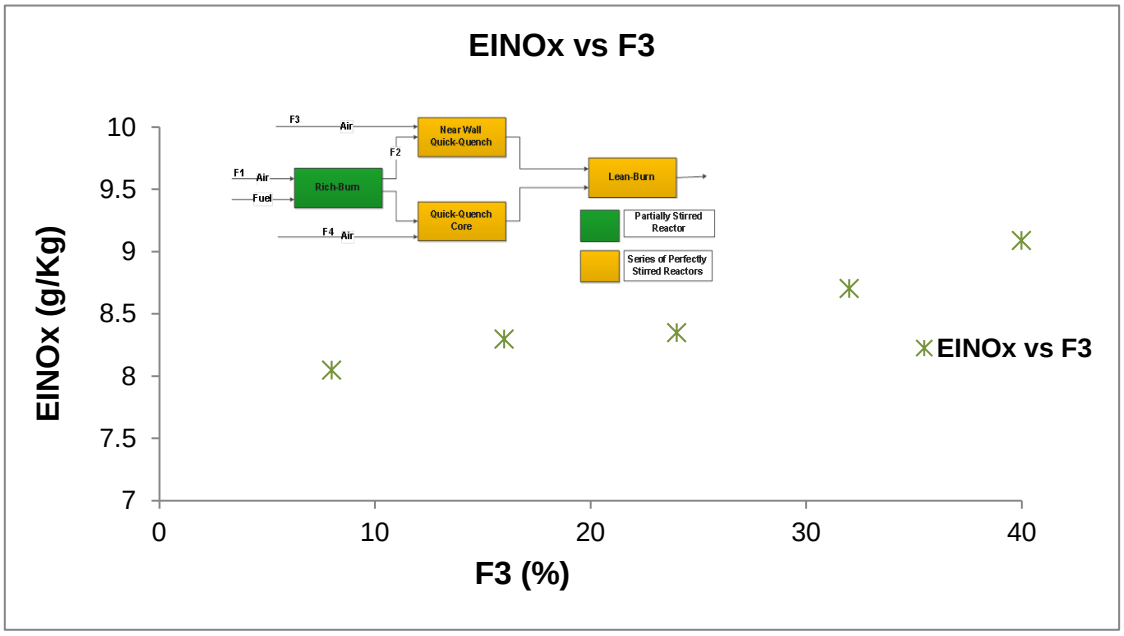

Figure 4-21: $EINO_X$ vs F3 (F1, F2, T3, P3, W_A and W_{ff} is constant)

It is observed from Figure 4-22 that the equivalence ratio increases with increase in F3. Rise in equivalence ratio towards the stoichiometric region raises the temperature to more than 1850 K as shown in the Figure 4-20. From section 2.5, it is inferred that the temperature has an exponential effect in increasing the NO_X formation in a combustor. Therefore, in Figure 4-21, NO_X increases with increase in F3 due to the rise in temperature in the core section of quick-quench region where almost all the combustion is taking place.

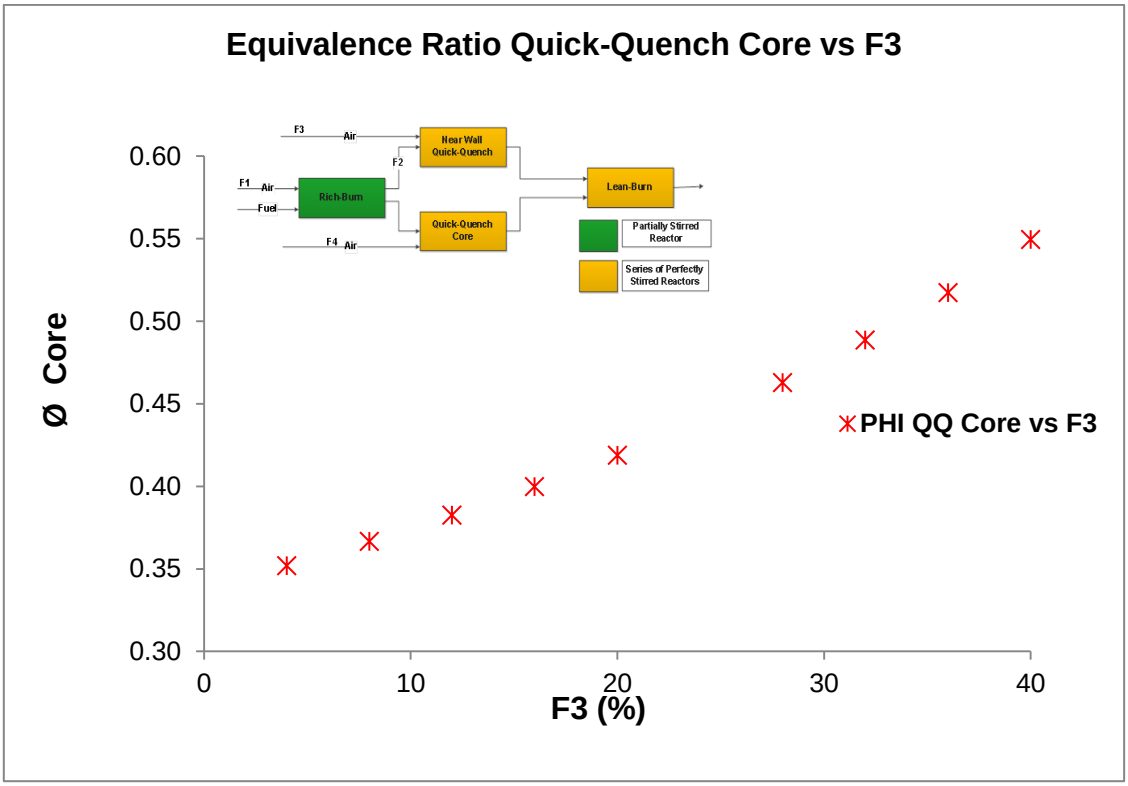

Figure 4-22: Equivalence Ratio Quick-Quench Core vs F3 (F1, F2, T3, P3, W_A,W_{ff} is constant)

The next section discusses the NO_X emission result from the RQL combustor for LTO cycle and compares with the International Civil Aviation Organisation (ICAO) LTO cycle NO_X regulations.

4.2.3 RQL combustor NOx prediction for LTO cycle

The section 2.4.3 describes the ICAO NO_X emission standard regulations set for the Landing and Take-Off (LTO) cycle for an aircraft engine. The LTO NO_X is calculated by computing the total NO_X emission from the aircraft engine at four modes (Take-off, approach, landing & taxi). The NO_X emission at a particular mode is the product of emission index, fuel-flow and time in that mode. The Table 4-2 shows all the values of CFM56-5B2 type CUTF1 engine from the ICAO emission databank. The DP/F_{oo} is the NO_X characteristics for LTO cycle given represented as the total NO_X in the LTO cycle divided by the take-off thrust as sea level static.

The Figure 4-23 shows various ICAO LTO cycle limits comparison for different overall pressure ratio. For higher overall pressure ratio, the combustor inlet temperature increases and hence the NO_X production in the combustor. It is observed from the Figure 4-23 that RQL combustor for the CUTF1 engine outperforms in terms of NO_X emission when compared to the conventional combustor counterpart.

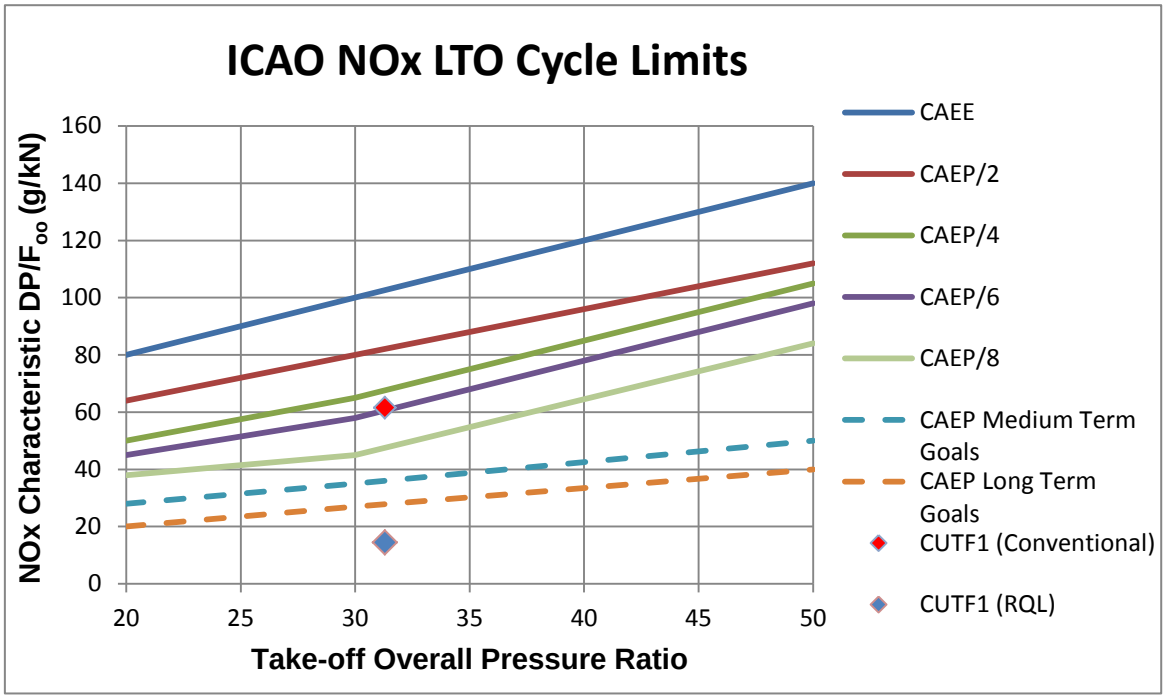

Figure 4-23: ICAO NO_X LTO Cycle limits

Although, the RQL combustor has advantage of NO_X reduction over the conventional combustor, its incorporation in the jet engine has certain constrains:-

- Firstly the size of the RQL combustor has to be similar to that of a conventional combustor in order to integrate it with the current jet engines. As, longer combustor (in case of this test rig NASA combustor) would require longer spool or shaft to connect the compressor and turbine which increases the weight and the torsion which may result in reduction of life of the engine.

- Secondly, the pressure loss across the combustor would be higher compared to a conventional annular combustor due to cold and hot losses as the NASA RQL combustor is longer.
- Thirdly, the NASA RQL combustor is a tubular combustor; therefore it would be much heavier compared to annular aero engine combustors.
- Although the RQL combustor has a wider stability limit compared to the lean premixed combustors, it is obligatory to check the altitude-relight capability of the combustor in case of a flame-blow out at higher altitude. A process where air flowing through an unlit engine causes spool rotation is called windmilling [99]. Windmilling is explained briefly in the next section.

The next section looks into these constraints of a jet engine for the incorporation of the RQL combustor in case of flame-blow out at higher altitude.

4.3 Case study: RQL Combustor at windmilling condition

In case of flame-blowout of an aero engine at higher altitude when there is no combustion taking place and the spool rotation is due to the air mass flow through the engine, it is called windmilling of the engine.

Relight at windmilling conditions are certification requirements for any novel combustor design. According to Fletcher [99], the key performance parameters vital for altitude relight during windmilling are:

- Combustor size, combustor entry pressure, temperature and mass flow
- Power which can be extracted from the engine
- The engine drag during windmilling, which is caused by the air slowing down as it passes through the engine

In order to estimate the combustor size, windmilling flame-out scenario is the basic requirement for a combustor in an aero engine. The theta parameter can be used to size a combustor as shown in Figure 2-14 and given by,

$$\theta = \left[\frac{P_3^{1.75} A_{ref} D_{ref}^{0.75} exp\left(\frac{T_3}{300}\right)}{\dot{m}_A}\right] \quad 4\text{-}2$$

As explained in the section 2.7.4, the combustor reference area A_{ref} and the diameter D_{ref} of the combustor inlet can be deduced from the equation 4-2 once the combustor inlet pressure, temperature and mass flow is known. The theta parameter can be plotted from the curve in Figure 2-14 for a given combustion efficiency.

In order to compute the inlet conditions (temperature, pressure and mass flow) for the jet engine combustor for a free windmilling case, charts from [99] for temperature and pressure ratios has been utilised.

The parameters required to calculate the combustor inlet conditions for the free windmilling and not locked rotor windmilling (where the high pressure spool is mechanically prevented from rotating) are:

- Design point bypass ratio
- Design point overall pressure ratio
- Maximum operating altitude of the aircraft,
- Mach number corresponding to the maximum operating altitude,
- Engine inlet area,
- Specific take-off thrust at sea level static

The combustor inlet pressure and temperature can be calculated from the Figure 4-24 and Figure 4-25 from [99].

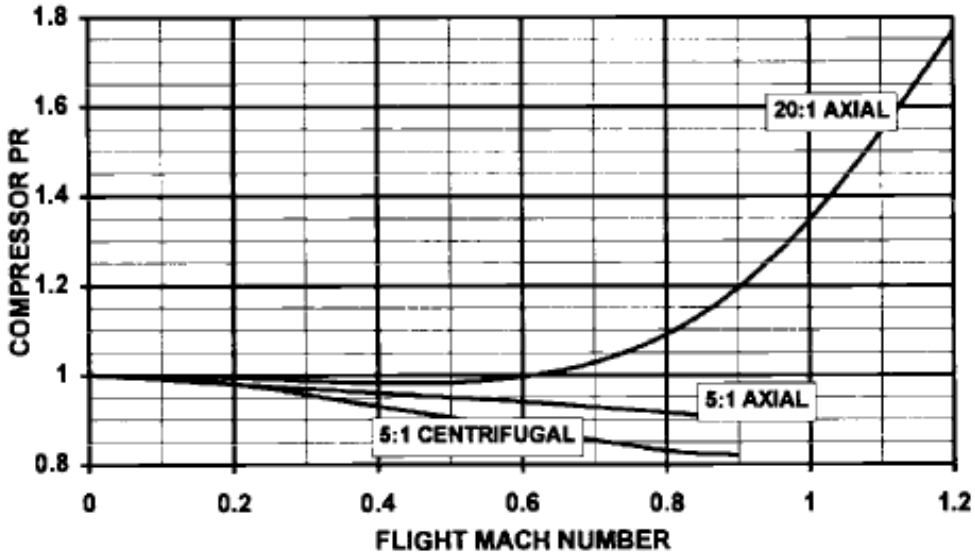

Figure 4-24: Compressor PR vs Flight Mach Number for one or two spool turbojet engine [99]

The ambient conditions at an altitude for pressure, temperature, relative humidity for a standard atmosphere, MIL-STD (Military standard) hot day and MIL-STD cold is summarised by Fletcher [99]. The charts can be used to define the inlet conditions at an altitude for the engine. In order to calculate the combustor inlet pressure and temperature, Figure 4-24 and Figure 4-25 provides the compressor pressure and temperature ratios which can be multiplied to the ambient MIL-STD conditions to give the combustor inlet pressure and temperature at an altitude for windmilling scenario for one or two spool turbojet engines.

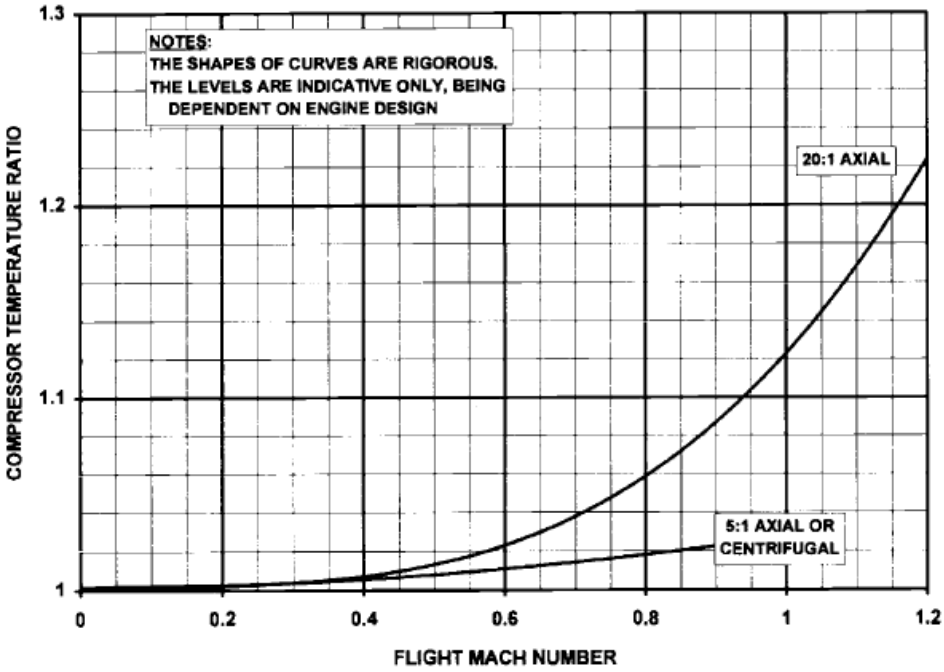

Figure 4-25: Compressor TR vs Flight Mach Number for one or two spool turbojet engine [99]

In case of windmilling in turbo fan engine, the bypass duct in the engine presents the least resistance to the ram pressure at the fan, hence most of the air mass flow bypasses the engine core. According to Fletcher [99], turbofan engines with bypass ratio of 5:1 has a windmilling bypass ratio of as high as 80:1 and for lower bypass ratios, it will be proportionally lower.

As, the bypass ratio increases during windmilling, the compressor pressure ratio falls gradually, thus a factor of around 0.6 must be applied to compressor delivery pressure for a turbofan of 5:1 bypass ratio relative to a turbojet.

The combustor inlet mass flow can be calculated from the two charts [99] as shown in Figure 4-26 and Figure 4-27.

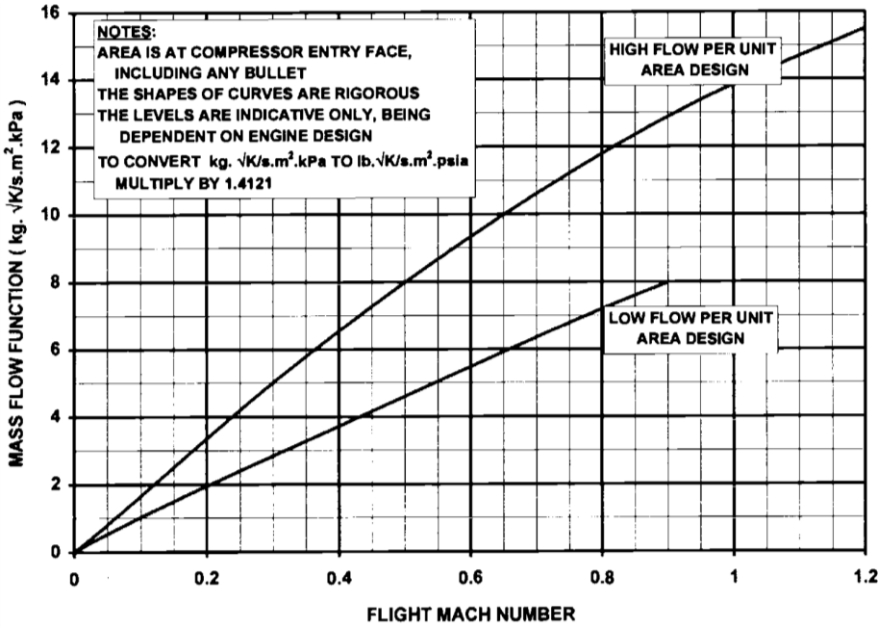

Figure 4-26: Turbojet windmlling: mass flow function vs flight Mach number

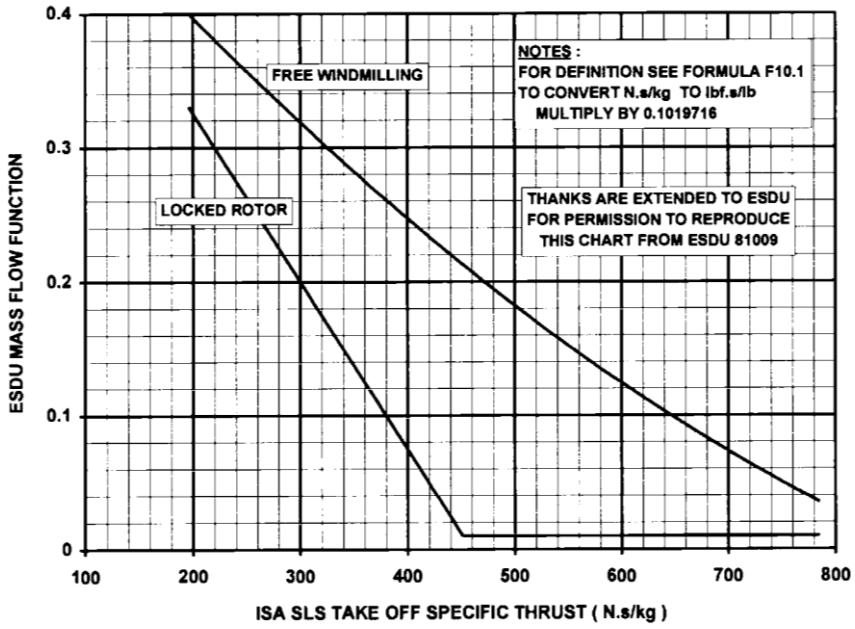

Figure 4-27: Turbojet and turbofan windmilling: ESDU mass flow function vs specific thrust

Engineering Sciences Data Unit (ESDU) mass flow function is the function of mass flow, gas constant, total temperature, area, total pressure and Mach number and is given in ESDU document [100] by the equation 4-3.

$$ESDU\ W_{flow\ Fn} = \left[\frac{\dot{m}_A * \sqrt{R * T_3}}{A_{inlet} * P_3 * fn(M_a)}\right] \quad \text{4-3}$$

Where,

$ESDU\ W_{flow\ Fn}$ = ESDU mass flow function

$\dot{m}_A$ = Combustor inlet air flow

R = Gas constant

T_3 = Combustor inlet temperature

A_{inlet} = Engine inlet area

P_3 = Combustor inlet pressure

$fn(M_a)$ = Mach number function which is given by:

$$= \left[\frac{M_a * \sqrt{\gamma}}{(1 + 0.5 * (\gamma - 1) * M_a^2)^{\left\{0.5 * \frac{(\gamma+1)}{(\gamma-1)}\right\}}}\right] \quad \text{4-4}$$

Where,

M_a = Mach number

γ = Gamma, ratio of the specific heat at constant pressure to that at constant volume

4.3.1 Case Study: Windmiling for NASA test rig experiment

The NASA test rig experiment as described in section 3.2 was conceded at sea level static temperature and pressure for emission prediction. As per the altitude relight requirement of a combustor, this section carries out a quantitative analysis of the NASA test rig combustor for flameout windmilling scenario if flown in an aero engine at an altitude 10,000m. Although the length of the combustor is 94 cm, which is long for an aero engine, this is assumed that no major change in the design of a single spool turbojet is done. The turbojet with an axial flow compressor of design point pressure ratio of 5:1 and an inlet area

of 0.1m^2 is free windmilling at 10,000m, standard day and 0.6 flight Mach number. From the Table 4-1, combustor inlet parameters are selected given in Table 4-3.

Table 4-3 Selected Engine Inlet Parameters from RQL NASA'S test rig

T3 (K)	P3 (atm)	Air mass flow (kg/s)	Fuel Flow (Kg/s)
585	5.4	2.717	0.1057

After carrying out the design point calculation for the above input parameters, specific thrust of 712 m/s is obtained.

According to Lefebvre [5], the minimum efficiency required for an altitude relight condition is 80%. Therefore, in this case, theta parameter is calculated for a single turbojet engine with an inlet of 0.1m^2, fitted with the NASA test rig combustor geometry which is windmilling after flame blowout at 10,000m.

In order to calculate the mass flow, pressure and temperature at the 10,000m, charts from the Walsh & Fletcher [99] is used as shown in Figure 4-24, Figure 4-25, Figure 4-26, and Figure 4-27. The chart is curve fitted to calculate various parameters with the polynomial equations as shown in

Figure 4-28,

Figure 4-29 and Figure 4-30.

Figure 4-28 shows the curve fitting of compressor temperature ratio for a given Mach number for an engine with pressure ratios of 20:1 and 5:1. The polynomial equation to calculate the temperature pressure ratio with PR of 20:1 is given by equation 4-5 with the error of 0%. Whereas, the equation to calculate the temperature pressure ratio with PR of 5:1 is given by equation 4-6 with the error of 0% in plotting the polynomial equation.

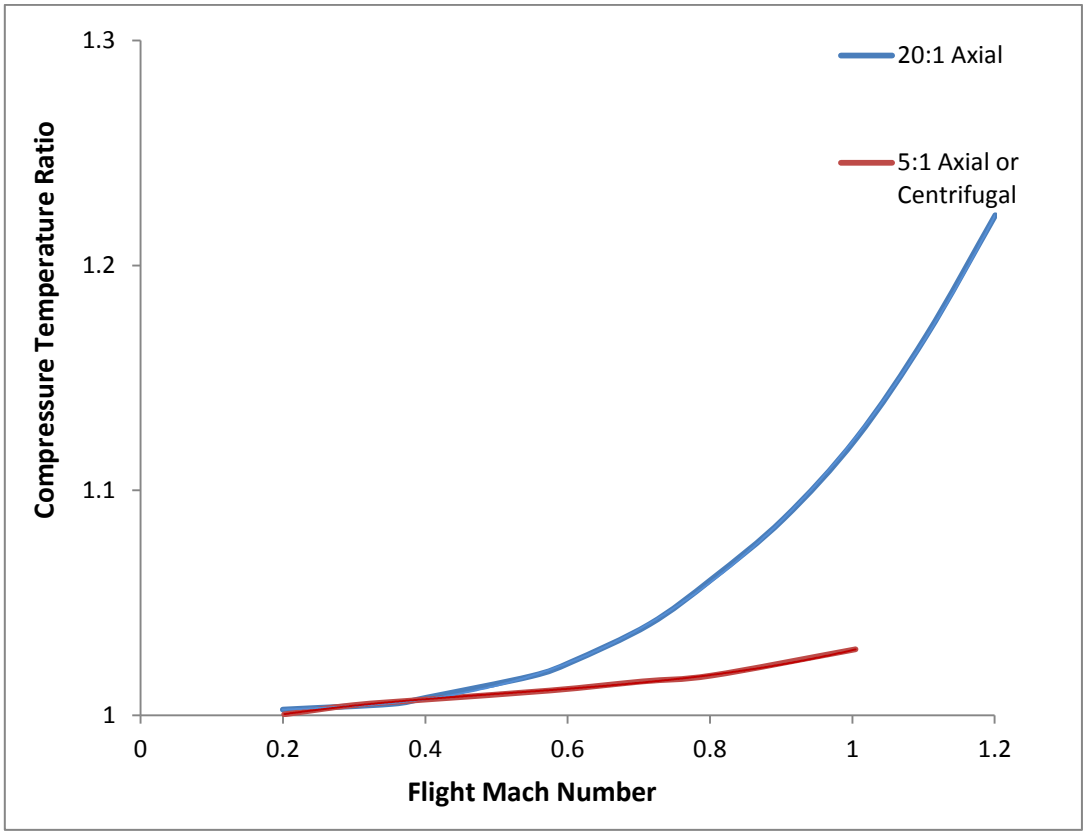

Figure 4-28: Curve fitting of Compressor TR vs Mach number

$$Temperature\ Pressure\ Ratio\ 20{:}1 = 0.1232Ma^5 - 0.4015Ma^4 + 0.6575Ma^3 - 0.3343Ma^2 + 0.0819Ma + 0.9948 \quad (4\text{-}5)$$

$$Temperature\ Pressure\ Ratio\ 5{:}1 = -0.0029Ma^4 + 0.081Ma^3 - 0.1208Ma^2 + 0.0839Ma + 0.9878 \quad (4\text{-}6)$$

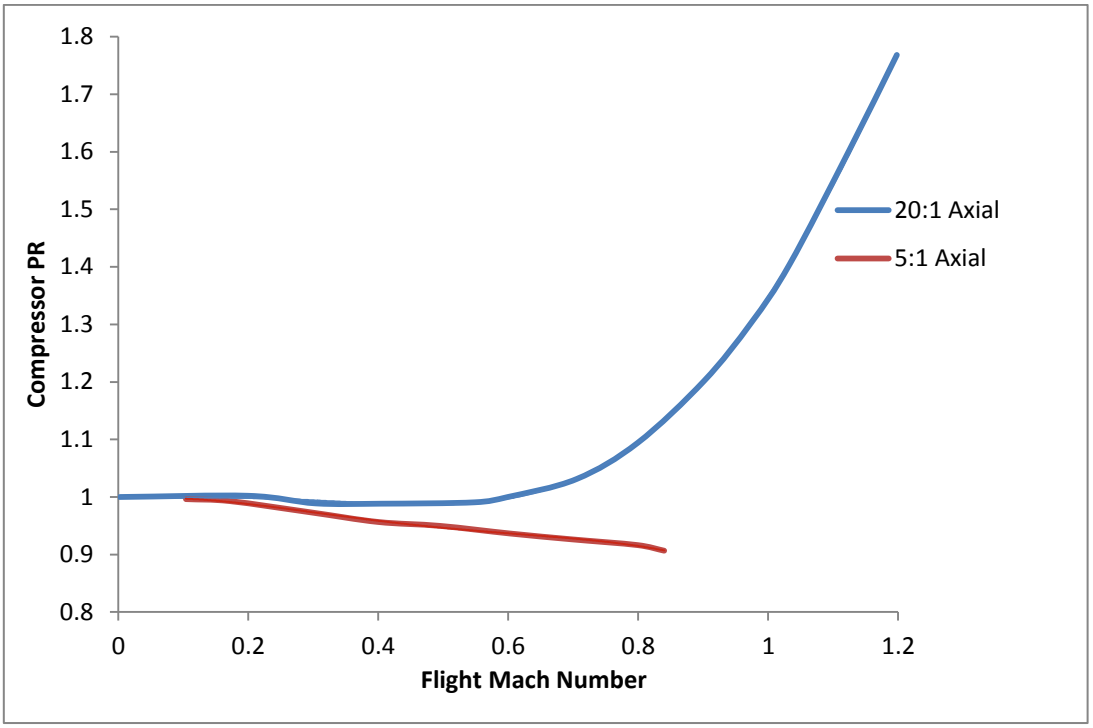

Figure 4-29: Curve fitting of Compressor PR vs Mach number

Figure 4-29 shows the curve fitting of compressor pressure ratio for a given Mach number for an engine with pressure ratios of 20:1 and 5:1. The polynomial equation to calculate the compressor pressure ratio of 20:1 is given by equation 4-7 and PR of 5:1 is given by equation 4-8.

$$Compressure\ Pressure\ Ratio\ 20{:}1 = -1.2249Ma^5 + 3.6112Ma^4 - 2.5773Ma^3 + 0.5931Ma^2 - 0.0546Ma + 1.0006 \quad (4\text{-}7)$$

$$Compressor\ Pressure\ Ratio\ 5{:}1 = -0.9783Ma^4 + 1.8026Ma^3 - 1.0935Ma^2 + 0.123Ma + 0.9941 \quad (4\text{-}8)$$

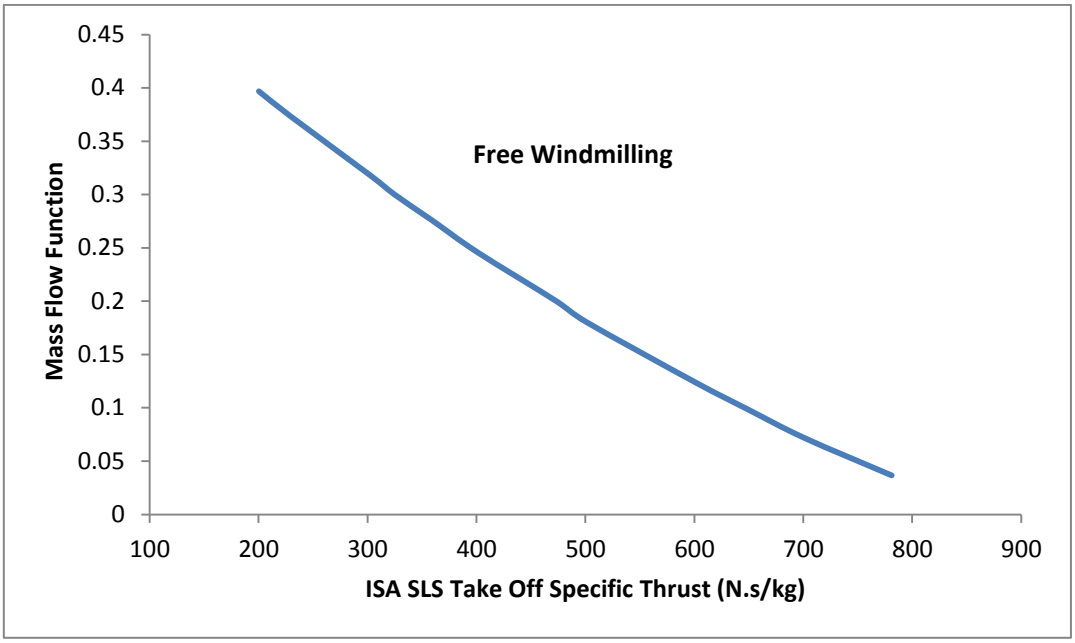

Figure 4-30: Mass Flow function from ESDU vs the Specific Thrust

$$ESDU\ Mass\ Flow\ Function\ = 3 * 10^{-7} * x^2\ -\ 0.001 * x\ +\ 0.5748 \qquad 4\text{-}9$$

Where $x =$ ISA SLS take-off specific thrust

The results for compressor pressure ratio, temperature ratio, ambient temperature (T1) and pressure (P1) at 10,000m, combustor inlet temperature (T3) and pressure (P3) and the mass flow function from the plotted charts for specific thrust 712 m/s and Mach number 0.6 is shown in Table 4-4:

Table 4-4: Results from the charts for combustor input parameters

Compressor PR	Temperature PR	T1 (K)	P1 (kPa)	T3 (K)	P3 (kPa)	Mass Flow Function
0.95	1.01	223.2	26.435	225.43	25.11	0.07

In order to calculate the inlet mass flow $\dot{m}_A$ of the combustor , all the values from the Table 4-4 is placed in equation 4-3 which can be re-written as

$$0.07 = \left[\frac{\dot{m}_A * \sqrt{287.05 * 225.43}}{0.1 * 25110 * fn(M_a)}\right] \quad 4\text{-}10$$

In order to calculate$fn(M_a)$ for the mass flow function, equation 4-4 can be re-written after putting all the values as:

$$fn(M_a) = \left[\frac{0.6 * \sqrt{1.4}}{(1 + 0.5 * (1.4 - 1) * 0.6^2)^{\left\{0.5 * \frac{(1.4+1)}{(1.4-1)}\right\}}}\right] \quad 4\text{-}11$$

$$fn(M_a) = 0.576$$

Therefore after putting the value of $fn(M_a)$ in equation 4-10,

$\dot{m}_A$ = 0.42 kg/s

Now, putting the values of P3, T3, mass flow, A_{ref} and D_{ref} (Table 3-1), theta parameter is calculated as shown by equation 4-12.

$$\theta = \left[\frac{25110^{1.75} * 0.031 * 0.152^{0.75} * exp\left(\frac{225.43}{300}\right)}{0.42}\right] \quad 4\text{-}12$$

$$\theta = 0.19 * 10^7$$

In order to be able to predict the combustor ignition ability for blame blowout at higher altitude, theta parameter is plotted by fitting curve against the efficiency of the combustor from Figure 2-14, Lefebvre [5; 68]. The curve fitting of the theta parameter is shown in Figure 4-31.

The above result of $\theta = 0.19 * 10^7$ is plotted in Figure 4-31 (blue star) for the combustion efficiency of 0.8, which generally is the minimum efficiency required for the altitude relight [5]. It is found from Figure 4-31, that the curve of theta parameter is close to 0 and outside the plotted area of combustion region. Hence, the sizing assessment of NASA test rig RQL combustor design doesn't meet the necessary certification criteria for altitude relight at 10000m. This

implies that for a given Dref T3, P3, and mass flow, the NASA test rig geometry cross sectional area of the combustor is not designed large enough to be able to sustain a relight at the altitude of 10,000m.

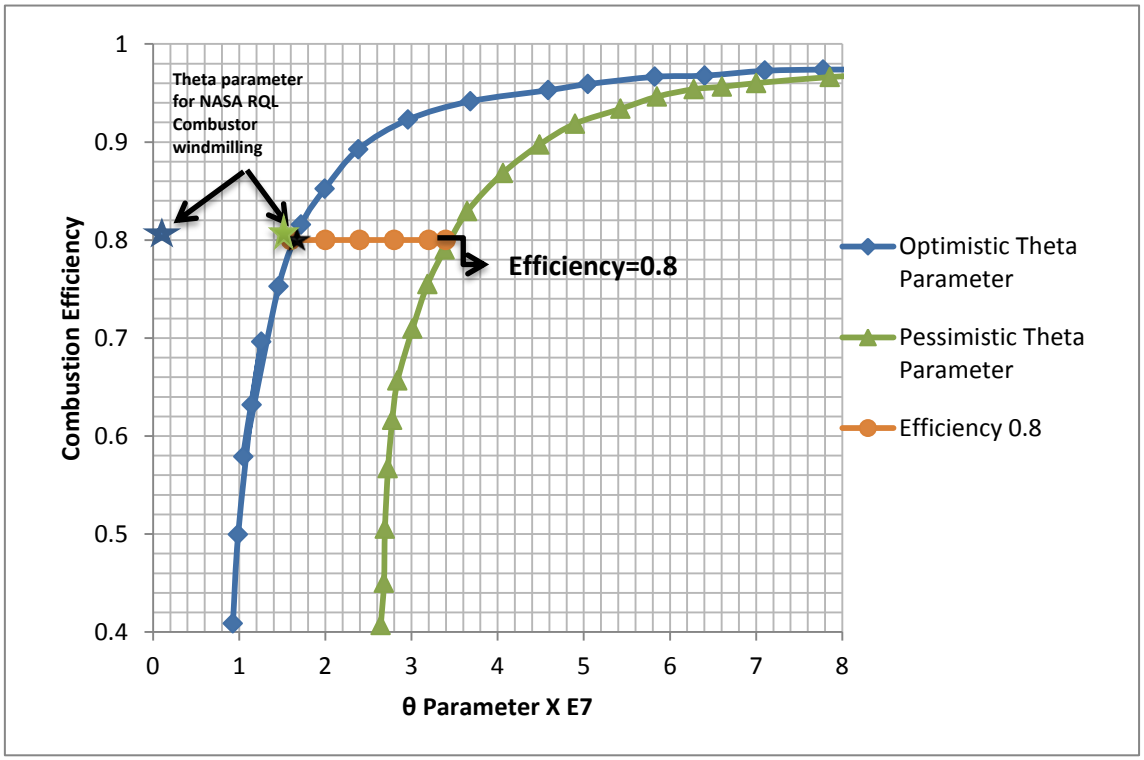

Figure 4-31: Curve fitting of the Theta Parameter

As, NASA RQL combustor is a single tube combustor which is a section representation of an axial combustor and the theta curve method used in this study is based on the axial combustor. Therefore, the modification in NASA's combustor geometry is needed in order to relight at 10,000m altitude.

In order to calculate the reference area for the NASA's combustor geometry, a theta parameter for the worst scenario of altitude relight condition is selected. Lefebvre [5] has proposed that generally combustion efficiency of 80% is required for the altitude relight condition. Therefore, according to Figure 4-31, a theta parameter of 1.6*10^7 is selected (green star) for combustion efficiency of 80% for the smallest combustor size.

Now, putting all the values of P3, T3, mass flow, theta parameter and Dref in equation 4-12, the Aref is calculated to be 0.26m^2.

Liu [101] carried out a study for the combustor sizing using Lefebvre's theta parameter [5]. The ratio of reference area to reference diameter of a combustor was found to be 1.8. Using this relation the reference area of the NASA test rig RQL combustor geometry would be 0.274m^2 (where D_{ref}=0.152m from Table 3-1).

Putting this new value of reference area in 4-12 keeping all other parameters as same from the previous case, the resultant theta parameter $\theta = 1.68 * 10^7$. The plotted point (black star) in Figure 4-31 shows this modified combustor geometry for the combustion efficiency of 0.8 suitable for relight. Figure 4-31 shows that the theta parameter is within the envelope of defined combustion area and hence the relight is possible at 10,000m for the RQL combustor.

4.3.2 Case Study: Windmiling for V2500 combustor

In order to verify the methodology used to analyse the sizing requirement in the case of the NASA test rig experiment, another working aircraft engine combustor (V2500) is considered. The V2500 engines' flange to flange length is 3.2m and fan tip diameter is 1.6m [102].

As V2500 engine is already in service, it must have passed the altitude relight certification criteria. Janes Aero-engine [102] provides the geometry of the jet engine, which gives A_{ref}=0.2315 m^2 and D_{ref}=0.284m. The theta parameter is calculated for V2500 combustor for attitude relight at 10,000m and plotted in the theta parameter versus combustion efficiency graph shown in Figure 4-32 (small green star). The Figure 4-32 shows that the theta parameter for V2500 combustor is within the required envelope of altitude relight.

It clearly shows that V2500 combustor certifies the altitude relight scenario with the existing geometry and verifies the methodology which has been taken in this report for the altitude relighting capability of the NASA test rig combustor.

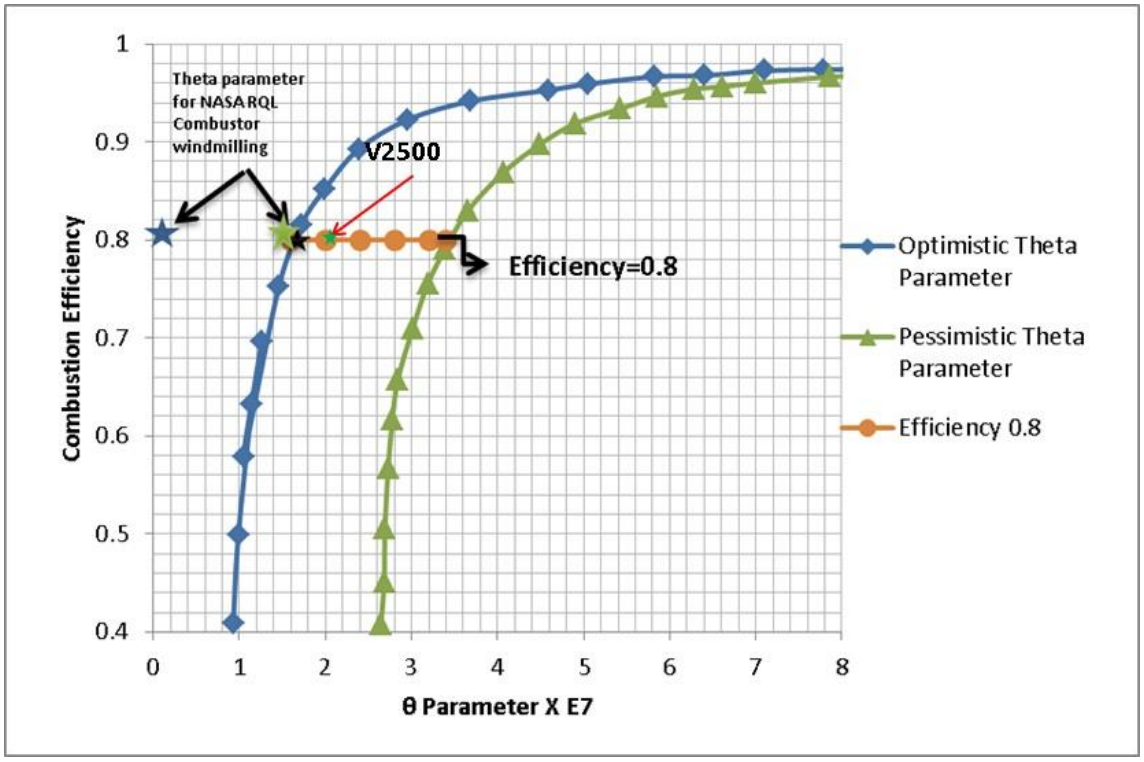

Figure 4-32 Theta parameter for V2500 combustor

The sensitivity analysis of NASA RQL combustor geometry is performed with change in theta parameter for the altitude re-light conditions at 10,000m.

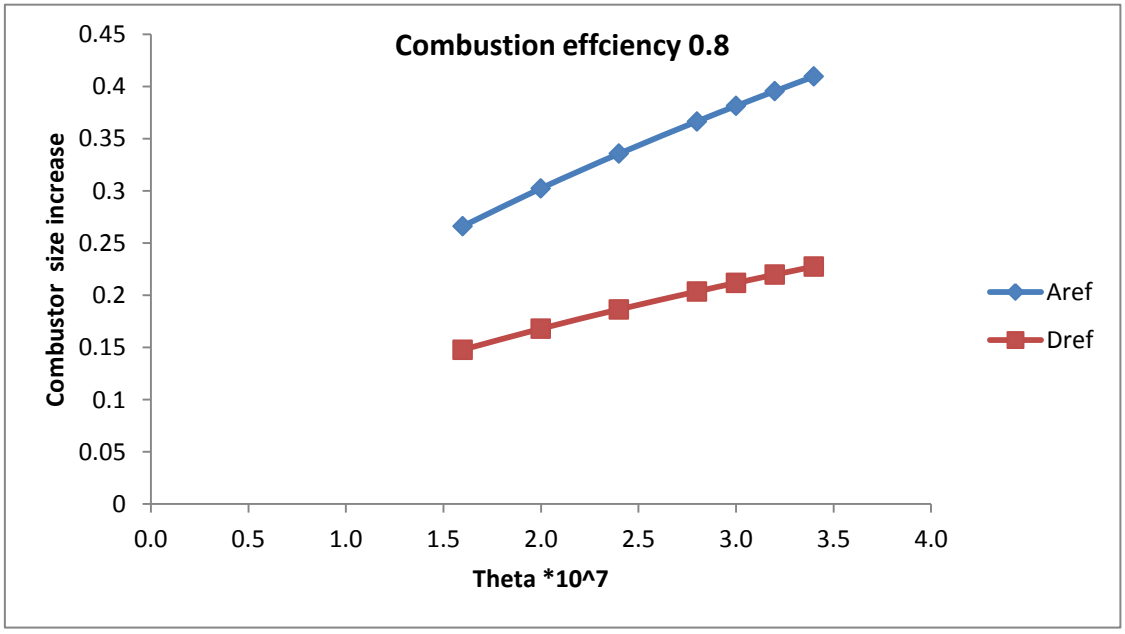

Figure 4-33: Combustor RQL geometry variation: Combustion Efficiency 0.8

Figure 4-33 shows the reference area and diameter of the combustor increases as the theta parameter increases from the optimistic scenario of 1.6*10^7 to maximum 3.4*10^7 which a pessimistic scenario for 80% combustion efficiency. Therefore, the reference area of the combustor varies from 0.27m^2 to 0.40m^2 and the reference diameter of the combustor varies from 0.14m to 0.22m for the altitude relight condition. Below the optimistic theta parameter of 1.6*10^7, the combustor will not ignite due to rich ignition limit and small size of the combustor. The pessimistic theta parameter of 3.4*10^7 and above lies outside the shaded area of the combustion from Figure 4-31, hence there will be no ignition as the size of the combustor is substantially large for the given mass flow, pressure and temperature at 10,000m for altitude relight at combustion efficiency of 80%.

As the efficiency of the combustor increases the shaded region between higher and lower theta parameter value from Figure 4-31, becomes narrower, thus limiting the size of the combustor for altitude relighting at higher efficiency.

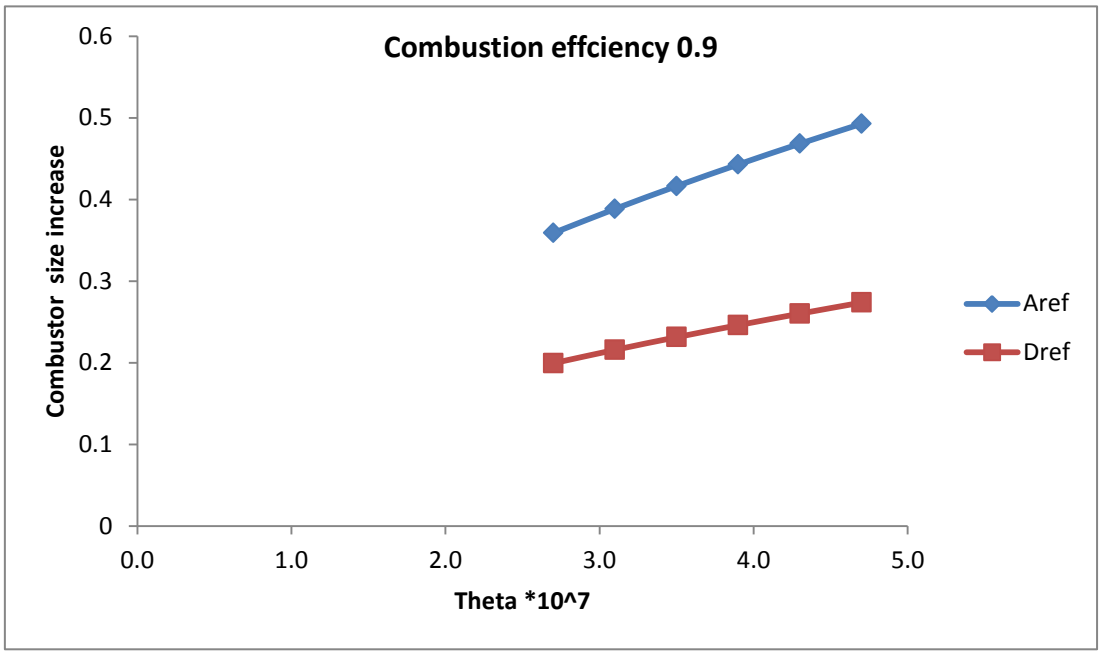

Figure 4-34: Combustor RQL geometry variation: Combustion Efficiency 0.9

Figure 4-34 also shows that the reference area and diameter of the combustor increases as the theta parameter increases from minimum of 2.7*10^7 to maximum 4.7*10^7 for 90% combustion efficiency. Therefore, the reference area of the combustor varies from 0.36m^2 to 0.49m^2 and the reference diameter of the combustor varies from 0.20m to 0.27m for the altitude relight condition. Below theta parameter of 2.7*10^7, the combustor will not relight due to the rich ignition limit at 90% efficiency and small size of the combustor for this case.

The theta parameter of 4.7*10^7 and above lies outside the shaded area of the combustion from Figure 4-31, hence there will be no ignition as the size of the combustor is substantially large for the given mass flow, pressure and temperature at 10,000m for altitude relight at combustion efficiency of 90%.

Hence, after carrying out the additional assessment to assess the sizing requirements for the RQL combustor design to meet the certification criteria for altitude relight at 10000m. The results suggest that for successful relight, the minimum reference area required is 0.40m^2 and a reference diameter of 0.22m for a “pessimistic” θ parameter curve and 0.27m^2 and 0.14m respectively for an “optimistic” θ parameter curve as shown in Figure 4-33 for the NASA test rig combustor.

5 CONCLUSION AND SUGGESTIONS FOR FURTHER WORK

5.1 Conclusion

The objectives of this doctoral research were based on the research questions presented in the first chapter. The primary aim of the research was to analyse the suitability of the stirred reactor method and develop a model to predict NO_X emissions for a novel aero-engine combustor. Based on the stirred reactor method, an RQL NO_X emission model was developed and assessed with the public domain data of a NASA test rig experiment.

The main conclusions which were drawn with respect to the research questions introduced in the first chapter are as follows:

- The preliminary RQL stirred reactor model is able to predict the NOx emissions reasonably comparative to the public domain NASA test rig experiment data. The model has successfully predicted NOx emissions trend for the RQL combustor for a CFM56 type engine for different power settings described in the chapter 4. After comparing the ICAO and conventional combustor design, the RQL model predicted the NO_X to be more than 70% lower. This has demonstrated that the model is capable of fairly capturing the chemical kinetics process inside the RQL combustor and can provide a representative estimation of NO_X for an RQL combustor.

- The parametric study on varying the amount of air in various zones in an RQL combustor with respect to lower NO_X and CO was conducted. It was observed that the lowest NO_X is predicted when the rich-burn section was at an equivalence ratio of 1.8 and quick-quench was at 0.5. The model was able to predict NOx by varying the amount of air in various zones (F1, F2, F3, and F4), but in order to carry out the test rig equivalent scenario, major design changes needs to be taken for the RQL combustor. The varying geometry RQL combustor would be able to vary the amount of air in different zones.

- An additional assessment was performed to assess the sizing requirements for the RQL combustor design to meet the certification criteria for altitude relight at 10000m. The results suggest that for successful relight, the minimum reference area required is 0.4m^2 and a reference diameter of 0.22m (for a “pessimistic” θ parameter curve) and 0.27m^2 and 0.14m respectively (for an “optimistic” θ parameter curve) as shown in Figure 4-33.

- Windmiling scenario for the existing V2500 combustor is carried out to verify the methodology for the sizing of the combustor. It was found that V2500 combustor certified the altitude relight scenario with the existing geometry with the methodology of this report for the altitude relighting capability. This verifies that the methodology for the NASA test rig combustor sizing.

The RQL model developed in this study has proved to be quick and reasonable to be integrated in the future with the multi-trajectory optimisation framework. The emission prediction model can be further developed for different novel combustor designs. To the author’s best knowledge the application of a stirred reactor modelling approach to compute NOx emissions of an RQL combustor has not been done before and is therefore the contribution to knowledge of this research.

5.2 Further Work

After carrying out the research on the stirred reactor RQL emission prediction method in this thesis and the limitations of the model discussed in chapter 3, some of the recommendations for further work are as follows:

- The comparison of the model and the NASA test rig experiment for the NO_X emission is shown in Table 4 1. It is inferred from the results that the NO_X is higher for the higher “J” (Jet-to-Crossflow Momentum Flux Ratio). Where J is directly proportional to the square of quick-quench air inlet jet velocity and inversely proportional to the square of main chamber jet

velocity. Therefore, higher the jet velocity, slightly higher the NO_X emission as it penetrates deeper in the main jet effluent gases emanating from the rich-burn section. One of the assumptions while modelling the RQL combustor for the NO_X emission prediction is not taking the "J" factor into account. It would be of interest to look at the impact on NO_X emission results in the model, once the "J" factor is introduced in the stirred reactor model for RQL combustor quick-quench section.

- CFD modelling: This doctoral research has used the stirred reactor method to predict NO_X emissions for the RQL combustor and modelled that in the in-house emission prediction software "Hephaestus". It would be interesting to look at NO_X prediction trends in a developed CFD model for an RQL combustor. A comparison can be carried out with the available stirred reactor model predictions and the results from the CFD modelling. As stirred reactor method gives a holistic view of the combustion process inside the combustor and unable to capture the fine nuances of chemical kinetics. Therefore, the CFD modelling would be of greater interests for the RQL emission prediction method to be integrated in Hephaestus. Further to add to the author's previous recommendations, "J" factor and the size of the quick-quench holes impacts the mixing and penetration of the jet entering the quick-quench region of the RQL combustor. And, these factors influence the NO_X emission. Therefore, in order to capture the chemical kinetics in fine details, CFD method could be used to model the RQL combustor by incorporating these factors to predict a fairer NO_X emission compared to stirred reactor model.

- In order to avoid an increase in level of uncertainties, the developed preliminary NO_X emission prediction stirred reactor model for RQL combustor doesn't include processes such as fuel evaporation and combustion unsteadiness. But, the fuel evaporation plays a major role in the NO_X emission production. Therefore, in order to enhance the level of

accuracy of NO_X emission prediction for the developed RQL stirred reactor model, it is recommend the inclusion of aforesaid processes.

- The stirred reactor RQL model predicts the NO_X emission to be much lower than the conventional combustor. Therefore, incorporation of the RQL NO_X emission prediction model in a trajectory optimisation framework could benefit in presenting the optimised trajectory for lowest NO_X emissions for an aircraft. It would be of great interest to look at the further development of this RQL stirred reactor model to be integrated with the trajectory optimisation framework.

- The RQL model in this study is based on various assumptions and constraints and the sensitivity study which was carried out for the effect of air inflow spits inside the RQL combustor on NO_X emission was inconclusive. A detailed and in-depth sensitivity analysis of the model is required in order to assess the RQL model's uncertainty level in the NO_x prediction levels when parameter such as J is introduced in the model.

- Furthermore, the low conversion of FBN into NO_X in the RQL combustor makes it an appropriate candidate in novel combustor design to be investigated further for the power generation gas turbine engine. Generally, gas turbine power generation runs on alternative fuels such as natural gas which contains some amount of nitrogen. This aero engine RQL model could be further used to predict the NO_X trend in a stationary gas turbine engine for power generation.

- This preliminary modelling of the RQL combustor has predicted reasonably comparative NO_X emissions with the NASA test rig results. Similarly, other novel combustors which are discussed in the chapter 2 of literature review such as staged combustors, Lean Direct Injection (LDI), Twin Annular Premixed Swirl (TAPS) and Partially Evaporated & Rapid Mixing (PERM) combustors are all promising novel concepts which

would reduce the NO_X emission while maintaining the reliability and combustion efficiency of the engine.

- This model is able to predict the NO_X emission for the RQL combustor but it is not able to predict the temperature traverse at the end of the combustor which is critical for the life of the turbine blades. It would be of interest to model the RQL combustor in the CFD and look at the temperature traverse quality of the combustor.

- Due to the modular design of the emission prediction model, it is relatively easier to add fuels to test the effects on the NO_X emissions. This study has added four shale gases as a fuel for the conventional jets engine combustor in the emission prediction model and predicted their impacts on NO_X emissions. It would be of greater interest to look at the impact various additions of alternative fuels with different compositions on NO_X emissions once added to the emission prediction model.

REFERENCES

[1] Ponater, M., Sausen, R., Feneberg, B. and Roeckner, E. (1999), "Climate effect of ozone changes caused by present and future air traffic", *Climate Dynamics,* vol. 15, no. 9, pp. 631-642.

[2] Pervier, H. (2012), Emissions Modelling for Engine Cycle and Aircraft Trajectory Optimisation, PhD thesis, Cranfield University.

[3] A new beginning for European Aviation Research (2015), available at: http://www.acare4europe.com/about-acare (accessed 02/03/15).

[4] Protecting the environment and the energy supply (2015), available at: http://www.acare4europe.com/sria/flightpath-2050-goals/protecting-environment-and-energy-supply-0 (accessed 20/08/15).

[5] Lefebvre, A. H. and Ballal, D. R. (2010), Gas Turbine Combustion-Alternative Fuels and Emissions, Book, Third edition, CRC Press.

[6] EPA United States Environmental Protection Agency (2015), National Service Center for Environmental Publications, available at: https://www.epa.gov/nscep (accessed 13/12/2015).

[7] Environmental Protection Agency (EPA) (2015), Standards of Performance for Stationary Combustion Turbines: July 6th 2006, available at: http://www.federalregister.com/Browse/Document/usa/na/fr/2006/7/6/06-5945 (accessed 21/12/2015).

[8] Environmental Protection Agency (EPA) (2015), Standards of Performance for Stationary Gas Turbines: A Proposed Rule by the Environmental Protection Agency on 08/29/2012, available at: https://www.federalregister.gov/articles/2012/08/29/2012-20524/standards-of-performance-for-stationary-gas-turbines-standards-of-performance-for-stationary (accessed 21/12/2015).

[9] Office of Energy Efficiency and Renewable Energy. (2015), Sustainable and Holistic Integration of Energy Storage and Solar PV (SHINES), available at: http://energy.gov/eere/sunshot/about-sunshot-initiative (accessed 01/12/2015).

[10] Parker, R. and Lathoud, M. (2010), "Green aero-engines: Technology to mitigate aviation impact on environment", Proceedings of the Institution of Mechanical Engineers, Part C: Journal of Mechanical Engineering Science, vol. 224, no. 3, pp. 529-538.

[11] Antoine, N. E. and Kroo, I. M. (2005), "Framework for aircraft conceptual design and environmental performance studies", *AIAA Journal,* vol. 43, no. 10, pp. 2100-2109.

[12] Holdeman, J. D. and Chang, C. T. (2001), "Low Emissions RQL Flametube Combustor Component Test Results", Technical Report, 20030056585, NASA/TM-2001-210678, NASA Glenn Research Center, Cleveland, OH, United States

[13] North Atlantic Treaty Organization, Advisory Group for Aerospace Research and Development. Propulsion and Energetics Panel (1993), Fuels and combustion technology for advanced aircraft engines, Agard, Neuilly-sur-Seine.

[14] Singh, R. P. (2006), "Causes and consequences of the greenhouse gases", Bulletin of Pure and Applied Sciences - Section F Geological Sciences, vol. 25, no. 1-2, pp. 13-17.

[15] Grossblatt, N. "Ozone and Other Photochemical Oxidants", Technical Report, United States: National Academy of Sciences, Washington, DC, USA, 1977.

[16] Ozone Poisoning (2015), available at: http://floridaindoorairquality.com/content/ozone-poisoning (accessed 08/03/15).

[17] Grewe, V., Dahlmann, K., Matthes, S. and Steinbrecht, W. (2012), "Attributing ozone to NOx emissions: Implications for climate mitigation measures", Atmospheric Environment, vol. 59, no. 0, pp. 102-107.

[18] Skowron, A., Lee, D. S. and De León, R. R. (2013), "The assessment of the impact of aviation NOx on ozone and other radiative forcing responses – The importance of representing cruise altitudes accurately", Atmospheric Environment, vol. 74, no. 0, pp. 159-168.

[19] Fan, L., Yang, S.L. and Kundu, K.P., 1996. "Evaluation of water injection effect on NOx formation for a staged gas turbine combustor", American Institute of Aeronautics and Astronautics, Washington, D.C.

[20] Anderson, D. (1975), "Effects of Equivalence Ratio and Dwell Time on Exhaust Emissions from an Experimental Premixing Pre-vaporizing Burner", American Society of Mechanical Engineers (Paper), no. 75 -GT-69.

[21] Loftin, L. K. (1985), Quest for performance: The evolution of modern aircraft, Scientific and Technical Information Branch, National Aeronautics and Space Administration.

[22] Pilidis, P. (Cranfield University), (2011), Gas Turbine Theory and Performance (unpublished MSc Thermal Power Course Notes), Cranfield.

[23] Darling, D. (2015), Turbofan Engine-The world of David Darling, available at: http://www.daviddarling.info/images/turbofan_engines.jpg (accessed 23/05/15).

[24] Aviation and the Global Atmosphere (2015), available at: http://www.ipcc.ch/ipccreports/sres/aviation/index.php?idp=96 (accessed 15/05/15).

[25] International Civil Aviation Organization, "ENVIRONMENTAL REPORT", (2013), available at: http://www.icao.int/environmental-protection/Pages/EnvReport13.aspx(accessed 15/05/14)

[26] International Civil Aviation Organization, "ENVIRONMENTAL REPORT" (2010), available at: http://www.icao.int/environmentalprotection/Pages/EnvReport10.aspx (accessed 12/02/12)

[27] International Civil Aviation Organization Engine Exhaust Emissions Data Bank, available at:http://www.caa.co.uk/default.aspx?catid=702&pagetype=68&gid=704 (accessed 10/07/11)

[28] Clean Sky. (2015), Clean Sky- about us, available at: http://www.cleansky.eu/content/homepage/about-us (accessed 23/01/15).

[29] Colmenares Quintero, R. F. (2009), *"Techno-economic and environmental risk assessment of innovative propulsion systems for short-range civil aircraft"*, PhD Thesis, Cranfield University.

[30] Sirag, A. (2011), "A TERA Approach to Aero Engine Performance Assessment", MSc Thesis, Cranfield University.

[31] Stephen, S., Pilidis, P. and Vishal, S. (2009), "Power Plant Selection in a Carbon Constrained World: The TERA (Technoeconomic Environmental Risk Analysis)", *Journal of Aerospace Power,* vol. 24, no. 4, pp. 1.

[32] Ogaji, S., Pilidis, P. and Hales, R. (2007), "TERA-a tool for aero-engine modelling and management", *Second World Congress on Engineering Asset Management and the Fourth International Conference on Condition Monitoring,* 11-14 June 2007, Harrogate, UK.

[33] Kyprianidis, K., Di Lorenzo, G., Ogaji, S. O. and Pilidis, P. (2008), "The TERA Approach-A Methodology for Technoeconomical, Environmental and

Risk Analysis of Multidisciplinary Systems", *Cranfield University Multi-Strand Conference.*

[34] Skalska, K., Miller, J. S. and Ledakowicz, S. (2010), "Trends in NOx abatement: A review", *Science of the Total Environment,* vol. 408, no. 19, pp. 3976-3989.

[35] Zeldovich, Y. B. (1946), "The Oxidation of Nitrogen in Combustion and Explosions", in *Acta Physicochimica,* U.R.S.S. 21: pp. 577–628.

[36] Bowman, C. T. (1975), "Kinetics of pollutant formation and destruction in combustion", *Progress in Energy and Combustion Science,* vol. 1, no. 1, pp. 33-45.

[37] Celis, C. (2010), “Evaluation and Optimisation of Environmentally Friendly Aircraft Propulsion Systems”, *PhD Thesis* (https://dspace.lib.cranfield.ac.uk/handle/1826/4686), Cranfield University, Cranfield, UK.

[38] Lieuwen, T. C. and Vigor Yang, e. (2013), *Gas Turbine Emissions*, Book, 1st edition, Cambridge University Press, Cambridge.

[39] Fenimore, C. P. (1971), "Formation of nitric oxide in premixed hydrocarbon flames", *Symposium (International) on Combustion*, vol. 13, no. 1, pp. 373-380.

[40] De Soete, G.G., 1975, December. Overall reaction rates of NO and N 2 formation from fuel nitrogen. *In Symposium (international) on combustion* (Vol. 15, No. 1, pp. 1093-1102). Elsevier.

[41] Bozzelli, J. W. and Dean, A. M. (1995), "O + NNH: A Possible New Route for NOx Formation in Flames", *International Journal of Chemical Kinetics*, vol. 27, no. 1097-109.

[42] Konnov, A. A. and De Ruyck, J. (2001), "Temperature-dependent rate constant for the reaction NNH + O → NH + NO", *Combustion and Flame Journal*, vol. 125, no. 4, pp. 1258-1264.

[43] Dagaut, P., Glarborg, P. and Alzueta, M. U. (2008), "The oxidation of hydrogen cyanide and related chemistry", *Progress in Energy and Combustion Science,* vol. 34, no. 1, pp. 1-46.

[44] Shakariyants, S. A., Van Buijtenen, J. P., Visser, W. P. J. and Tarasov, A. (2005), "A generic approach to aero-engine exhaust emission simulation", *Proceedings of ISABE 2005,* .

[45] Lefebvre, A. H. (1984), "Fuel Effects on Gas Turbine Combustion - Liner Temperature, Pattern Factor and Pollutant Emissions", *AIAA/SAE/ASME 20th Joint Propulsion Conference,* Cincinnati, Ohio, AIAA, New York, USA.

[46] Rizk, N. and Mongia, H. (1994), "Emissions predictions of different gas turbine combustors", 32nd Aerospace Sciences Meeting and Exhibit. American Institute of Aeronautics and Astronautics, Reno, NV, U.S.A.

[47] Odgers, J. and Kretschmer, D. (1985), "The Prediction of Thermal NOx in Gas Turbines, Proceedings of the ASME Turbo Expo 1985.

[48] Baughcum, S. L., Boeing Company Commercial, A. G. and Langley, R. C. (1996), *Scheduled civil aircraft emission inventories for 1992: Database development and analysis,* National Aeronautics and Space Administration, Langley Research Center.

[49] NEPAIR (2003), *Development of the technical basis for a New Emissions Parameter Covering the Whole Aircraft Operation: NEPAIR,* NEPAIR/WP4/WPR/01, Final Technical Report.

[50] Chandrasekaran, N. and Guha, A. (2012), "Study of Prediction Methods for NOx Emission from Turbofan Engines", *Journal of Propulsion and Power,* vol. 28, no. January–February.

[51] Shakariyants, S. A. (2008), *Generic Methods for Aero-Engine Exhaust Emission Prediction,* Dissertation, ISBN 978-90-9023346-8, *TU Delft, Delft University of Technology*

[52] Shakariyants, S. A., Van Buijtenen, J. P. and Visser, W. P. J. (2004), "Aero-gasturbine emission reduction and simulation technology: Philosophy and approach", *2004 ASME Turbo Expo,* Vol. 2, 14 June 2004 through 17 June 2004, Vienna, pp. 165.

[53] Aksit, I. M. and Moss, J. B. (1996), "Stochastic modelling of NOx and smoke production in gas turbine combustors", *ASME 1996 International Gas Turbine and Aeroengine Congress and Exhibition, GT 1996,* Vol. 3.

[54] Hammond, D. C. and Mellor, A. M. (1971), "Analytical Calculations for the Performance and Pollutant Emissions of Gas Turbine Combustors", *Combustion Science and Technology,* vol. 4, no. 1, pp. 101-112.

[55] Hammond, D. C. and Mellor, A. M. (1973), "Analytical Predictions of Emissions from and Within an Allison J-33 Combustor", *Combustion Science and Technology,* vol. 6, no. 5, pp. 279-286.

[56] Fletcher, R. and Heywood, J. (1971), "A model for nitric oxide emission from aircraft gas turbine engines", in *9th Aerospace Sciences Meeting* (p. 123), American Institute of Aeronautics and Astronautics.

[57] Kundu, K. P., Deur, J. M., (1994), "Simplified NOx formation mechanism for CFD use", *30th Joint Propulsion Conference and Exhibit, Joint Propulsion Conferences, American Institute of Aeronautics and Astronautics*, Indianapolis, IN, U.S.A.

[58] ICAO. (2015)*, Aircraft Engine Emissions*, available at: http://www.icao.int/environmental-protection/Pages/aircraft-engine-emissions.aspx (accessed 08/03/15).

[59] Zhang, M., Fu, Z., Lin, Y. and Li, J. (2012), "CFD study of NOx emissions in a model commercial aircraft engine combustor", *Chinese Journal of Aeronautics,* vol. 25, no. 6, pp. 854-863.

[60] Lee, D., Park, J., Jin, J. and Lee, M. (2011), "A simulation for prediction of nitrogen oxide emissions in lean premixed combustor", *Journal of Mechanical Science and Technology,* vol. 25, no. 7, pp. 1871-1878.

[61] McBeath, G., Ghorashi, B., Chun, K., (1993), "A thermal NOx prediction model: Scalar computational module for CFD codes with fluid and kinetic effects", *29th Joint Propulsion Conference, American Institute of Aeronautics and Astronautics, Society of Automotive Engineers, American Society of Mechanical Engineers and American Society for Engineering Education,* Monterey, CA, U.S.A.

[62] Gobbato, P., Masi, M., Toffolo, A., Lazzaretto, A. and Tanzini, G. (2012), "Calculation of the flow field and NOx emissions of a gas turbine combustor by a coarse computational fluid dynamics model", *Energy,* vol. 45, no. 1, pp. 445-455.

[63] Talpallikar, M. V., Smith, C. E., Lai, M. C. and Holdeman, J.D. (1992), "CFD analysis of jet mixing in low NOx flametube combustors" NASA Technical Memorandum 104466, ASME-91-GT-217.

[64] Falcitelli, M., Pasini, S., Rossi, N. and Tognotti, L. (2002), "CFD+reactor network analysis: an integrated methodology for the modeling and optimisation of industrial systems for energy saving and pollution reduction", *Applied Thermal Engineering,* vol. 22, no. 8, pp. 971-979.

[65] Frassoldati, A., Frigerio, S., Colombo, E., Inzoli, F. and Faravelli, T. (2005), "Determination of emissions from strong swirling confined flames with an integrated CFD-based procedure", *Chemical Engineering Science,* vol. 60, no. 11, pp. 2851-2869.

[66] Falcitelli, M., Pasini, S. and Tognotti, L. (2002), "Modelling practical combustion systems and predicting NOx emissions with an integrated CFD based approach", *Computers & Chemical Engineering,* vol. 26, no. 9, pp. 1171-1183.

[67] Kiameh, P. (2002), *Power Generation Handbook: Selection, Applications, Operation, Maintenance, ISBN-13: 063-9785336006,* 1st edition, McGraw-Hill Professional.

[68] Lefebvre, A. (1966), "Theoretical aspects of gas turbine combustion performance", *College of Aeronautics, Department of Propulsion, 1966,* vol. 163 of Note: Cranfield College of Aeronautics.

[69] Briehl, D., Schultz, D. F. and Ehlers, R. C. (1983), "Variable-Geometry Combustor Used To Study Primary and Secondary Zone Stoichiometry", Joint Power Generation Conference, ASME, *NASA Technical Memorandum, NASA-TM-83372, Indianapolis, U.S.A.*

[70] Saintsbury, J. A. and Sampath, P. (1975), "Emissions Research on a Simple Variable Geometry Gas Turbine Combustor", *American Society of Mechanical Engineers (Paper),* no. 75 -WA/GT-12.

[71] Saintsbury, J. A. and Sampath, P. (1975), "Atmospheric tests of a variable combustor geometry for reducing gas turbine emissions", *Journal of Fluids Engineering - ASME,* vol. 97, no. 1-3, pp. 327-333.

[72] Saintsbury, J. A. and Sampath, P. (1974) "Variable Combustor Geometry for Reducing Gas Turbine Emissions", pp. 217-232, *Fluid Mechanics of Combustion, Symposium,* Montreal, Quebec, Canada.

[73] Leonard, G. and Stegmaier, J. (1994), "Development of an aeroderivative gas turbine dry low emissions combustion system", *Journal of Engineering for Gas Turbines and Power,* vol. 116, no. 3, pp. 542-546.

[74] Tacina, R. R., Wey, C., Choi, K. J., (2001), *Flame tube NOx emissions using a lean-direct-wall-injection combustor concept,* 37th Joint Propulsion Conference and Exhibit, American Institute of Aeronautics and Astronautics, American Society of Mechanical Engineers, Society of Automotive Engineers and American Society for Engineering Education NASA/TM-2001-21105, E-12950, AIAA Paper 2001-3271, NAS 1.15:211105*,* Salt Lake City, UT, U.S.A.

[75] Wilfert, G., Sieber, J., Rolt, A., Baker, N., Touyeras, A. and Colantuoni, S. (2007),"New environmental friendly aero engine core concepts", in *International symposium on Air Breathing engines, AIAA*, Beijing, China.

[76] Tacina, R. R. (1990), "Low NOx Potential of Gas Turbine Engines", *NASA Technical Memorandum 102452,* no. AIAA-90-0550.

[77] Foust, M. J., Thomsen, D., Stickles, R., Cooper, C. and Dodds, W. (2012), "Development of the GE aviation low emissions TAPS combustor for next generation aircraft engines", *50th AIAA Aerospace Sciences Meeting Including the New Horizons Forum and Aerospace Exposition.*

[78] Mosier, S. A. and Pierce, R. M. (1980), *Advanced Combustor Systems for Stationary Gas Turbine Engines, Phase I. Review and Preliminary Evaluation, Final Report,* Contract 68-02-2136, FR-11405, Volume I, U.S. Environmental Protection Agency, US.

[79] Jacobson, N. S. (1992), "High-Temperature Durability Considerations for HSCT Combustor", *NASA Technical Paper 3162,* no. NASA-TP-3162 19920007852.

[80] McKinney, R. G., Sepulveda, D., Sowa, W. and Cheung, A. K. (2007), "The Pratt & Whitney TALON X low emissions combustor: Revolutionary results with evolutionary technology", *Collection of Technical Papers - 45th AIAA Aerospace Sciences Meeting,* Vol. 7, pp. 4697.

[81] Singh, R. and Sethi, V. (2015), *Gas Turbine Combustors, Volume 3* (unpublished Lecture Supplements), Cranfield University.

[82] Peterson, C. O., Sowa, W. A. and Samuelsen, G. S. (December 2002), "Performance of a Model Rich Burn-Quick Mix-Lean Burn Combustor at Elevated Temperature and Pressure", *University of California, Irvine, California,* no. NASA/CR-2002-211992.

[83] Martin, F. J. and Dederick, P. K. (1977), "NOx from fuel nitrogen in two-stage combustion", *Symposium (International) on Combustion,* vol. 16, no. 1, pp. 191-198.

[84] Nakata, T., Sato, M., Ninomiya, T. and Hasegawa, T. (1996), "A study on low NOx combustion in LBG-fueled 1500°C-class gas turbine", *Journal of Engineering for Gas Turbines and Power,* vol. 118, no. 3, pp. 534-540.

[85] Smith, C. E., Talpallikar, M. V. and Holdeman, J. D. (1997), *"A CFD Study of Jet Mixing in Reduced Flow Areas for Lower Combustor Emissions*, 27th Joint Propulsion Conference, AIAA, SAE, ASME,and ASEE", June 24-27, Sacramento, California, U.S.A.

[86] Rizk, N. K. and Mongia, H. C. (1990), "Ultra-low NOx rich-lean combustion", *American Society of Mechanical Engineers,* International Gas Turbine and Aeroengine Congress and Exposition, *Paper No. 90-GT-087, pp. V003T06A022*.

[87] Holdemann, J. D. and Chang, C. T. (2008), "Mixing of Multiple Jets with a Confined Subsonic Crossflow: Part III-The Effects of Air Preheat and Number of Orifices on Flow and Emissions in an RQL Mixing Section", Technical Report, NASA/TM-2008-215151, E-16378

[88] Samuelsen, S. (2006), "Rich Burn, Quick-Mix, Lean Burn (RQL) Combustor", *The Gas Turbine Handbook, US Department of Energy, Office of Fossil Energy, National Energy Technology Laboratory, DOE/NETL2006-1230,* , pp. 227-233.

[89] Margason, R. J. (1993), "Fifty years of jet in cross flow research", *In AGARD, Computational and Experimental Assessment of Jets in Cross Flow 41 p (SEE N94-28003 07-34),* Vol. 1, .

[90] Ji, Y., Mao, R., Yuan, Y., Shen, S. and Ge, B. (2015), "Numerical Investigation on Mixing Characteristics in Quenching Zone of Annular RQL Combustors", *First International Conference on Information Sciences, Machinery, Materials and Energy,* Atlantis Press, .

[91] Hossaini, M. K. (2014), "Review of the New Combustion Technologies in Modern Gas Turbines", in *Progress in Gas Turbine Performance, Dr. Ernesto Benini (Ed.), ISBN: 978-953-51-1166-5, Intech, DOI: 10.5772/54403. Available from:http://www.intechopen.com/books/progress-in-gas-turbine-performance/review-of-the-new-combustion-technologies-in-modern-gas-turbines (accessed 15/06/2015)*.

[92] Gordon, S. and McBride, B., J. (1994), *Computer Program for Calculation of Complex Chemical Equilibrium Compositions and Applications. Part 1: Analysis,* Technical Report, NASA-RP-1311, E-8017, NAS 1.61:131, NASA Lewis Research Center, Cleveland, OH, U.S.A.

[93] McBride, B., J. and Gordon, S. (1996), *Computer Program for Calculation of Complex Chemical Equilibrium Compositions and Applications. II. User's Manual and Program Description,* Technical Report, NASA-RP-1311, E-8017-1, NAS 1.61:1311, NASA Lewis Research Center, Cleveland, OH, U.S.A.

[94] Williams, F. E. (1994), *Combustion Theory: The Fundamental Theory of Chemically Reacting Flow Systems,* 2nd edition, Benjamin/ Cummings Publishing, Company, California, U.S.A.

[95] Sturgess, G. J., Zelina, J., Shouse, D. and Roquemore, W. (2005), "Emissions reduction technologies for military gas turbine engines", *Journal of Propulsion and Power,* vol. 21, no. 2, pp. 193-217.

[96] Allaire, D. L., Waitz, I. A. and Willcox, K. E. (2007), "A comparison of two methods for predicting emissions from aircraft gas turbine combustors", *Proceedings of the ASME Turbo Expo,* Vol. 2, pp. 899.

[97] *Cranfield University, 1999, "The Turbomatch Scheme" (unpublished MSc Thermal Power Course Notes).*

[98] ICAO, available at: http://www.icao.int/about-icao/Pages/default.aspx (accessed 12/02/2015).

[99] Walsh, P. P. and Fletcher, P. (2004), *Gas turbine performance, Book,* John Wiley & Sons.

[100] *Estimation of Windmill Drag and Airflow of Turbojet and Turbofan Engines, Performance Volume 4, ESDU,* (1981), ESDU 81009, ESDU, London.

[101] Liu, A. (2014), *Towards the Development of a Preliminary Combustor Design and Sizing Computational Software, Part I: Preliminary Aerodynamic Design* (MSc thesis), Cranfield University, Cranfield.

[102] Gunston, B. (1996), *Jane's Aero- Engines,* 26th edition, Jane's Information Group, ISBN 0710614055, 9780710614056.

[103] Stevens, P. (August 2012), "The 'Shale Gas Revolution': Developments and Changes", *Energy, Environment and Resources,* [Online], no. EERG BP 2012/04.

[104] *Where Our Natural Gas Comes From?* (2015), available at: http://www.eia.gov/energyexplained/index.cfm?page=natural_gas_where (accessed 19/06/15).

[105] *The Shale Gas Boom and U.S. Energy Security* (2015), available at: https://worldpittsburgh.wordpress.com/2014/01/17/the-shale-gas-boom-and-u-s-energy-security/ (accessed 19/06/15).

[106] George, D. L. and Bowles, E. B. J. (2011), "Shale Gas Measurement And Associated Issues", *Pipeline and Gas Journal,* [Online], vol. 238, no. 7, pp. 06/19/2015 available at: http://www.pipelineandgasjournal.com/shale-gas-measurement-and-associated-issues?page=show.

[107] Sehgal, V. (2014), *Preliminary Assessments of Potential of Liquefied Shale Gas for Civil Aviation* (MSc thesis), Cranfield University, Cranfield.

APPENDICES

Appendix A List of Publications

1. Prakash, A., “Prediction of NOx Emissions using a Stirred Reactor Modelling Approach for an Aero-Engine with RQL Combustor”, Technical Paper, accepted 52nd AIAA/SAE/ASEE Joint Propulsion Conference, AIAA Propulsion and Energy Forum and Exposition 2016

2. Prakash, A., Kadambari, L., Kamthe, A. and Sethi, V., *“Advanced Novel Jet Engines Emission Modelling to Predict NO_X & CO_2 by Physics Based Model”*, 49th AIAA/ASME/SAE/ASEE Joint Propulsion Conference, 2013

3. Prakash, A., Kadambari, L., and Sethi, V., “Stirred Reactor Approach for Cryoplane Engines’ NOX Prediction”, 49th AIAA/ASME/SAE/ASEE Joint Propulsion Conference, 2013

4. Kadambari, L., Prakash, A., Sethi, V., Goodger, E., Pilidis, P., “*Life Cycle Assessment of Life Cycle Emissions of Bio-SPKs in Jet engines”*; American Society of Mechanical Engineers; ASME International Gas Turbine Institute., ASME TURBO EXPO 2013

Appendix B : Hephaestus Input for NASA test rig

```
!   **********************
!   HEPHAESTUS - Input file
!   **********************

!   Author: Cesar Celis
!   Cranfield University (CU), 2010

!     This file contain the input data for the CU Gaseous Emissions Prediction Model HEPHAESTUS
!   Four slashes (////) indicate the data beginning
!   Everything before the four slashes (////) is ignored

!   Data is read sequentially. POINT must start at 1 (one), and follow a sequential order
!   This input data format is used in order to allow the computation of multiple points easily

!   Input file is divided in sections starting with a keyword 'METHOD' (sequential METHOD numbering is required)
!   Each section (except the first one) represents a different emissions prediction methodology
!   First section (METHOD 0) deals with the initial settings of HEPHAESTUS

!   Each section has two lines/rows of '==...' characters. Everything inside these two rows is ignored
!   Data is read immediately after the second row of '==...' characters until a line of blank ones is found

!   Lines/rows of blank characters must be avoided between the keyword 'METHOD' and the first line/row of '==...' characters
!   Lines/rows of blank characters must be avoided between the second line/row of '==...' characters and the actual data lines/rows

!   Only the first section (METHOD 0) is read at all times
!   Other sections are read only when required (according to the first section settings)
!   Input data is required according to the particular emissions prediction method utilised

////
METHOD 0
================================================================================================
!   MODEL 0 is NOT a model. It is a generic section dealing with HEPHAESTUS initial settings
!   Only one (1) line or row of data (first one) is need. All other data lines/rows are ignored

!   Description of the input parameters:

!   PMTYP       Prediction method type (1: Reactor; 2: Correlation; ...)            [--]
!   CTYP        Combustor type (1: Conventional; 2: RQL; ...)                   [--]
!   FTYP        Fuel type (1: Jet-A(g) (C12H23); 2: Biofuel1 (C8H18,isooctane); 3: Blended Jatropha-JetA ...    [--]
!   BLPER       If a blended fuel is used, input the percent of blending referred to the first fuel (otherwise put 0.0) [--]

POINT   PMTYP         CTYP        FTYP      BLPER
[---]   [--]          [--]        [--]      [--]
================================================================================================
1     1           2           1        0.0
METHOD 1
================================================================================================
================================================================================================
!   MODEL 1 uses a stirred reactor-based approach to predict GT combustor gaseous emissions

!   Description of the input parameters:

!   POINT       Calculation point               [---]
!   HAMB        Ambient (flight) altitude           [m]
!   TAMB        Ambient temperature             [K]
!   RHAMB       Ambient relative humidity           [---]
!   TA      Air total temperature                   [K]
!   PA      Air total pressure                  [atm]
!   WA      Total air mass flow rate                [kg/s]
!   FRAIRFF         Flame front air mass flow rate fraction         [---]
!   FRAIRP      Primary air mass flow rate fraction     [---]
!   FRAIRI      Intermediate air mass rate flow fraction    [---]
!   FRAIRD      Dilution air mass flow rate fraction        [---]
!   WF      Fuel mass flow rate             [---]
!   TF      Fuel total temperature                  [K]
!   FFIA        Flame front inlet area              [m2]
!   FFOA        Flame front outlet area             [m2]
!   FFL     Flame front length              [m]
!   PZIA        Primary zone inlet area             [m2]
!   PZOA        Primary zone outlet area            [m2]
!   PZL     Primary zone length             [m]
!   IZIA        Intermediate zone inlet area            [m2]
!   IZOA        Intermediate zone outlet area           [m2]
!   IZL     Intermediate zone length            [m]
!   DZIA        Dilution zone inlet area            [m2]
!   DZOA        Dilution zone outlet area           [m2]
!   DZL     Dilution zone length                [m]
!   FACT1       Fuel fraction reaching FF NWR           [---]
!   FACT2       Air fraction going to FF core reactor       [---]
!   FACT3       Comb gases fraction reaching PZ NWR     [---]
!   FACT4       Fraction of FRAIRP going to PZ NWR      [---]
!   FACT5       Fraction of FRAIRI going to IZ NWR      [---]


POINT   HAMB   TAMB        RHAMB       TA     PA          WA        FRAIRFF   FRAIRP  FRAIRI  FRAIRD  WF              TF         FFIA
[---]   [m]  [K]         [---]       [K]    [atm]       [kg/s]    [---]     [---]   [---]   [---]  [kg/s]           [K]
================================================================================================
1   0.00000 288.15000   0.55000 583.1500    10.48000    2.567000    0.28000 0.72000 0.00000 0.00000 0.098400        420.00000   0.03097 0.01290
2   0.00000 288.15000   0.55000 795.0000    8.306000    2.808000    0.28000 0.72000 0.00000 0.00000 0.089400        420.00000   0.03097 0.01290
3   0.00000 288.15000   0.55000 585.7056    5.470900    2.717000    0.28000 0.72000 0.00000 0.00000 0.105700        420.00000   0.03097 0.01290
4   0.00000 288.15000   0.55000 797.0000    8.165520    3.048000    0.28000 0.72000 0.00000 0.00000 0.088900        420.00000   0.03097 0.01290
5   0.00000 288.15000   0.55000 583.1500    10.14000    2.784149    0.22000 0.78000 0.00000 0.00000 0.098883        420.00000   0.03097 0.01290
6   0.00000 288.15000   0.55000 848.1500    10.00280    3.361000    0.23000 0.77000 0.00000 0.00000 0.104780        420.00000   0.03097 0.01290
7   0.00000 288.15000   0.55000 763.0000    8.505750    3.633000    0.13000 0.87000 0.00000 0.00000 0.103400        420.00000   0.03097 0.01290
```

Appendix C : ALTERNATIVE FUEL: SHALE GAS NO_X EMISSIONS

This part focuses on the NO_x prediction of the CUTF1 engine with shale gas as a fuel in the conventional combustor. The first part has discussed the shale gas and its formation. The second part explains the chemical composition of the chosen four shale gases and the last part describes the NO_x prediction with comparison for the LTO cycle.

C.1 Introduction

The matter of alternative way to harness the fuel from the planet acquired more urgency in 1973, the time of the first real “fuel crisis”. Oil based fuel prices tripled overnight and there were various reviews of alternative fuels for subsonic commercial air transport by the big airframe companies such as Lockheed and others. There is an increasing urgency to find alternative sources of energy as petroleum reserves are diminishing. Combustion of fuels with higher number of carbon creates the most harmful greenhouse gas emissions “CO_2”, for the Earth’s atmosphere.

C.2 Shale Gas

Shale is a sedimentary rock fine grained together with the pre-existing minerals and composed of mixtures of clay flakes. Therefore, shale gas is a natural gas found trapped within that shale formation. According to the paper published “The Shale Gas Revolution” [103], in 2000, shale gas provided only 1% of U.S. natural gas production; but it was providing over 20% by 2010. The U.S. government's Energy Information Administration predicts that by 2035, 46% of the United States' natural gas supply will come from shale gas [104].

Figure 5-1 shows the natural resources available for harnessing the conventional fuel. Therefore, in the light of increasing energy demand and environmental awareness, alternative fuels have been perceived as one of the potential solutions.

Recent developments in hydraulic fracturing (fracking) technology have provided access to large reserves of shale natural gas. Natural gas is relatively a cleaner fuel compared with other hydrocarbon fuels like Jet A. Additionally, due to its higher hydrogen content the luminous emissivity from the combustion of natural gas is lower than that from Jet A and this has implications on both NOx emissions and combustor life.

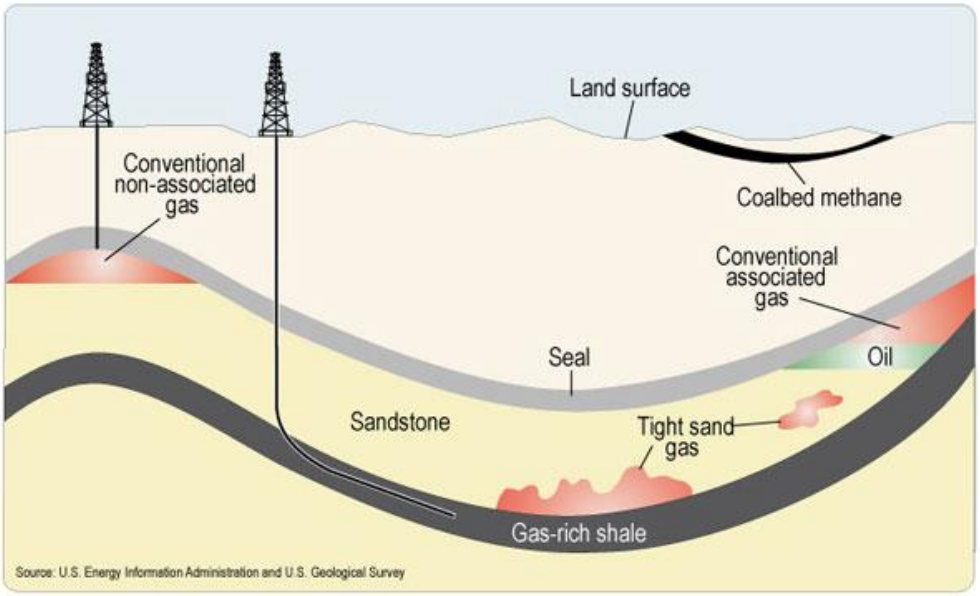

Figure 5-1: Natural Gas Resources [104]

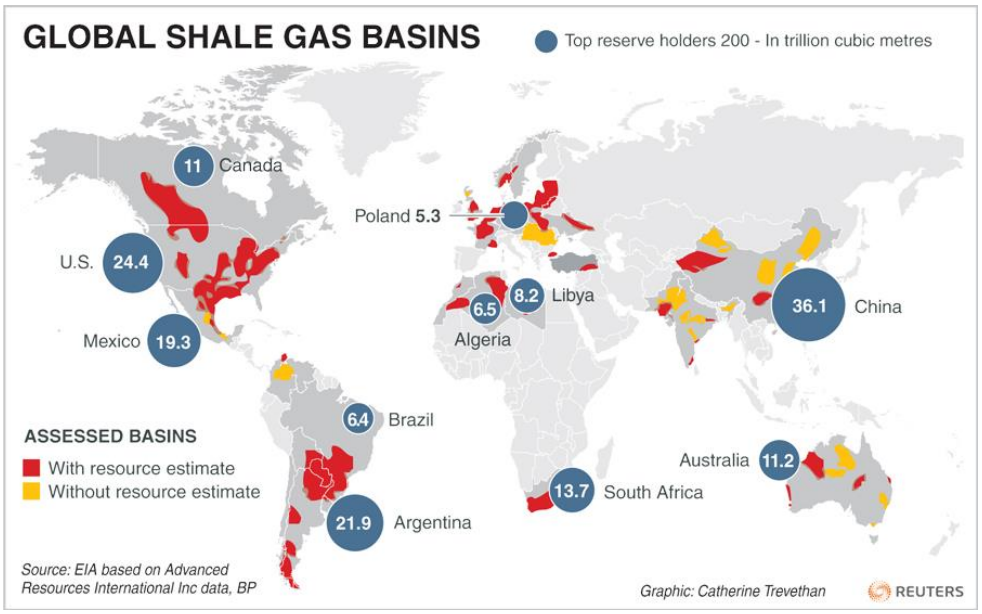

Figure 5-2: Shale reserves around the world [105]

USA has the second largest shale reserves after china in the world as shown in Figure 5-2. This study focuses on the shale excavation sites in USA because the extraction of Shale gas has already started on large scale in USA and the literature is available for US sites already. Figure 5-3 shows all the excavation sites in the USA. Four sites were selected as the chemical composition of these shale gases data is available.

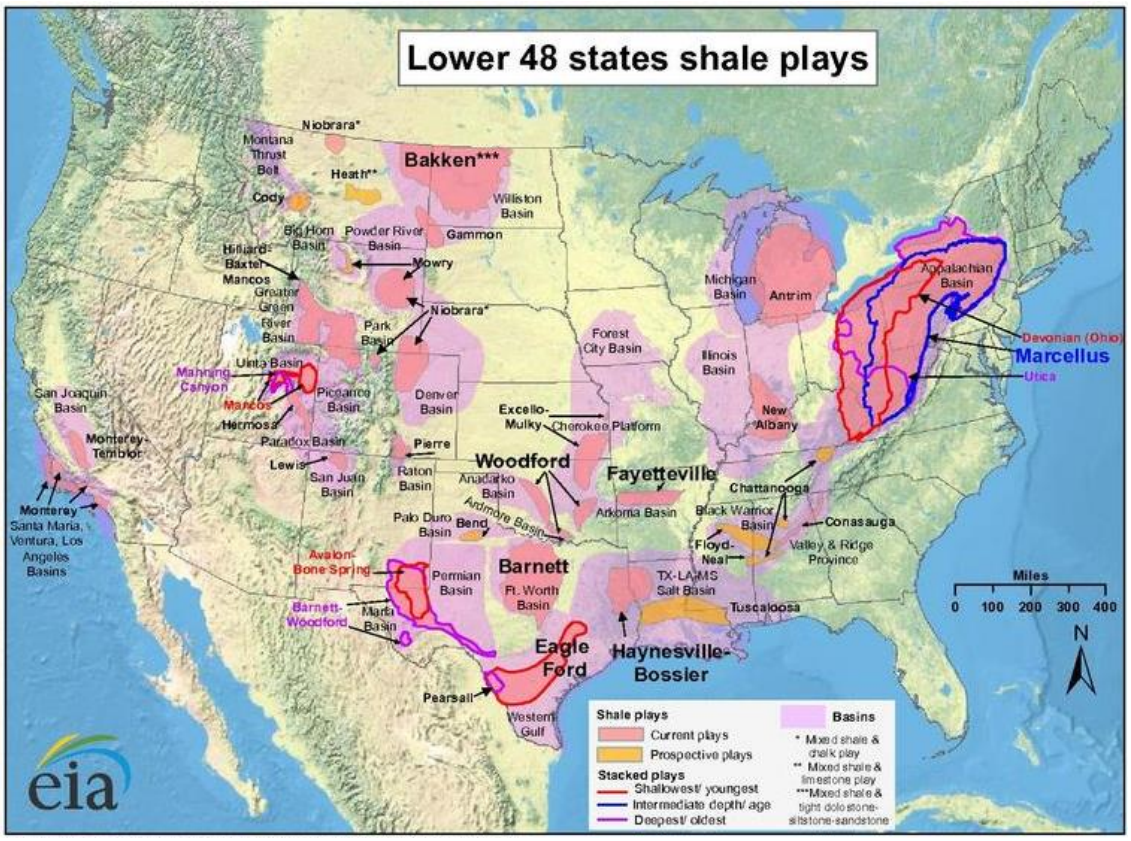

Figure 5-3: Shale gas extraction sites in US [104]

The shale gases chosen are from Marcellus, Appalachian, Eagle Ford and Haynesville sites. Based on the chemical composition given by George and Bowles [106], the molar properties of the shale gas sites were calculated by Sehgal [107]. Table 5-1 shows the mass fraction of the constituents in the shale gas at different sites which is used to implement in the Hephaestus for conventional combustor.

The performance model for CUTF1 engine discussed in section 4.2 was carried out and verified with natural gas by Sehgal [107]. This study has taken the

combustor input parameters; pressure, mass flow, temperature and fuel flow from the CUTF1 engine performance model to estimate the NO_X emission for the shale gas as a fuel in the conventional combustor design.

Table 5-1: Mass Fraction of constituents for shale gas sites

	Marcellus	Appalachian	Eagle Ford	Haynesville
Methane	0.9700	0.7908	0.7460	0.9630
Ethane	0.0244	0.1771	0.1382	0.0120
Propane+	0.0022	0.0060	0.0988	0.0031
Carbon Dioxide	0.0004	0.0007	0.0154	0.0182
Nitrogen	0.0030	0.0254	0.0016	0.0037

C.3 Results and Discussion

There is no literature available to verify the NO_X emission results for the CUTF1 engine. Therefore a comparison is shown in Table 5-2 between the different shale gases and the ICAO data with Jet-A as fuel for conventional combustor.

Table 5-2: $EINO_X$ vs Power Setting for different shale gas for CUTF1

		$EINO_X$ (g/Kg Fuel)			
Power Settings (%)	ICAO Jet-A	Marcellus	Appalachian	Eagle Ford	Haynesville
100	37.8	20.7	21.5	22.2	20.4
85	28.5	16.4	17.1	17.6	16.1
30	11	7.5	7.8	8.1	7.4

9	4.7 (7%)	5.8	6.1	6.3	5.7

The results from Table 5-2, shows that the NO_X formation in the CUTF1 engine for shale gas is much lower than that for Jet-A. The reason behind the difference in $EINO_X$ is mentioned below:-

- Mixture of shale gas and air is homogenous in the combustion (air and gas mixture), whereas in case of Jet-A, the mixture (air and liquid) is heterogeneous. Therefore, small pockets of Jet-A fuel during the fuel/air mixture create local stoichiometric region or local hot spot region increasing temperature thus aggravating the formation of NO_X.
- Shale gas is mostly methane with high hydrogen to carbon ratio whereas, Jet-A has high carbon content compared to methane. The carbon or soot produces luminous radiation which increases the flame temperature leading to increase in NO_X production in Jet-A fuel.

However, at the lower power setting the NO_X formation for shale gas and Jet-A is in close approximation. As the engine performance calculation was performed in Turbomatch [97] by Sehgal [107], the compressor had surged at lowest power setting of 9%. This limitation of Turbomacth restricted the exact comparison of shale gas and Jet-A $EINO_X$ for 7% power settings.

Moreover, testing the robustness of the model by looking into the trend of NO_X emission characteristics was the primary focus for the introduction of shale gases in the Hephaestus model and the result shows, the shale gas reduces NO_X formation in the conventional combustor when burned, compared to the Jet-A fuel.

Since the shale gas reduces the NO_X formation in the conventional combustor of CUTF1, a LTO cycle NO_X calculation is performed. The section 2.4.3 explains the ICAO LTO cycle limits for NO_x production by aircraft engines. Figure 5-4 shows the comparison of shale gas LTO NO_x and where it stands with the CAEP limits for the CUTF1 engine including the comparison with Jet-A.

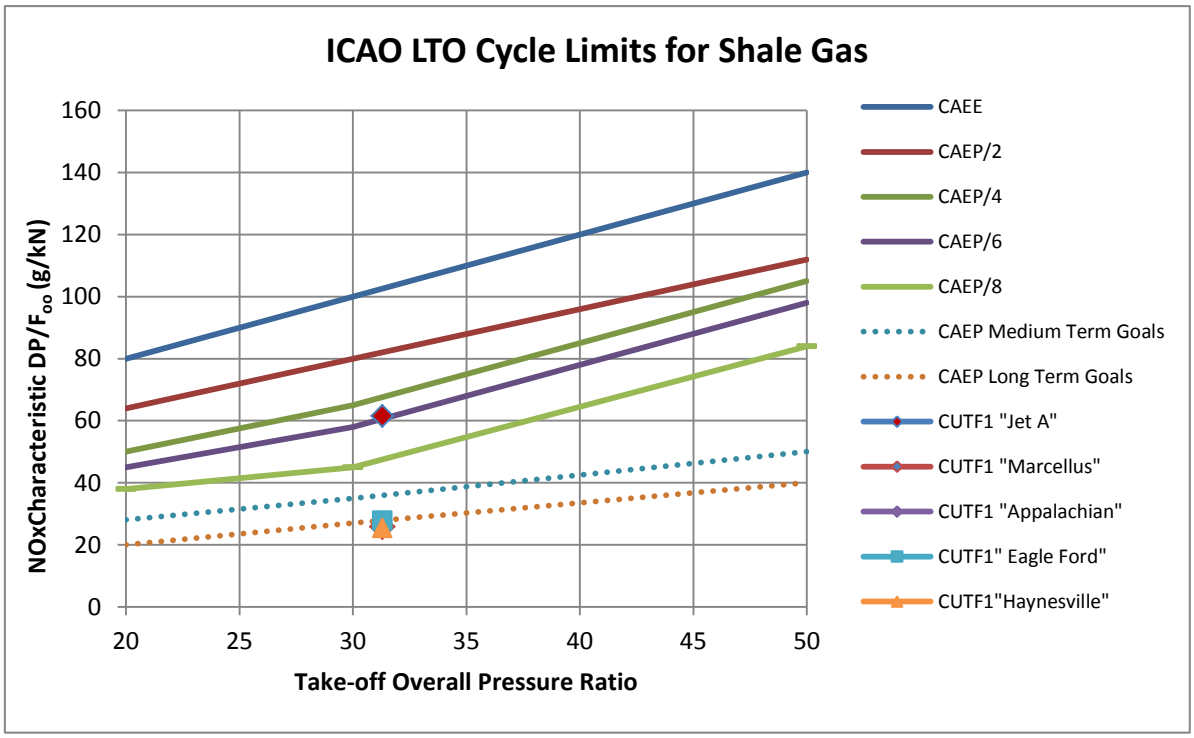

Figure 5-4: Comparison of NOx characteristics: shale gas in LTO Cycle

The NO_X prediction from the model shows that the shale will abide by the CAEP long term goals whereas the Jet-A fuel is way higher in the NO_X production for the LTO cycle.

In order to use the natural gas as a fuel in an aircraft engine, it has to be liquefied when stored on board an aircraft. This poses a design limitation for it to be used in current aero engines. Especially designed fuel tank is needed to accommodate the liquefied natural gas for an aircraft.

As the primary focus of this study was to check the robustness and flexibility of the prediction model to accommodate new fuels, the design of an aero engine fuel tank is not covered in this study. Sehgal [107] has reviewed and suggested some design changes in an aircraft to accommodate the shale gas storage on board an aircraft.